7773 U-005-307.22

# TRANSITE CHARACTERIZATION TREATABILITY STUDY FINAL REPORT, PREPARED FOR USDOE, FERNALD AREA OFFICE, FERNALD, OHIO - (USED AS A REFERENCE IN OU3 RI/FS/PP REPORT, MAIN REFERENCE LIST)

10/01/95

TCT-FO-013
UC FERMCO
200
FINAL REPORT

7773

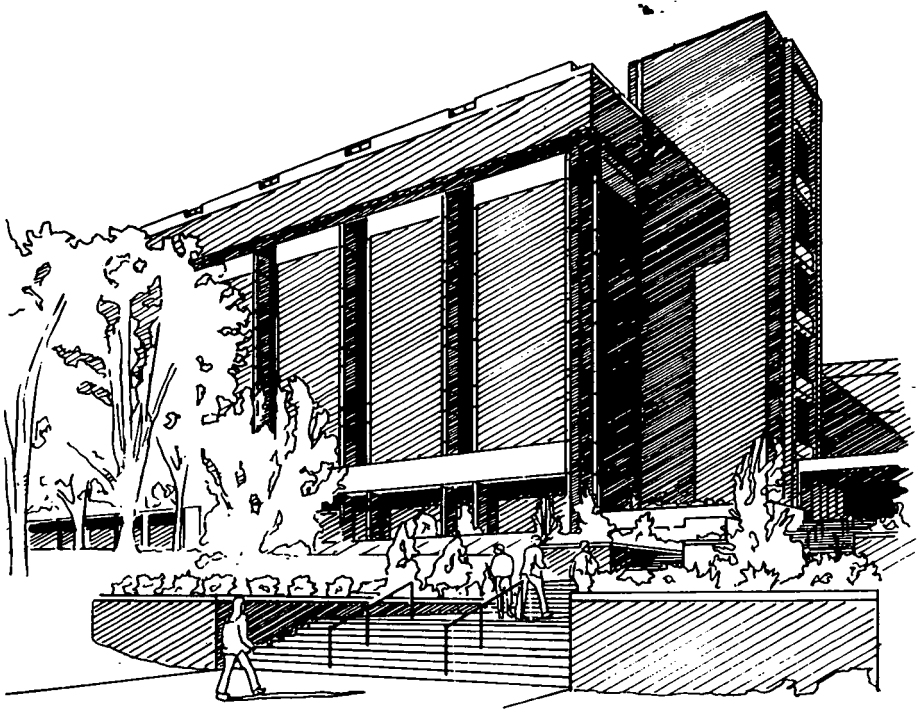

UNIVERSITY OF CINCINNATI
COLLEGE OF ENGINEERING

DOC. #TCT-FO-013

**ALTER**

Accelerated Life Testing and Enviromnental Research

# TRANSITE CHARACTERIZATION TREATABILITY STUDY

**Final Report**
Submitted to:

FERNALD ENVIRONMENTAL REMEDIATION MANAGEMENT COMPANY OF OHIO

October 1995

000001

# University of Cincinnati - College of Engineering

Transite Characterization Treatabiliy Study
Final Report

Performed and Reported
by

John Valentine
Linda Rieser
Ali Houshmand
William Russ
Wei Chung
Laura Ollier
Nathalie Tracez

# TABLE OF CONTENTS

PAGE

1.0 INTRODUCTION ..... 1–1

2.0 TRANSITE SAMPLES ..... 2–1

3.0 TECHNIQUES INVESTIGATED ..... 3–1
- 3.1 NEUTRON ACTIVATION ANALYSIS (NAA) ..... 3–1
- 3.2 PROTON INDUCED X-RAY EMISSION (PIXE) ..... 3–2
- 3.3 ATOMIC ABSORPTION SPECTROMETRY (AAS) ..... 3–2
- 3.4 X-RAY FLUORESCENCE (XRF) ..... 3–2
- 3.5 BACKSCATTER SPECTROMETRY ..... 3–3
- 3.6 INDUCTIVELY COUPLED SPECTROSCOPY- AES AND MS ..... 3–3
- 3.7 ULTRAVIOLET FLUORESCENCE ..... 3–3
- 3.8 AUTORADIOGRAPHY ..... 3–4
- 3.9 GAMMA-RAY SPECTROSCOPY ..... 3–4

4.0 TECHNIQUES USED ..... 4–1
- 4.1 DESTRUCTIVE RADIOLOGICAL TECHNIQUES ..... 4–1
- 4.2 NON-DESTRUCTIVE RADIOLOGICAL TECHNIQUE ..... 4–5
  - 4.2.1 COMPUTATIONAL TECHNIQUES ..... 4–5
    - 4.2.1.1 Mathematical Representation of the Detector Responses ..... 4–5
    - 4.2.1.2 Diffusion in Solid Materials ..... 4–8
      - 4.2.1.2.1 Instantaneous contamination exposure ..... 4–9
      - 4.2.1.2.2 Constant surface contamination exposure ..... 4–10
  - 4.2.2 DISTINGUISHING SPATIAL DISTRIBUTIONS ..... 4–12
    - 4.2.2.1 Detector Responses to Surface and Volumetric Sources ..... 4–12
    - 4.2.2.2 Contamination on One Side ..... 4–13
    - 4.2.2.3 Contamination on Two sides ..... 4–13
  - 4.2.3 TECHNIQUE REQUIREMENTS ..... 4–17
- 4.3 METALS CHARACTERIZATION TECHNIQUES ..... 4–18
  - 4.3.1 LEACHING PROCEDURE ..... 4-18
  - 4.3.2 SURFACE DIGESTION ..... 4-20

PAGE

5.0 RESULTS ..... 5–1
5.1 RADIOLOGICAL CHARACTERIZATION RESULTS BASED ON DESTRUCTIVE TECHNIQUES ..... 5–1
5.2 RADIOLOGICAL CHARACTERIZATION RESULTS BASED ON NON-DESTRUCTIVE TECHNIQUES ..... 5–1
5.2.1 Linear Attenuation Coefficient of Transite ..... 5–1
5.2.2 Technique Validation ..... 5–9
5.3 METALS CHARACTERIZATION RESULTS ..... 5–13
5.3.1 Metals Characterization Results– Leaching Procedure ..... 5–13
5.3.2 Metals Characterization Results– Surface Digestion ..... 5–14

6.0 CONCLUSIONS ..... 6–1

APPENDIX A - RADIOLOGICAL TECHNIQUES INVESTIGATED ..... A–1

APPENDIX B - INITIAL SURVEY DATA FOR ALL PANELS ..... B–1

APPENDIX C -RADIOLOGICAL CHARACTERIZATION SAMPLE SPECIFIC RESULTS BASED ON DESTRUCTIVE ANALYSIS TECHNIQUES ..... C–1

APPENDIX D -RADIOLOGICAL CHARACTERIZATION SAMPLE SPECIFIC RESULTS BASED ON GAMMA-RAY SPECTROSCOPY TECHNIQUE ..... D–1

REFERENCES ..... R–1

# 1.0 INTRODUCTION

A typical decontamination and decommissioning concern for both Department of Energy (DOE) facilities and nuclear power industry facilities is accurately determining the depth to which radiological contamination has penetrated building materials. The optimal means of decontaminating or disposing of such materials will often be dependent on this penetration depth. The building material of primary concern in this study is transite, an asbestos-cement material used for both internal and external walls at process buildings at the DOE Fernald site. Transite was used extensively as building panels at DOE sites prior to the implementation of asbestos-controlling regulations. Uranium processing at the Fernald site has resulted in the radiological and chemical contamination of these panels. In the current era of remediation, prior to the disposal of these transite panels, the multiple concerns of toxic (asbestos containing) and radioactive/chemical (process contaminated) waste must be addressed. Such a mixed waste is much more costly to dispose of than singularly contaminated waste. It is therefore desirable to minimize the amount of mixed wastes. In the case of transite, surface decontamination might be able to restore the bulk of the material to the simpler toxic waste form. The viability of decontamination hinges on the distribution of the contamination through the thickness of the transite panels. Consequently, characterizing this contamination distribution is the first step in the disposal of the transite. Note: the term " contamination distribution" will be used in this report to indicate the distribution of contamination through the thickness of transite samples, and does not refer to the distribution of contamination on the surface of the samples unless specifically mentioned.

The University of Cincinnati was contracted by FERMCO to develop a methodology to determine the depth of radiological contamination for transite samples from the Fernald site. This methodology development was to include a review of potential techniques and analysis of Fernald transite samples using one or a few of the most promising techniques identified by this review. In addition, an analysis of the metals contamination was requested. The penetration of lead through the thickness of transite was of particular interest as windows and doors were hung using lead washers and casings.

The potential exists for a variety of destructive and non-destructive techniques to be used to characterize the contamination distribution through the thickness of transite. Destructive methods primarily involve a sequential layer removal and subsequent analysis of the exposed surfaces. Such destructive techniques are very limiting due to the difficulties in handling

radiologically contaminated friable asbestos and the resulting constraints on sample size. Consequently, a non-destructive technique capable of being implemented on site is preferred, as this would bypass some difficulties in handling, and would minimize reliance on inferential statistics by allowing a much larger scale sampling plan.

# 2.0 TRANSITE SAMPLES

Transite is the brand name of an asbestos-cement construction material consisting of chrysotile asbestos (magnesium silicate) and portland cement. Manufacturing consisted of multiple layers of material bonded in a hydraulic press to form composite laminar panels. At the Fernald site, these panels typically have the dimensions of 4'x10' and are either flat or corrugated in form. The flat panels have a nominal thickness of 1/4" whereas the corrugated panels have a nominal thickness of 3/8". In general, the flat panels were used for internal walls and the corrugated panels were used for external walls. Transite was chosen as a building material for its strength and ability to resist moisture, heat and corrosion. It has a density of about 100 $lbs/ft^3$ or 0.16 $g/cm^3$

The samples used in this study to develop a methodology for determining contamination distribution were taken from two different buildings at the Fernald site with very different process histories. One was building 7A where very little process contamination occurred, and the other was building 2A where more process contamination occurred. Initially, 3 groups or blocks of panels (A, B, and C) were taken from these buildings for analysis. Each of these groups consisted of 6 panels of approximately 10"x10". Group A were flat panels from the interior of building 7A. Group B were corrugated panels from the exterior of building 7A. Group C were flat panels from the interior of building 2A. Examples of the panels from these three groups are shown in Figure 2–1. Each panel was further labeled 1 through 6 in each group, resulting in panels A1 through A6, B1 through B6, and C1 through C6. Furthermore, these panels were subdivided into 9 samples each, a through i. For example, panel C5 was divided into approximately 3"x3" squares C5a through C5i, as shown in Figure 2–2. Each of these samples represents the basic unit of analysis. This presumes a certain degree of contamination homogeneity while allowing sufficient area for practical application of analytic methods.

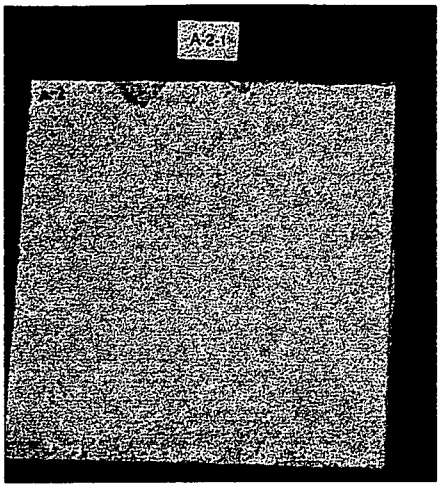


(a)

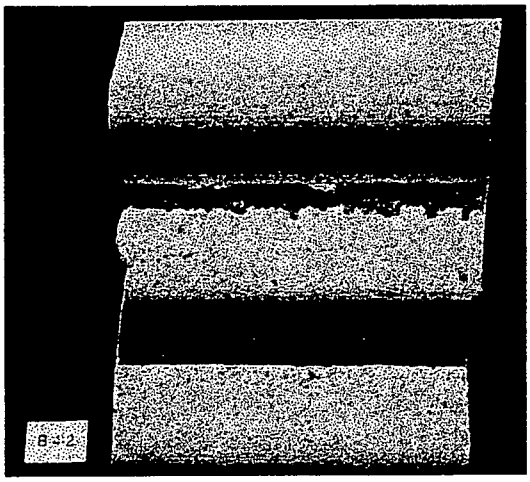


(b)

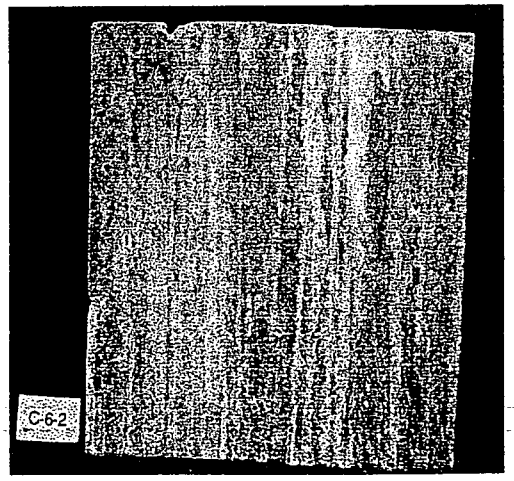


(c)

Figure 2–1: Examples of transite panels from a) Group A (Building 7 – Interior), b) Group B (Building 7 – Exterior), and c) Group C (Building 2 – Interior).

| | | |
|---|---|---|
| C5a | C5b | C5c |
| C5d | C5e | C5f |
| C5g | C5h | C5i |

**Figure 2–2 Sample labeling**

# 3.0 TECHNIQUES INVESTIGATED

After developing a set of criteria for which a technique must meet in order to be useful for transite characterization, as many techniques as possible were identified and evaluated. These techniques can be grouped into three categories based on the ability of the technique to provide information about the contamination distribution in the sample: 1) destructive techniques which require destroying the sample to provide any information, 2) non-destructive techniques which only provide information about the surface of the sample and therefore require destructive analysis to determine the contamination distribution, and 3) non-destructive techniques which directly provide information about contamination distribution. As previously noted, entirely non-destructive techniques (category 3) are preferred. The following techniques were considered in an attempt to provide an encompassing range of possibilities while still remaining within the realm of desired criteria. Such criteria consist of minimizing cost, ability to perform in-house, time constraints, quantitative or qualitative nature of the results, ability to measure contamination penetration distribution, accuracy, and precision. A more complete description of each technique, including benefits and limitations, is presented in Appendix A.

## 3.1 NEUTRON ACTIVATION ANALYSIS

Activation analysis consists of first activating the sample and then measuring the resultant induced activity. Activation is the process whereby an element is converted to an unstable state, creating a radioactive material. In the case of NAA, activation is accomplished using a high neutron flux which can penetrate deeply and relatively uniformly. The target material captures the incident neutrons and becomes unstable. The subsequent decay of the target material can be measured with a high resolution gamma-ray detector such as a high-purity germanium (HPGe) detector. The measured spectrum is characteristic of the material, allowing identification of its constituent isotopes. No direct depth information is provided by standard NAA and a large source of neutrons (typically a research reactor) is required. While means of providing depth information can be envisioned, including the gamma-ray spectroscopy technique discussed in section 3.9, most would result in using destructive analysis with NAA (category 1 and possibly 3).

### 3.2 PROTON INDUCED X-RAY EMISSION (PIXE)

An energetic proton beam is created and directed onto the target. This results in the target atom inner electron shell becoming excited. In returning to the stable ground state, the target atom gives up the excitation energy in the form of an X-ray which has an energy characteristic of that element. Typically, a Si(Li) detector is used to detect these X-rays and the resultant spectrum allows elemental identification. The quantity of a particular element in a sample is determined based on the assumption that the peak area is proportional to the amount of that element in the sample. In general, PIXE is a non-destructive technique used for surface or near-surface analysis and requires a proton accelerator. Consequently, PIXE would require destructive analysis to provide definitive information about the contamination distribution in transite samples (category 2).

### 3.3 ATOMIC ABSORPTION SPECTROMETRY

A parallel beam of photons is created by a hollow cathode atomic spectral lamp. The beam passes through an atomized sample of the material of interest. The sample will attenuate the continuum of radiation at frequencies corresponding to the target atom resonance transition energies. The attenuated product radiation passes through a monochromator that filters through the range of frequencies characteristic of the element of interest. Finally, a detector measures the resultant radiation intensity. This method is normally based on analyzing for a single element dependent on the monochromator. It is destructive (category 1) and provides no depth information although it does result in a measure of the concentration.

### 3.4 X-RAY FLUORESCENCE (XRF)

Similar to PIXE in outcome, the source of incident radiation with X-ray fluorescence is high energy photons such as gamma-rays and X-rays. Again this incident radiation causes vacancies in the inner electron shells of the target material. The resultant transition of electrons to fill these desirable, low potential positions results in the release of X-rays that are characteristic of the element. A high energy resolution detector, such as a HPGe detector which is able to discern the adjacent photopeaks, measures the resultant spectrum to identify the material. This technique works best with a homogeneous solid material, and primarily provides surface or near surface information. Consequently, XRF would require destructive analysis to provide definitive information about contamination penetration depth (category 2).

## 3.5 BACKSCATTER SPECTROSCOPY

A source, such as a Van deGraaf accelerator, that can provide a beam of collimated and monenergetic particles directs these particles onto a very flat and thin target material. Most of the particles will pass through the target while a few will be backscattered. A detector placed at very large angles (> $160^0$) measures the energy of these backscattered particles. A kinematic analysis based on knowledge of the initial and final energies and angle of scattering indicates the mass of the target atoms. Quantitative analysis is subsequently performed through knowledge of the scattering cross section of the material and number of scatters. This technique requires an extremely uniform surface and would require destructive analysis to provide contamination penetration depth information (category 2).

## 3.6 INDUCTIVELY COUPLED SPECTROSCOPY (ICP) - ATOMIC EMISSION SPECTROSCOPY (AES) AND MASS SPECTROSCOPY (MS)

An inert gas, usually Argon, is inductively coupled with a high frequency electrical field. The resulting ionization of the circulating gas creates a very high temperature controlled plasma. A sample of the material of interest is dissolved, dissociated and atomized before injection into the plasma. This results in the material atoms being excited and emitting light at frequencies that are unique to the material. The intensity and wavelength of the light is then measured by either an emission spectrometer or a mass spectrometer. Quantitative analysis is based on the intensity when compared to a standard sample. This method requires that the sample be in solution capable of being atomized and provides no direct depth information (category 1).

## 3.7 ULTRAVIOLET (UV) FLUORESCENCE

When uranium is exposed to an oxygen containing environment, such as air, uranyl ions ($UO_2^{+2}$) are formed. These ions fluoresce visible green light when exposed to ultraviolet (UV) light. The concentration of contamination is proportional to the intensity at which the material fluoresces. The presence of uranium contamination can be determined qualitatively by direct observation. Image analysis through the use of standards to determine relative intensities could likely produce quantitative results. However, such a quantitative analysis would require extremely consistent photography. This method, developed by UC ALTER in 1992, provides only surface information (category 2), but it is very quick, simple, and inexpensive.

## 3.8 AUTORADIOGRAPHY

Autoradiography differs from typical radiography only in that the source of radiation is provided by the sample itself and a separate radioactive source is not required. Typical radiography also involves capturing the image of the sample on a photographic plate based on the attenuation of the radiation from the separate source by the intervening sample, while autoradiography captures the actual pattern and intensity of contamination from the sample. The only requirements are film and a means of handling the light sensitive media for exposure purposes. Since autoradiography also provides a spatial representation of contamination, it can be used for comparison to the UV photography results for verifying which regions contain uranium contamination. The greatest drawback to autoradiography is the lengthy time requirement which can be as much as several days for sufficient exposure. Autoradiography provides surface or near surface information and would require destructive analysis to determine the contamination distribution through the thickness of the transite panels (category 2).

## 3.9 GAMMA-RAY SPECTROSCOPY

While providing spectral data from a source of gamma-rays using a detector and multi-channel analyzer is not a new concept, using such data with a knowledge of the source material attenuation coefficient to determine the contamination penetration distribution is a pioneering application of the existing technology. The greatest advantage of this technique is the ability to obtain penetration data directly without having to remove layers of the material destructively (category 3). In order to obtain sufficient photopeak areas for analysis, some samples may require lengthy counting times on the order of days, depending on the degree of contamination. A HPGe detector is recommended for high energy resolution to discern adjacent photopeaks.

# 4.0 TECHNIQUES USED

To determine the contamination distribution in transite panels, the following were determined the most appropriate methods, in accordance with the considered criteria, allowing use of current in-house equipment to minimize cost while providing sufficient accuracy and precision in a timely manner. These techniques include ICP for metals analysis, autoradiography, UV fluorescence, and gamma-ray spectroscopy for radiological characterization. Of these, the only technique to directly provide information about the contamination penetration distribution through the thickness of the sample is the gamma-ray spectroscopy. This novel non-destructive technique initially required the use of other techniques to provide verification. In order for the other destructive techniques to provide information about the contamination penetration distribution, successive layers of material must be removed to allow analysis at the various depths. One possible concern with using the destructive techniques to verify the non-destructive technique is that the latter provides a continuous distribution while the former provides data at discrete thicknesses. However, the random nature of the thickness of layer removal and a sufficiently large number of data points ensure that interpolation between analysis depths is valid for comparison.

## 4.1 DESTRUCTIVE RADIOLOGICAL TECHNIQUES

Converting the surface analysis provided by UV fluorescence and autoradiography into a form that reveals the contamination distribution in the depth of the transite requires the removal of layers. Figure 4-1 shows an example of UV fluorescence and antoradiograph results compared to a photograph in ambient light. Also, the data provided by these techniques is essentially qualitative and verification of the non-destructive method requires a comparison with a quantitative distribution. This quantitative data is provided by a Geiger-Mueller $\beta - \gamma$ survey meter with measurements at each depth analyzed. A 3'x 2'x 4' HEPA filtered glove box containment built specifically for this project (see Figure 4-2) was used to deal with the unique challenge of the neccessary creation of friable radioactive asbestos resulting from layer removal. Samples of transite are placed in the containment along with an 18" belt sander , 1" micrometer, and double bagged $\beta - \gamma$ survey meter with a circular probe. Measurements of contamination are conducted in-situ using the $\beta - \gamma$ survey meter. Measurements of thickness are performed with the micrometer at the positions indicated by Figure 4–3.

Each sample is then placed in a vise attached to a wooden base inside the containment such that about half of the sample thickness extends above the top of the vise. The belt sander with rough grit sandpaper is applied to remove layers of material. Applying the sander in a variety of directions maximizes even removal. The thickness of the layer removed is dependent on both the amount of pressure applied manually and the amount of time spent sanding. Through meticulous sander control and technique, it is possible to remove a fairly even layer with a minimum thickness of approximately 0.01". The variation in the thickness measured by the micrometer at the eight positions is a measure of the evenness.

Before and after each of these layer removals, the sample is analyzed with the Geiger-Mueller detector, UV photography, and autoradiography. The detector is used in the glove box by placing the probe, which is about the same size as the sample, on the sample face and obtaining a visually averaged reading from the meter face on slow response. For the UV photography, the sample is placed in a light box equipped with ultraviolet fluorescent bulbs which emit light at a 254 nanometer wavelength. A 35 mm camera is attached to the viewport with 200 speed film, and the exposure is of 4 second duration. For comparative purposes, consistent settings and development are crucial. Different levels of contamination result in varied intensity hues and shades of iridescent green. Optically scanning the image into a digital format allows some image enhancement to emphasize the actual contamination. Correct interpretation of the UV images often requires comparison to the equivalent autoradiograph. The autoradiographs are produced using standard X-ray imaging film with a central polymeric base coated on both sides with a thin emulsion covered with an anti-scratch layer. Two triple closure light-tight boxes were constructed for film storage and sample exposure. The film is placed in direct contact with a sample and stored in one of the boxes for an exposure time of either 24 or 48 hours, depending on the contamination level. It has been empirically determined that a Geiger-Mueller detector reading of about 1000 cpm or greater can be exposed for 24 hours with a sufficient image. Lesser activity requires a 48 hour exposure. Consistent developing is provided by a standard automated developer. One concern with this method of layer removal was the possibility of cross-contamination between subsequent layers due to removal by abrasion. The results have indicated that this effect is negligible.

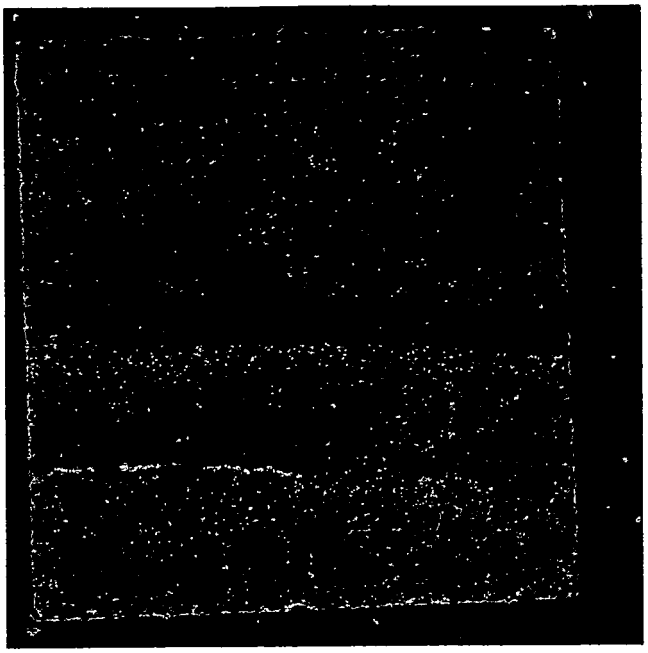

(a)

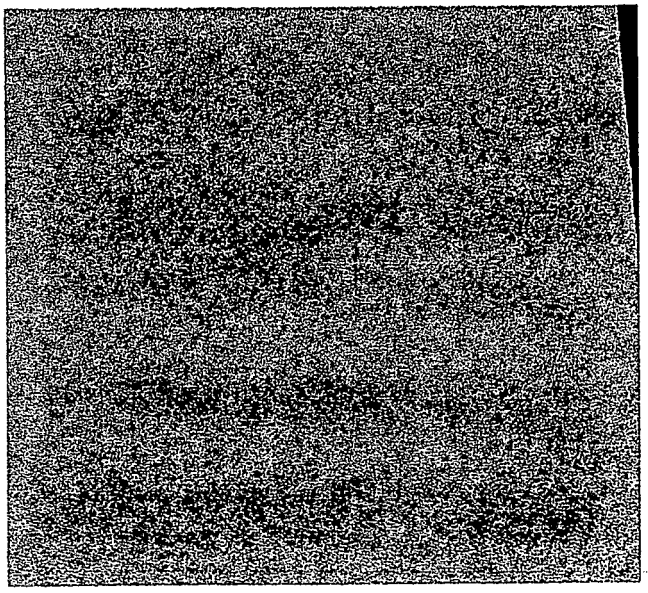

(b)

Fig. 4–1: Example of results from a) UV photography and b) autoradiography of a transite sample. The dark areas in b) correspond to regions with relatively high radiological contamination and have associated dark green regions in a).

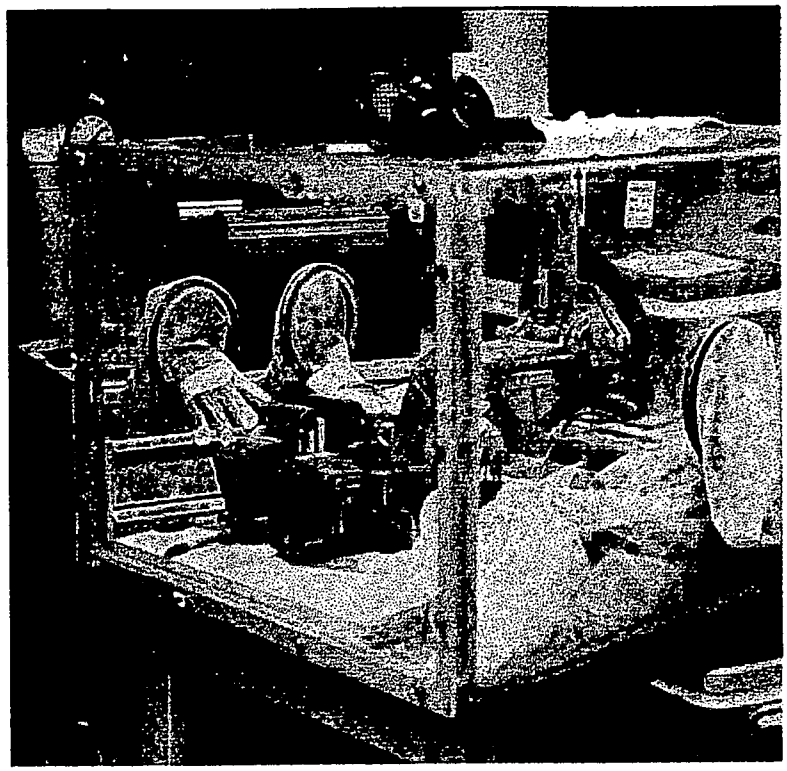

Fig. 4–2: HEPA Filtered Glove Box for Destructive Transite Analyses.

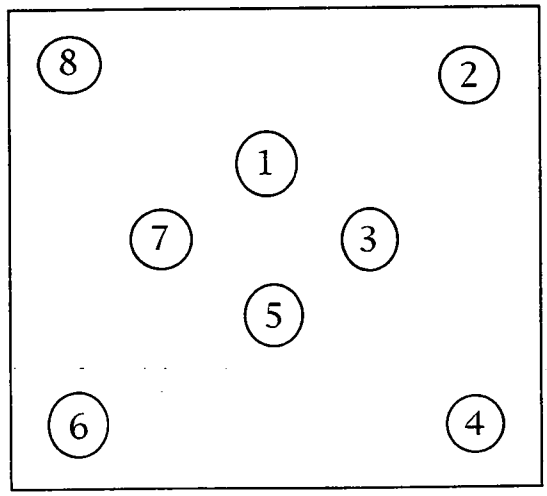


Figure 4–3 - Thickness Measurement Locations

## 4.2 NON-DESTRUCTIVE RADIOLOGICAL TECHNIQUE

A non-destructive method of measuring the contamination penetration distribution, which is based on measuring the gamma-ray spectra from both sides of the sample is proposed and validated in this study. In conjunction with knowledge of the gamma-ray linear attenuation coefficient of the sample material and proper diffusion or leaching models representative of how the material was contaminated, the ratio of photopeak areas at several energies from these spectra can be used to infer the most-probable distribution of the contamination. Figure 4–4 illustrates the implementation of this technique. A high-purity germanium (HPGe) detector provides sufficient energy resolution to discern all of the photopeaks of interest. Comparing the measured ratio of the respective photopeak areas from both sides of the panel (Figure 4–4b) over a range of energies to computer-generated ratios for possible contamination distributions allows determination of the most-probable distribution (Figure 4–4c). While discussion of this technique in this study is focused on its use with Fernald transite, the technique can be used with any material for which gamma-ray spectra can be acquired on both sides of the sample.

### 4.2.1 Computational Techniques

*4.2.1.1 Mathematical Representation of the Detector Responses*

The number of gamma-rays detected from some spatially extended source will vary as the geometric or material conditions of the medium change. Detecting gamma rays from both sides of radiologically contaminated planar samples as in the currently proposed technique presents such a situation. Fortunately, the point kernel technique has been a widely and successfully used for modeling such radiation transport problems. In the point kernel technique, the fundamental assumption is that the extended radiation source can be regarded as consisting of differential isotropic point sources. Additionally, the effect of the radiation from the whole source at the points of interest (the detectors in this method) can be obtained by summation of the contributions from the individual differential sources that comprise the entire source region. In most practical applications, the assumption that the original nuclear radiation is emitted isotropically is physically valid when considering effects on a macroscopic scale.

In this application, only full-energy gamma rays are considered. This implies that only the uncollided gamma-ray flux reaching the detectors from the source is considered. Consequently, the computational complexity of the technique is greatly simplified and no generality is lost since only photopeak count rates are being considered. Additionally, it has been assumed that the contamination distribution is uniform in the *x-y* plane on both sides, but not in the z direction.

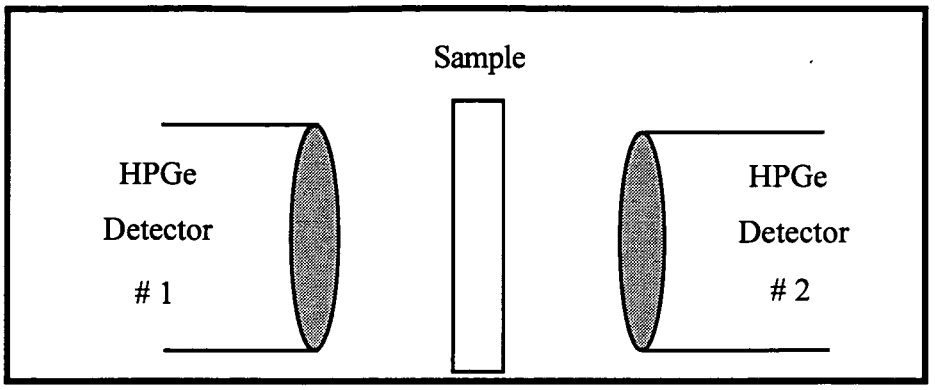


a

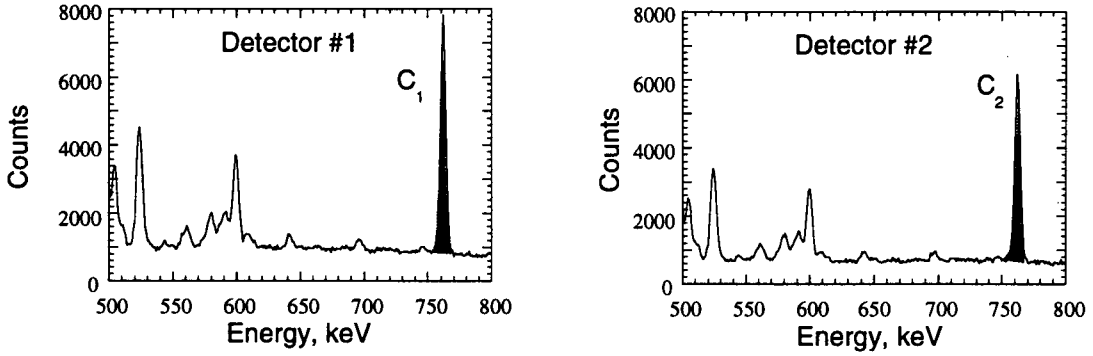


b

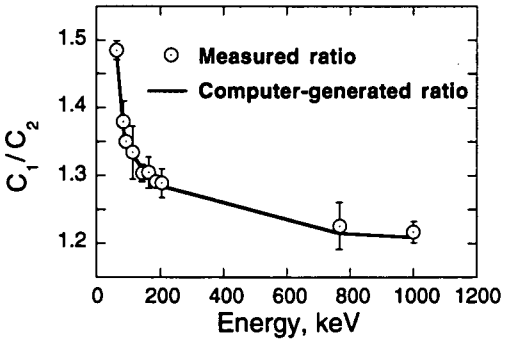


c

**Figure 4–4 Demonstration of the gamma-ray spectrometry technique using two detectors to determine the contamination penetration distribution in the sample; a) shows the sample-detector geometry; b) the gamma-ray spectra recorded by the detectors and one of the full-energy peaks; c) shows the relationship of measured response ratios as a function of gamma-ray energy compared to the computer-generated ratios.**

Furthermore, the term contamination distribution will be used to refer only to the variation in the $z$ direction (the thickness of the sample). In the $z$ direction, the contamination has been assumed to penetrate through a certain thickness. Therefore, the transite panels are assumed to be a finite volumetric radiation source with some kind of contamination distribution in the $z$ direction.

When a detector is set before a finite planar volumetric source, the response of the detector, $f(E)$,to the source at a particular energy $E$ can be written as:

$$\phi(E) = \iiint_{v_s} dv \iint_{s_d} ds\, g(z)\, f(x,y,z,r,\theta,E), \tag{4–1}$$

$$f(x,y,z,r,\theta,E) = \frac{S_0\, r\, e^{-\mu(E)\, z\, \rho/(a+t-z)}}{4\pi\, \rho^2}, \tag{4–2}$$

and

$$\rho = (x^2 + y^2 + r^2 + (a+t-z)^2 - 2r(x^2+y^2)^{1/2} \cos(\tan^{-1}\frac{y}{x} - \theta))^{1/2}, \tag{4–3}$$

where:

$f(E)$ is the uncollided gamma-ray current reaching the detector surface;
$f(x,y,z,r,\theta,E)$ is the kernel function;
$g(z)$ is the unknown source distribution function in $z$ direction;
$\mu(E)$ is the linear attenuation coefficient of the source material;
$E$ is the gamma-ray energy;
$S_0$ is the source strength, particles per unit volume per unit time;
$v_s$ is the source volume;
$s_d$ is the detector surface area;
$t$ is the sample thickness;
$a$ is the distance between the source surface and detector surface;

Consequently, the response ratio $R(E)$ for a finite volumetric source at energy $E$ can be written as:

$$R(E) = \frac{\phi_1(E)}{\phi_2(E)} = \frac{\iiint_{v_s} dv \iint_{s_d} ds\, g(z)\, f_1(x,y,z,r,\theta,E)}{\iiint_{v_s} dv \iint_{s_d} ds\, g(z)\, f_2(x,y,z,r,\theta,E)}, \tag{4–4}$$

where $f_1(E)$ and $f_2(E)$ are the uncollided gamma-ray currents over the surfaces of two detectors. Due to the relative coordinates, the forms in kernel functions $f_1$ and $f_2$ will be slightly different.

Let $C(E)$ be the detector count rate, then $C(E)=ef(E)$, where $e$ is a constant accounting for the detection efficiency. For two identical detectors symmetrically positioned on both sides of the source, $e$ is approximately equal. Consequently, the detector response ratio $R(E)$ can be expressed as:

$$R(E) = \frac{\phi_1(E)}{\phi_2(E)} = \frac{C_1(E)}{C_2(E)}, \tag{4–5}$$

where $C_1(E)$ and $C_2(E)$ are the count rates for two detectors, respectively.

Note that surface contamination is the limiting case of a volumetric distribution with the penetration depth approaching zero. Therefore, the mathematical expression for a surface source is similar to that of a volumetric source.

The major complication in solving the integral equation (4–4) for $g(z)$ is that the solution strongly depends upon the conditions of the kernel functions $f_1$ and $f_2$, function $R$ as it varies with energy, and the relations of $f_1$, $f_2$, $R$, and $g$. When the kernel functions are nonlinear functions, as in our case, and function $R$ is also a nonlinear function, it is difficult to obtain the solution using either analytical or numerical methods. In some situations, no solutions exist. However, if the unknown distribution function $g(z)$ can be constrained to a properly chosen mathematical expression in terms of physically valid assumptions, equation (4–4) can be efficiently and dependably solved. On the basis of this fundamental idea, resolving equation (4-4) becomes possible and, as it will be shown later, this is an efficient approach for determining the contamination distribution. In the computation process, the Gauss-Legendre integration method is used for multidimensional integrals.

*4.2.1.2 Diffusion in Solid Materials*

To select potential unknown distribution functions $g(z)$ in equation (4–4), the manner in which the sample was contaminated should be considered to obtain the proper analytical models. One common situation which may occur when solid materials are radiologically contaminated is the process of diffusion transport, during which the radioactive particles migrate into the material. Although there are different models describing diffusion phenomena with various considerations for different diffusion mechanisms (such as the bulk diffusion model, bulk diffusion with partial fixation model, bulk diffusion with linear adsorption model, and some empirical models which emphasize different diffusion mechanisms and conditions), all can be generalized into a fundamental form. The major differences in such models are reflected by the expression of the diffusion coefficient parameter. In general, if only considering the cumulative contamination effect, the lumped parameter (or effective diffusion coefficient) can be used. The diffusion

process is described by transport theory and can be used to obtain the theoretical solution given specific initial and boundary conditions.

Generally, the one dimensional, time-dependent problem is represented by Fick's second law and can be written as:

$$\frac{\partial J}{\partial z} = -\frac{\partial c}{\partial t}, \tag{4–6}$$

where $J$ is the flux of particles, $c$ is the concentration of diffusion species. In a homogeneous system, equation (4–6) can further be reduced to:

$$\frac{\partial c}{\partial t} = D\frac{\partial^2 c}{\partial z^2} \quad , \tag{4–7}$$

where $D$ is the diffusion coefficient or diffusivity of the sample material.

For some specific initial conditions and boundary conditions, equation (4–7) can be solved analytically. For the case of Fernald transite, two special cases are considered herein. Other cases, and possibly other models (such as leaching), may be more appropriate for different contamination scenarios.

*4.2.1.2.1 Instantaneous Contamination Exposure*

If the diffusing species is deposited as a "thin" layer, or an instantaneous contamination, on the surface of the sample, the initial condition is:

$$c(z,0)=s_0\,\delta(z)\ , \tag{4–8}$$

where $\delta$ is the Dirac delta function, defined by:

$$\delta(z) = \begin{cases} 0, & z \neq 0 \\ 1, & z = 0 \end{cases}\ , \tag{4–9}$$

and

$$\int_0^{+\infty} c\,dz = s_0\ , \tag{4–10}$$

where $s_0$ is the quantity of diffusing particles deposited per unit area. Under these conditions, the analytical solution to equation (4–7) is:

$$c(z,t) = (s_0 / 2(\pi Dt)^{1/2})\ exp(-z^2 / 4Dt). \tag{4–11}$$

Equation (4–11) is the Gaussian distribution function and Figure 4–5 shows the contamination penetration profile at two different times. Note the total amount of contamination remains constant at $s_0$, while the penetration depth increases with time.

#### *4.2.1.2.2 Constant Surface Contamination Exposure*

If the sample is being continuously exposed to a constant concentration of the diffusing species, a different situation arises. In this case, with initial condition:

$$c(z,0) = c_0 , \tag{4–12}$$

and boundary condition:

$$c(0,t) = c_s , \tag{4–13}$$

the analytical solution is:

$$\frac{c - c_s}{c_0 - c_s} = erf\left(\frac{z}{2\sqrt{Dt}}\right) , \tag{4–14}$$

where, "*erf*" indicates the error function:

$$erf(x) = \frac{2}{\sqrt{\pi}} \int_0^x e^{-u^2} du . \tag{4–15}$$

Since the transite panels were not radiologically contaminated when the buildings were constructed, $c_0$, represents the material background concentration which is approximately zero compared to the contamination concentrations. Therefore, equation (4–14) can be further simplified as:

$$c(z,t) = c_s \, erfc(z / 2(Dt)^{1/2}), \tag{4–16}$$

where "*erfc*" is the complementary error function (*erfc*=1-*erf*). $c_s$ has the physical meaning of concentration of the constant source of the diffusing species at the surface of sample. Figure 4–6 shows the contamination penetration profile at two different times. Again the surface activity or contamination remains constant with time, while the penetration depth increases with time.

Equations (4–11) and (4–16) are the analytical solutions of equation (4–7) for a planar geometry. These distribution functions have been simplified into the following formats to consistently represent the contamination distribution function *g(z)* in the detector response ratio equation (4–4).

$$g(z) = S_{01} \, exp(-\lambda_1 z^2) , \tag{4–17}$$

and

$$g(z) = S_{02} \, erfc(\lambda_2 z) , \tag{4–18}$$

where it is assumed that effective diffusion coefficient $D$ and time $t$ are constant for a specific point in time. Therefore, $S_0$ has the lump meaning of $S_{01}=s_0/2(pDt)^{1/2}$, $S_{02}=c_s$, and $\lambda$ has the

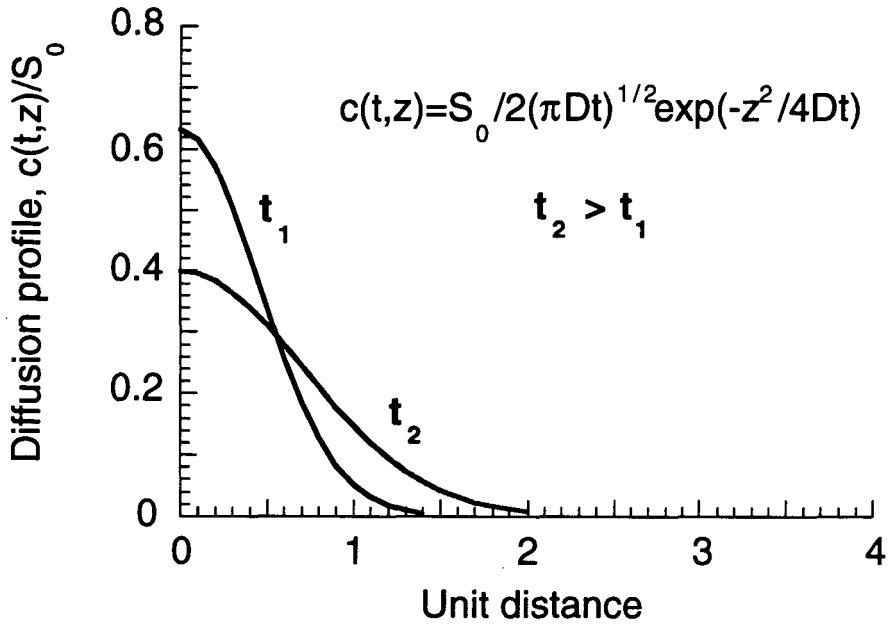


**Figure 4–5 Contamination distribution (Gaussian distribution) through thickness of sample due to instantaneous contamination exposure using diffusion model at two times, $t_1$ and $t_2$, after the exposure.**

meaning $\lambda_1 = 1/4Dt$, $\lambda_2 = 1/2(Dt)^{1/2}$. Both parameters ($S_0$ and $\lambda$) are expressed by the diffusion coefficient and duration of time since the initial exposure to contamination.

A major objective in developing this non-destructive technique is to predict the possible contamination distributions that may occur in the transite panels by using computer simulation of the experimental measurement. Such simulation provides insight into how the radiation is attenuated due to the different geometry and photon energies, and uses these characteristic differences to evaluate the contamination distribution. Furthermore, this simulation not only performs the calculation to resolve the equation (4) when the distribution function $g(z)$ is given, but also generates the optimum parameters to predict the most probable contamination distribution , such as the $\lambda$ and $S$ parameters in the diffusion model. These optimum parameters are determined using a least-squares fit.

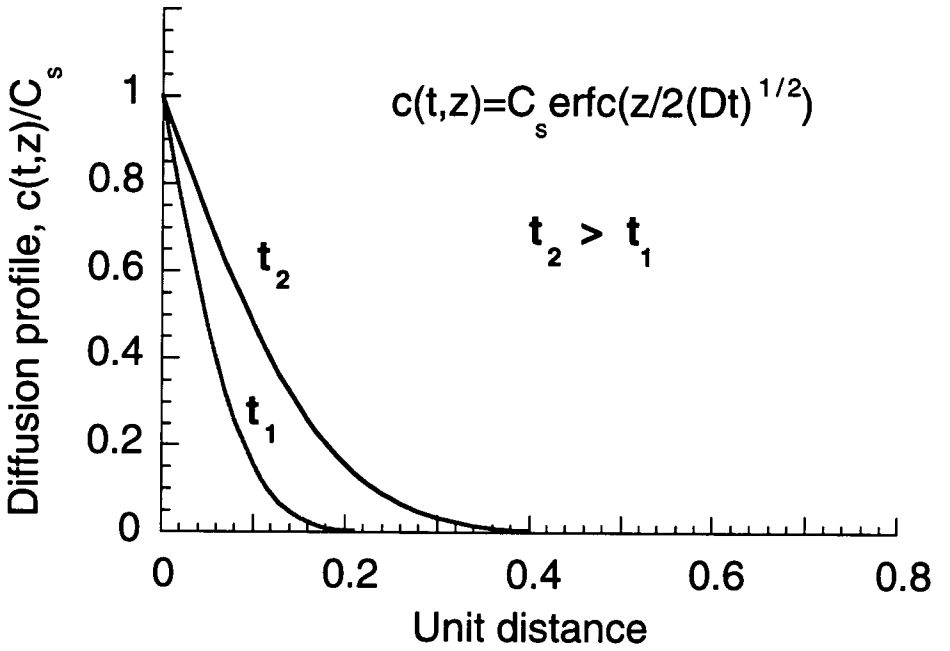


**Figure 4–6 Contamination distribution (complimentary error function) through thickness of sample due to constant contamination exposure using diffusion model at two times, $t_1$ and $t_2$, after the initial contamination.**

### 4.2.2 Distinguishing Spatial Distributions

*4.2.2.1 Detector Responses to Surface and Volumetric Sources*

The potential exists for both sides of Fernald transite panels to be radiologically contaminated. In almost all cases, this situation occurs. Consequently, the contamination will penetrate into the material from both sides. If the penetration depth is small, the material may be considered surface contaminated and could possibly be decontaminated. If the contamination has penetrated deeply into the material, it must be considered volumetric and could be distributed through the panel thickness in any of a nearly infinite number of distributions. Therefore, two problems should be considered: first, identifying whether the contamination is distributed on the surface only or is volumetric; and second, determining the contamination penetration depth along with the contamination distribution within the panel.

To address these two problems, two fundamental parameters which are used in the analysis are introduced. The first parameter is the *response ratio* which is defined as $C_1/C_2$, where $C_1$ and $C_2$ are the photopeak counting rates in detectors 1 and 2, respectively, at a particular energy. This ratio is used to reflect the difference in gamma-ray attenuation for the two sides and analytically corresponds to equation (4–4). The second parameter is the *boundary condition ratio* which is defined as $S_2/S_1$, where $S_1$ is the surface activity of the more contaminated side (hot side), and $S_2$ is the surface activity of the less contaminated side (cold side). This ratio presents the relationship of the boundary contamination levels on the two surfaces of a transite panel. By choosing the hot and cold sides as sides 1 and 2, respectively, the boundary condition ratio will always be less than or equal to unity ($S_2/S_1 \leq 1$). The response ratio, however, depends upon the geometry and gamma-ray energy.

*4.2.2.2 Contamination on One Side*

Some situations may exist where only one side of the transite panel is contaminated. This is represented by $S_2$ being equal to zero. If the measurement geometry is arranged as illustrated in Figure 4–7, the response ratio as function of gamma-ray energy will always be greater than unity ($C_1/C_2 \geq 1.0$) and vary depending on the contamination distribution.

The different contamination distributions, shown in Figure 4–8a, will generate the corresponding detector response ratios shown in Figure 4–8b. It should be noted that any contamination distribution approaches the behavior of a surface source as the penetration depth approaches zero. This is illustrated in Figs. 4–8a and 4–8b by volumetric source 1 (VS1) , and the surface source (SS). Different penetration depths will result in different response ratios ($C_1/C_2$) as a function of energy as shown in Figure 4–8b. These differences permit the quantitative analysis and distinguish the different source distributions. For example, if given a set of measured response ratios ($C_1/C_2$) for a transite panel, one can compare this data with the computed results to identify which distribution is most probable.

*4.2.2.3 Contamination on Two Sides*

When both sides of a transite panel are contaminated, the boundary condition ratio ($S_2/S_1$) becomes non-zero and the analysis is more complicated. The recommended measurement geometry for this technique when contamination exists on two sides is shown in Figure 4–9.

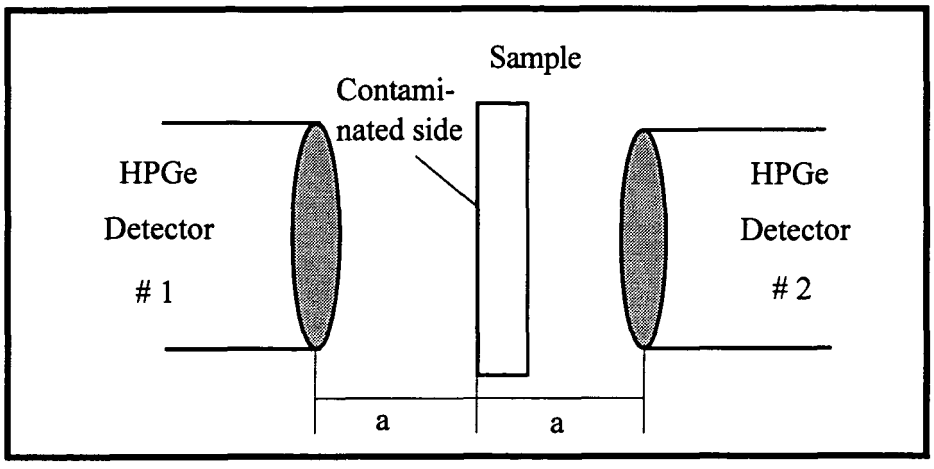


**Figure 4–7 Sample-detector geometry for samples contaminated on one side only.**

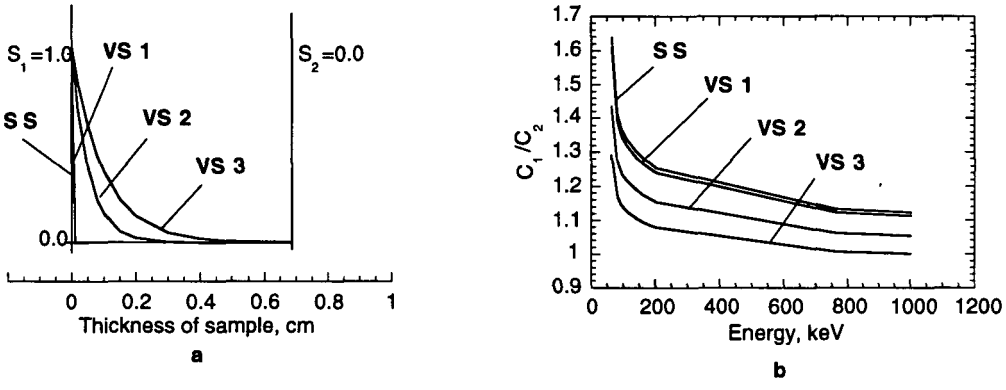


**Figure 4–8 a) Configuration of different contamination distributions used to model transite panels contaminated on one side only. b) Corresponding response ratios ($C_1/C_2$) for surface and volumetric sources shown in (a) for transite panels contaminated on one side only. (SS is surface source, VS is volumetric source.)**

The following analytical techniques were used to determine contamination distribution for such cases:

- When $S_2 \neq S_1$ and the boundary condition ratio ($S_2/S_1$) is known, a comparison between the measured data and the computed data is possible to determine the most likely distribution within the panel. For example, assume $S_2/S_1=0.15$ for the geometry in Figure 4–9. Several possible contamination distributions with this boundary condition ratio are shown in Figure 4–10a. However, each distribution will contribute differently to the response ratio, as shown

in and Figure 4–10b. When the proper distribution model is selected, such as selecting diffusion model equation (4–9) adapted for a two-sided case, then comparing these simulated results with the measured data, the true distribution can be identified.

- When $S_2 \neq S_1$ and the boundary condition ratio ($S_2/S_1$) is unknown, we may use relationships obtained by computer simulation to evaluate the maximum and minimum boundary condition ratios. This is accomplished by using the measured response ratios. Referring to Figure 4–11, the measured ratios $R_1$ and $R_2$ at energies 64 keV and 1001 keV, intersect with the simulated surface source results at points of 2 and 4, respectively. The vertical line formed by these points corresponds to the maximum possible ratio $(S_2/S_1)_{max}$ of approximately 0.30. If the shape of the distribution *g(z)* is known, as shown in Figure 4–11, the ratio $S_2/S_1$ can be determined by intersection points 1 and 3, and is approximately 0.15. Otherwise, when ratio $S_2/S_1$ is known, the distribution function *g(z)* can be determined by measured response ratios $R_1$ and $R_2$. Note that the minimum boundary condition occurs when $S_2/S_1$ is zero. If $R_1$ and $R_2$ are known and $S_2/S_1=0$, the distribution *g(z)* can be determined and provides the other limiting case. Furthermore, this case produces the maximum penetration depth of the contamination from the hot side of the panel. If $S_2/S_1$ is larger than zero, then the penetration depth of the contamination from the hot side will be smaller, and there will be some contamination on the cold side.

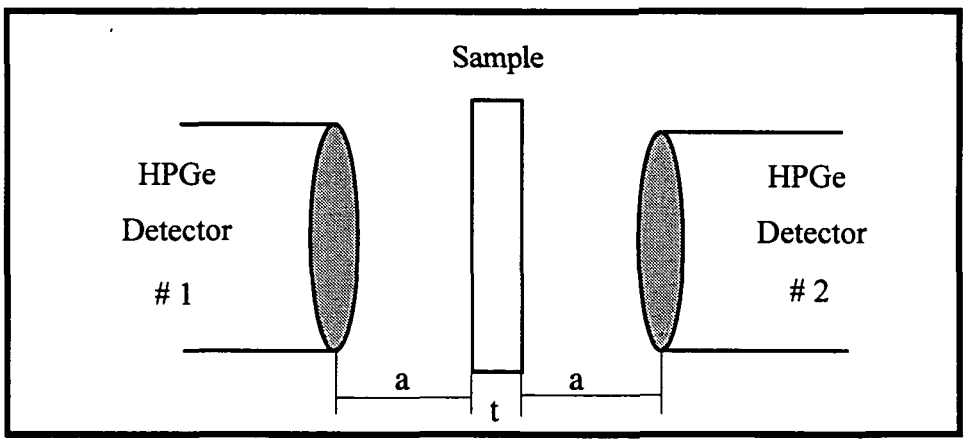


**Figure 4–9 Sample-detector geometry for transite panels contaminated on two sides**

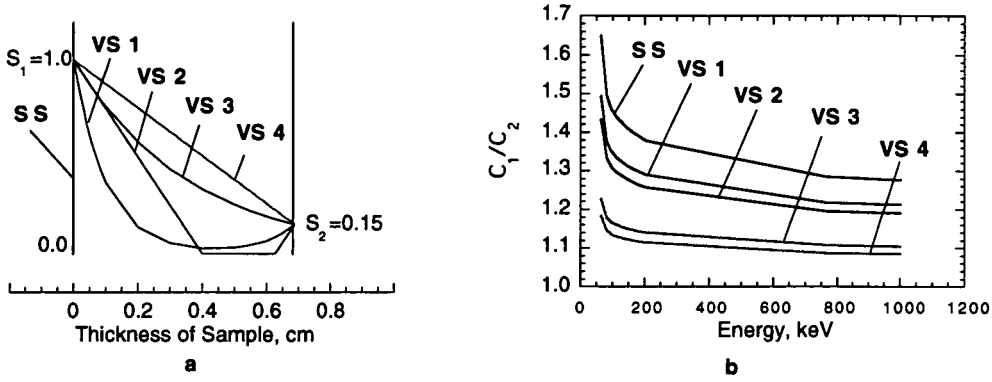


**Figure 4–10 a) Configuration of different contamination distributions in transite panels when $S_2/S_1$=0.15. b) Response ratios ($C_1/C_2$) for different contamination distributions shown in (a) when $S_2/S_1$=0.15. (SS means surface source, VS means volumetric source.)**

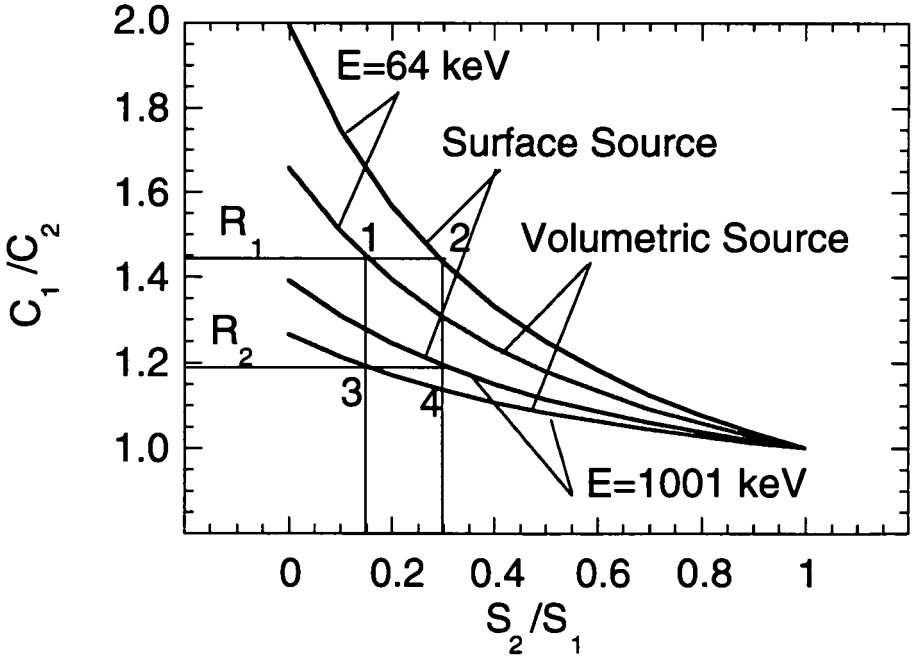


**Figure 4–11 Relationship of response ratio ($C_1/C_2$) and boundary condition ratio ($S_2/S_1$) (surface and volumetric sources for E=64 and 1001 keV).**

### 4.2.3 Technique Requirements

Implementing this technique requires both significant experimental response ratio data and the significant material and geometric input data for the simulation. Knowledge of the gamma-ray linear attenuation coefficient as function of energy and material is required to perform the computer simulations. As a result, the linear attenuation coefficient of transite was measured over the energy range of interest. These measurements were performed using a HPGe detector with standard gamma-ray sources (Cd-109, Am-241, and Eu-152) and multiple transite panels to provide variable thicknesses.

The accuracy of this technique increases with the number and energy range of detector response ratios used. As seen in Figs. 4–8b, 4–10b, and 4–11, the response ratio varies most significantly at low energies. Consequently, it is desirable to use as many response ratios as possible in the low energy region. Furthermore, choosing the gamma-ray energies for recording response ratios must be considered carefully. For the Fernald transite panels, it was first necessary to note that the contamination is primarily from uranium processing, thus the radionuclides on the transite panels are primarily U-235, U-238, and their daughters. Due to the relatively short period of time (short compared to uranium and uranium daughter half-lives) that the contamination has been on the transite panels (5-40 years), the number of gamma-ray energies to choose from is limited. More precisely, U-235 will likely be in equilibrium with daughter Th-231, but may not be in equilibrium with Pa-231 and its daughters; and U-238 will likely be in equilibrium with daughters Th-234 and Pa-234m, but may not be in equilibrium with U-234 and its daughters. These restrictions are due to the relatively long haft-lives of Pa-231 and U-234, respectively. Thus, gamma-ray energies were chosen only from those radionuclides which were believed to be in equilibrium with U-235 and U-238. Table 4–1 lists the resulting energies and radionuclides chosen for analysis of the Fernald transite panels.

To obtain the most accurate response ratios, a HPG detector is recommended. Although the technique calls for two detectors, only one HPGe detector is actually required. With one detector, an experimental arrangement similar to that shown in Figure 4–9 is achieved by turning the sample over and carefully controlling the geometric conditions. Furthermore, the high energy resolution of HPGe detector is necessary to ensure that all counts are associated with the correct full-energy gamma-ray peak.

**Table 4–1 Gamma-ray energies and associated radionuclides at which response ratio should be recorded for Fernald transite panels**

| Energy, keV | Radionuclide |
|---|---|
| 63.29 | Th-234 |
| 84.21 | Th-231 |
| 92.80 | Th-234 |
| 112.81 | Th-234 |
| 143.76 | U-235 |
| 163.35 | U-235 |
| 185.72 | U-235 |
| 205.31 | U-235 |
| 766.62 | Pa-234m |
| 1001.22 | Pa-234m |

## 4.3 METALS CHARACTERIZATION TECHNIQUES

Metals contamination of transite was measured indirectly by performing leach tests and directly by digestion of the transite surface layer. The following provides a description of the methods used. Results of the analyses are provided in Section 5.3

### 4.3.1 Leaching Procedure

Transite panels are identified as A, B, or C series, corresponding to Building 7 interior flat panels, Building 7 exterior corrugated panels and Building 2A interior flat panels, respectively. Building 7 interior panels (A series) were used for the initial metals analysis.

Samples are prepared by cutting transite panel A6 into approximately 4 in. by 4 in. squares. Panels were dry cut in a sealed glove box using a tile saw. Final dimensions of panel A6 samples are summarized in Table 4–2. The volume and surface area is calculated for each cut sample to determine the required amount of leachant.

The procedure developed for this study is similar to the ANS 16.1 leach test. To provide more aggressive leaching, without the destruction of the samples, the following changes were incorporated into the standard leach test: 1) the strength of the acetic acid leachant is increased from 0.04M to 0.4M and 2) the leachant was stirred continuously for all leach intervals.

## Table 4-2 Sample dimensions for transite panel A6

SAMPLE A6b

| LENGTH | mm | in | THICKNESS | mm | in |
|---|---|---|---|---|---|
| 1 | 103.09 | 4.059 | 1 | 6.14 | 0.242 |
| 2 | 99.99 | 3.937 | 2 | 6.68 | 0.273 |
| 3 | 103.32 | 4.068 | 3 | 6.13 | 0.240 |
| 4 | 99.88 | 3.932 | 4 | 5.84 | 0.231 |
| AVG(1&3) | 103.21 | 4.064 | AVERAGE | 6.20 | 0.247 |
| AVG(2&4) | 99.94 | 3.935 | | | |
| SURFACE AREA (cm ^ 2) | | | 231.46 | | |
| LEACHANT VOLUME REQ'D (mL) | | | 2315 | | |

SAMPLE A6c

| LENGTH | mm | in | THICKNESS | mm | in |
|---|---|---|---|---|---|
| 1 | 100.10 | 3.941 | 1 | 6.21 | 0.244 |
| 2 | 103.04 | 4.057 | 2 | 6.6 | 0.260 |
| 3 | 99.87 | 3.932 | 3 | 6.14 | 0.242 |
| 4 | 102.51 | 4.036 | 4 | 6.23 | 0.245 |
| AVG(1&3) | 99.99 | 3.937 | AVERAGE | 6.30 | 0.248 |
| AVG(2&4) | 102.78 | 4.047 | | | |
| SURFACE AREA (cm ^ 2) | | | 231.62 | | |
| LEACHANT VOLUME REQ'D (mL) | | | 2316 | | |

SAMPLE A6e

| LENGTH | mm | in | THICKNESS | mm | in |
|---|---|---|---|---|---|
| 1 | 95.42 | 3.757 | 1 | 5.35 | 0.211 |
| 2 | 100.05 | 3.939 | 2 | 5.57 | 0.219 |
| 3 | 95.17 | 3.747 | 3 | 5.46 | 0.215 |
| 4 | 99.97 | 3.936 | 4 | 5.33 | 0.210 |
| AVG(1&3) | 95.30 | 3.752 | AVERAGE | 5.43 | 0.214 |
| AVG(2&4) | 100.01 | 3.938 | | | |
| SURFACE AREA (cm ^ 2) | | | 211.81 | | |
| LEACHANT VOLUME REQ'D (mL) | | | 2118 | | |

SAMPLE A6f

| LENGTH | mm | in | THICKNESS | mm | in |
|---|---|---|---|---|---|
| 1 | 95.07 | 3.743 | 1 | 5.08 | 0.200 |
| 2 | 102.38 | 4.031 | 2 | 5.74 | 0.225 |
| 3 | 95.22 | 3.749 | 3 | 5.41 | 0.213 |
| 4 | 102.36 | 4.030 | 4 | 5.33 | 0.210 |
| AVG(1&3) | 95.15 | 3.746 | AVERAGE | 5.39 | 0.212 |
| AVG(2&4) | 102.37 | 4.031 | | | |
| SURFACE AREA (cm ^ 2) | | | 216.53 | | |
| LEACHANT VOLUME REQ'D (mL) | | | 2165 | | |

The leach vessels are constructed of unreactive polypropylene. To maximize the surface exposed to the leachant solution, samples were suspended on an inert stand.

At the end of each leaching interval the specimen is removed from the used leachant and placed into fresh leachant. The leachate is sampled and completely replaced after cumulative leach times of 2, 7, and 24 hours from initiation of the test. Subsequent leachate sampling and replacements are made at cumulative leach times of 48, 72 and 121 hours. Spent leachate is analyzed through inductively coupled plasma (ICP) spectroscopy. Prior to ICP analysis, the spent leachate is acid digested according to method SW-846:3050. ICP analysis is performed according to method SW-846:6010A.

### 4.3.2 Surface Digestion

Abraded material from the surface of transite panels was digested and analyzed for total extractable lead, uranium and barium content. Approximately 30 grams of dry, abraded transite material taken from the glove box was provided in a single 250 mL HDPE container from which all analytical samples were taken. The container was manually and randomly sampled to obtain 24 dry transite samples, labeled M1 through M24. Each sample consisted of approximately one-half (0.5 +/-) grams of dry transite material.

Transite samples were placed in separate 100 mL PFA-lined pressure vessels to which 10 mL of trace-metal grade nitric acid was added for digestion. Sample digestion was carried out in a Questron Q 45 EnviroPrep microwave digester. The sample digestion procedure followed USEPA SW-846, Method 3051 "Microwave Assisted Acid Digestion of Sediments, Sludges, Soils and Oils".

Once digestion was completed samples were analyzed for total extractable lead, uranium and barium content using a Perkin-Elmer Optima 3000 Inductively Coupled Plasma - Atomic Emission Spectrometer. The preparation, calibration and measurement of each analyte followed USEPA SW-846, Method 6010A "Inductively Coupled Plasma-Atomic Emission Spectroscopy". Calibration was carried out using a stock 10000 microgram/liter multi-element standard produced by SPEX Chemical Division of Metuchen, NJ. Three replicate readings were carried out for each analyte of each sample. The measured concentrations presented, based on 100 mL volume, are the arithmetic average of the three replicate readings for each analyte. These concentrations were then converted to analyte concentrations as milligram of analyte per kilogram of dry transite solids.

# 5.0 RESULTS

## 5.1 RADIOLOGICAL CHARACTERIZATION RESULTS BASED ON DESTRUCTIVE TECHNIQUES

Quantitative measurements with the Geiger-Mueller (G-M) detector allow the determination of a contamination penetration distribution. This method also has a lower threshold of detection than the qualitative techniques of UV photography and autoradiography. Below approximately 300 to 500 cpm on the G-M detector no contamination was visible under UV excitation nor after a 48 hour autoradiography exposure. It is possible that with a much longer exposure time, the autoradiography could theoretically match or better this threshold, but would be impractical for most applications.

Prior to performing any destructive analysis, the original uncut 10"x10" panels were surveyed with portable $\beta - \gamma$ and $\alpha$ detectors in each quadrant of both sides in order to determine an initial external contamination level. Figure 5–1 is a sample of this data. The remainder of this initial survey data is presented in Appendix B.

Table 5–1 is a sample of the β-γ count rate data collected using a G-M detector during the destructive layer removal, Figure 5–2 illustrates these results. Data for all other samples analyzed using this technique are presented in Appendix C. Figures 5–3 through 5–6 illustrate the qualitative results collected using UV photography and autoradiography after each layer removal.

## 5.2 RADIOLOGICAL CHARACTERIZATION RESULTS BASED ON NON-DESTRUCTIVE TECHNIQUE

### 5.2.1 Linear Attenuation Coefficient of Transite

The measurements of transite attenuation coefficients were performed by using HPGe detector with clean transite samples and three standard radiation sources. The major consideration in choosing the standard radiation sources is ensuring that the range of gamma-ray energies should cover the expected range of full-energy peaks for the transite sample. The measured linear attenuation coefficients of transite are listed in Table 5–2 and are shown in Figure 5–7.

**Samples from interior of Plant 7**

**Sample A-1**

Measurement Date: 10/21/94

| A-1 | |
|---|---|
| β–γ 100 cpm<br>α 10 cpm | β–γ 100 cpm<br>α 5 cpm |
| β–γ 110 cpm<br>α 10 cpm | β–γ 110 cpm<br>α 10 cpm |

Side 1* – Painted

| A-1 | |
|---|---|
| β–γ 90 cpm<br>α 0 cpm | β–γ 90 cpm<br>α 0 cpm |
| β–γ 80 cpm<br>α 0 cpm | β–γ 90 cpm<br>α 0 cpm |

Side 2 – Painted

| Background Activity | |
|---|---|
| β–γ | 50 cpm |
| α | 0 cpm |

**Figure 5–1 Example of initial survey data**

**Table 5–1 Example of layer removal results based on geiger-mueller detector β-γ measurements**

original thickness: 0.257 inches

*Sample C5a - side1*

| Total Thickness Removed (inches) | Activity (cpm) |
|---|---|
| 0 | 19000 |
| 0.022 | 1200 |
| 0.032 | 500 |
| 0.046 | 100 |
| 0.057 | 80 |
| 0.074 | 50 (background) |

*Sample C5a - side2*

| Total Thickness Removed (inches) | Activity (cpm) |
|---|---|
| 0 | 3500 |
| 0.008 | 700 |
| 0.029 | 300 |
| 0.049 | 100 |
| 0.058 | 50 (background) |

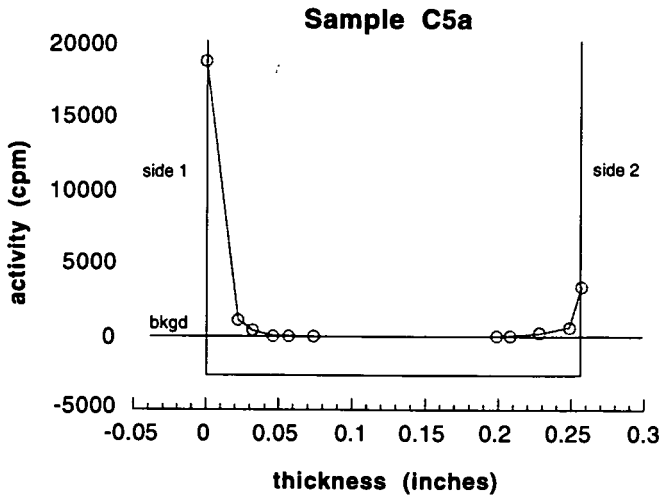


**Figure 5–2 Example of contamination penetration distribution for sample C5a**

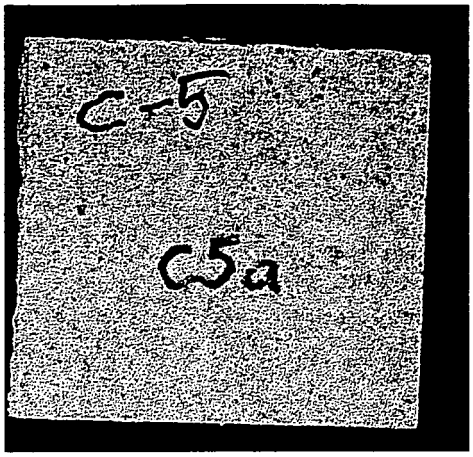


(a)

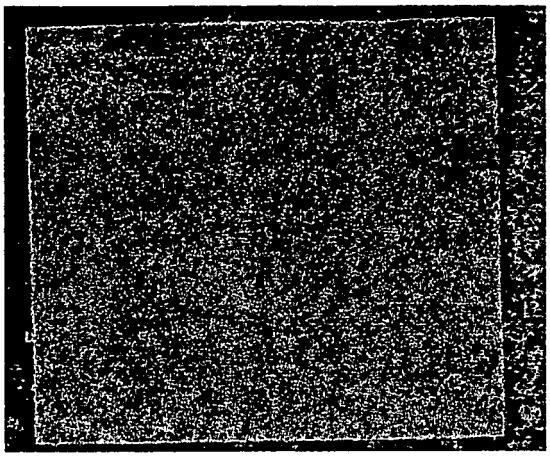

(b)

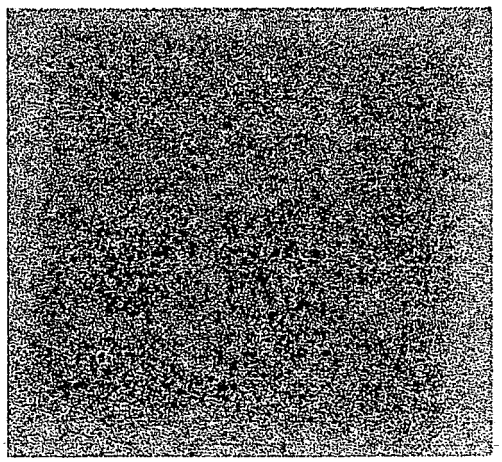

(c)

Fig. 5–3: Sample C5a prior to destructive analysis photographed under a) ambient light and b) UV light and c) after a 24 hour autoradiographic exposure.

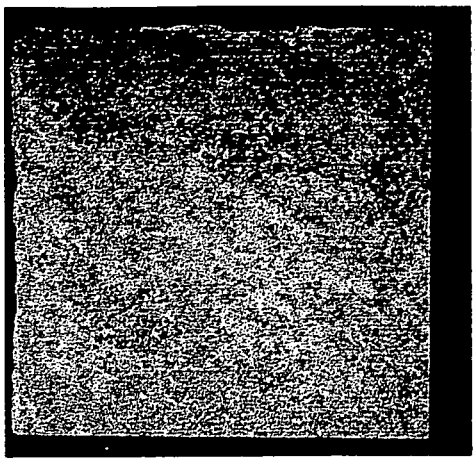

(a)

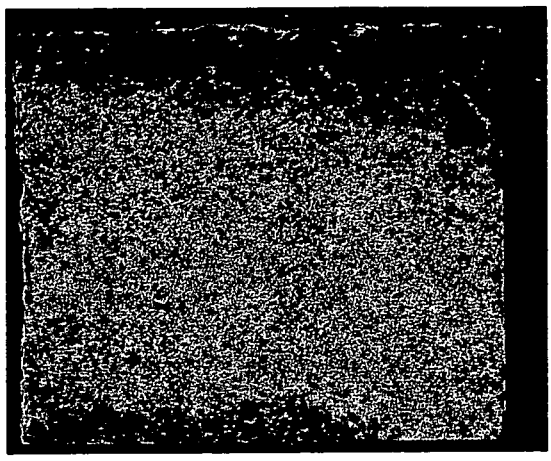

(b)

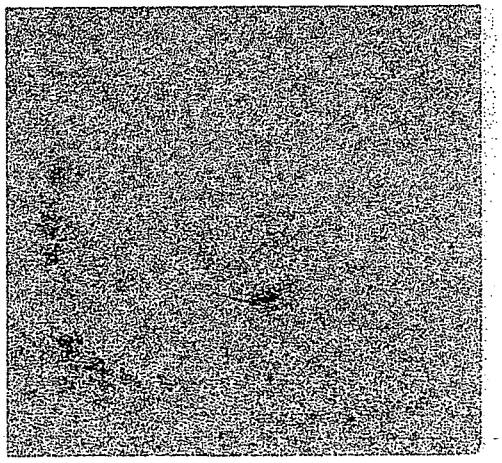

(c)

Fig. 5–4: Sample C5a after one layer removal, photographed under a) ambient light and b) UV light and c) after a 24 hour autoradiographic exposure.

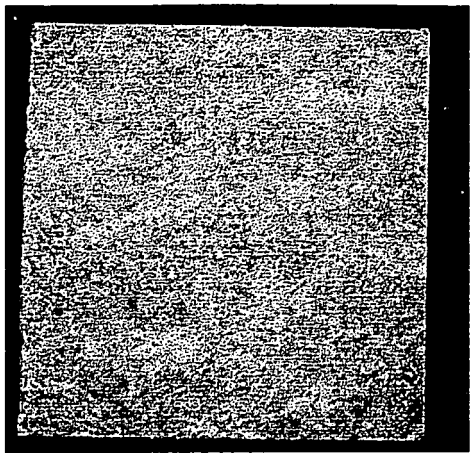

(a)

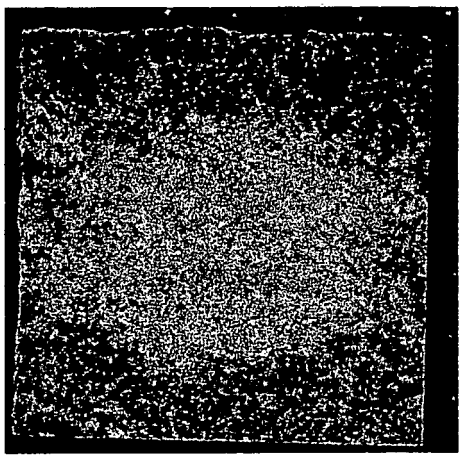

(b)

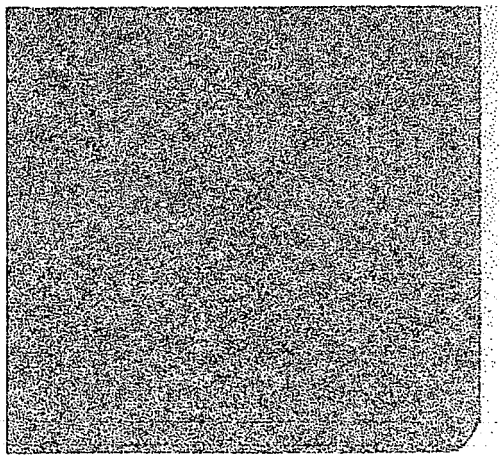

(c)

Fig. 5–5: Sample C5a after two layer removals, photographed under a) ambient light and b) UV light and c) after a 48 hour autoradiographic exposure.

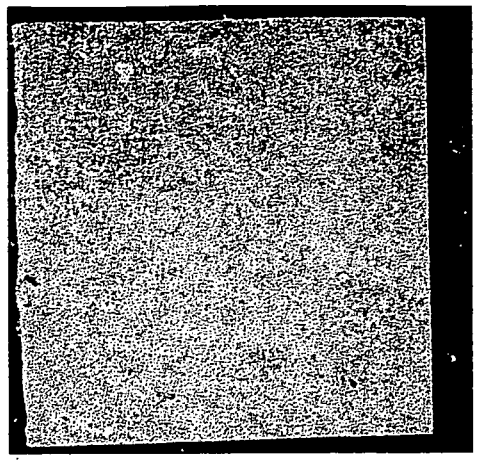

(a)

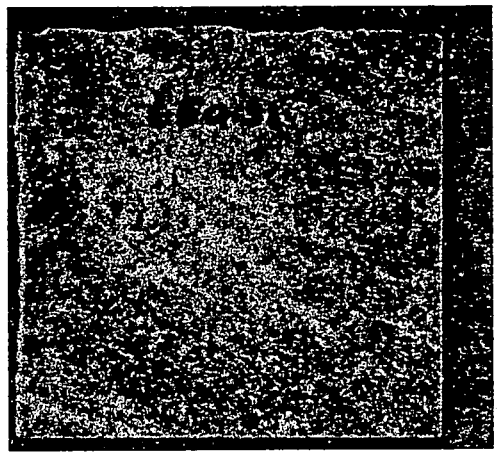

(b)

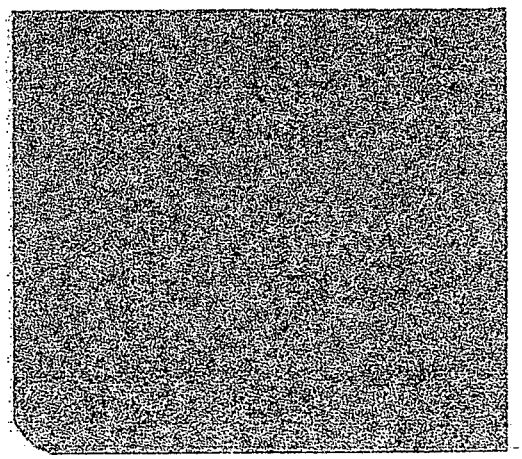

(c)

Fig. 5–6: Sample C5a after three layer removals, photographed under a) ambient light and b) UV light and c) after a 48 hour autoradiographic exposure.

**Table 5–2 Linear attenuation coefficients of transite**

| Gamma-ray Energy (keV) | Linear Atten. Coeff. ($cm^{-1}$) | Standard Deviation(σ) | Standard Source |
|---|---|---|---|
| 59.53 | 0.62711 | 0.035 | Am-241 |
| 88.05 | 0.37256 | 0.021 | Cd-109 |
| 121.63 | 0.30455 | 0.010 | Eu-152 |
| 244.63 | 0.22768 | 0.024 | Eu-152 |
| 344.06 | 0.20117 | 0.011 | Eu-152 |
| 410.88 | 0.19682 | 0.056 | Eu-152 |
| 443.75 | 0.19992 | 0.046 | Eu-152 |
| 778.66 | 0.13177 | 0.023 | Eu-152 |
| 867.81 | 0.14106 | 0.039 | Eu-152 |
| 963.81 | 0.12041 | 0.030 | Eu-152 |
| 1085.58 | 0.13128 | 0.034 | Eu-152 |
| 1111.80 | 0.12282 | 0.0264 | Eu-152 |
| 1407.7 | 0.09764 | 0.020 | Eu-152 |

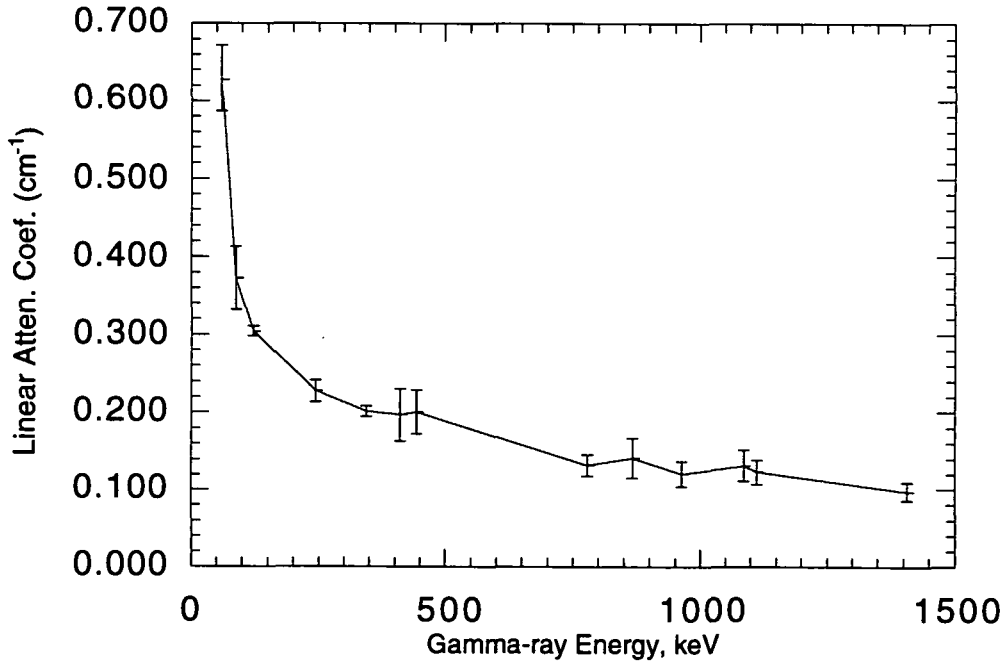


**Figure 5-7 Linear attenuation coefficients of transite**

### 5.2.2 Technique Validation

To simulate the contamination of Fernald transite panels, the complementary error function equation (4–18) (the diffusion transport solution for the constant contamination case) can typically be assumed. While some of the Fernald transite was almost continuously exposed to contaminants, most of the transite was exposed more discretely. However, these discrete (or instantaneous) exposures were repeated frequently enough over time to approximate a continuous exposure. This assumption of continuous exposure is certainly not rigorous, but is likely a good approximation. Based on equation (4–18), considering contamination on both sides of a sample, and normalizing the contamination level on the hot side to unity, the predicted contamination distribution can be expressed as:

$$g(z) = erfc(\lambda_1 z) + R_B\, erfc(\lambda_2 (t - z)) \quad , \qquad (5\text{–}1)$$

where $\lambda_1$ and $\lambda_2$ are the lumped effective diffusion coefficient and diffusion exposure time for side 1 and 2, respectively, $R_B$ is the boundary condition ratio, $t$ is the thickness of transite panel, and $z$ is the distance from the hot surface. Based on the experimental data the simulation performs a $\chi^2$ minimization[6] with $\lambda_1$, $\lambda_2$, and $R_B$ as fit parameters to determine the most probable contamination distribution.

As mentioned previously, the choice of an appropriate model is essential to accurately predicting the actual contamination distribution. This choice should be achieved by using physically valid assumptions in terms of analyzing the actual conditions under which the sample was contaminated. For Fernald transite, the diffusion transport theory can be used as a reasonable assumption. In other cases, the choice of models might differ.

To demonstrate the ability of this technique, a series of Fernald transite samples were used in the measurement geometry shown in Figure 4-9. For one such sample, C5a, the measured boundary condition ratio was $S_2/S_1 = 0.184 \pm 0.0535$ (as measured using a Geiger-Mueller detector). The measured response ratios are listed in Table 5–3 and Table 5–4, and shown in Figure 5–8 for two different spacings $a$=4.0 cm and $a$=7.1 cm, respectively. Note the sensitivity of the technique to small changes in the sample-detector geometry as indicated by the two different spacings. This sensitivity allows the computer program to accurately predict the contamination distribution based on the measured response ratios. In order to use the measured response ratio data to generate a contamination distribution using the computer simulation program, it was assumed that the distribution in the transite sample was represented by equation (5–1). With these conditions and assumptions, the computationally predicted contamination distributionfor $a$=4.0

cm spacing is $g(z) = erfc(22z) + 0.195\ erfc(22(t-z))$ and produces response ratios similar to the measured data, as shown in Figure 5–9. These gamma-ray spectroscopy technique results were verified using the destructive G-M detector technique results in order to establish the actual or true contamination distribution for sample C5a. The measured layer removal results are shown and compared to the best fit distribution of $g(z)= erfc(22z) + 0.195erfc(22(t-z))$ in Figure 5-10. The results for all other samples analyzed using this gamma-ray spectroscopy technique, along with the comparison to the G-M detector results, are presented in Appendix D.

Note, one fundamental assumption made in order to implement this technique is that the contamination distribution is uniform in the *x-y* plane throughout the sample. Actually, the Fernald transite samples were nonuniformly contaminated with randomly distributed contamination (as indicated by autoradiography) on the surfaces of both sides. Nevertheless, the computer-generated distribution accurately predicts the contamination distribution as measured using the destructive technique. These results imply that the technique is insensitive to the assumption of a uniform distribution in the *x-y* plane. Therefore, the proposed technique is not limited by the uniform contamination exposure case.

**Table 5–3 Measured response ratios ($C_1/C_2$) for C5a ($a$=4.0 cm)**

| Energy, keV | $C_1$ | $C_2$ | Ratio($C_1/C_2$) | $\sigma$ |
|---|---|---|---|---|
| 63.91 | 42226 | 28435 | 1.4805 | 0.01417 |
| 84.60 | 17157 | 12497 | 1.3794 | 0.03042 |
| 93.11 | 209302 | 155066 | 1.3498 | 0.0035279 |
| 113.24 | 8886 | 6661 | 1.3340 | 0.04905 |
| 144.09 | 36945 | 28331 | 1.3040 | 0.01321 |
| 163.56 | 15722 | 12051 | 1.3046 | 0.02270 |
| 185.54 | 188186 | 145789 | 1.2908 | 0.004821 |
| 205.35 | 14697 | 11403 | 1.2889 | 0.02118 |
| 765.35 | 5841 | 4765 | 1.2258 | 0.03452 |
| 1001.00 | 15564 | 12795 | 1.2164 | 0.01578 |

Where, $C_1$ is the net photopeak area for detector 1;
$C_2$ is the net photopeak area for detector 2.

**Table 5–4 Measured response ratios ($C_1/C_2$) for C5a ($a$=7.1 cm)**

| Energy, keV | $C_1$ | $C_2$ | Ratio($C_1/C_2$) | σ |
|---|---|---|---|---|
| 63.91 | 41539 | 29618 | 1.4025 | 0.01340 |
| 84.60 | 17467 | 13175 | 1.3258 | 0.02953 |
| 93.11 | 209305 | 159248 | 1.3143 | 0.00508 |
| 113.24 | 9637 | 7575 | 1.2722 | 0.03651 |
| 144.09 | 37653 | 30367 | 1.2399 | 0.01335 |
| 163.56 | 16626 | 13476 | 1.2337 | 0.02331 |
| 185.54 | 188966 | 152397 | 1.2399 | 0.00463 |
| 205.35 | 15126 | 12327 | 1.2271 | 0.02529 |
| 765.35 | 9157 | 7907 | 1.1581 | 0.02389 |
| 1001.00 | 15826 | 13740 | 1.1518 | 0.01452 |

Where, $C_1$ is the net photopeak area for detector 1;
$C_2$ is the net photopeak area for detector 2;

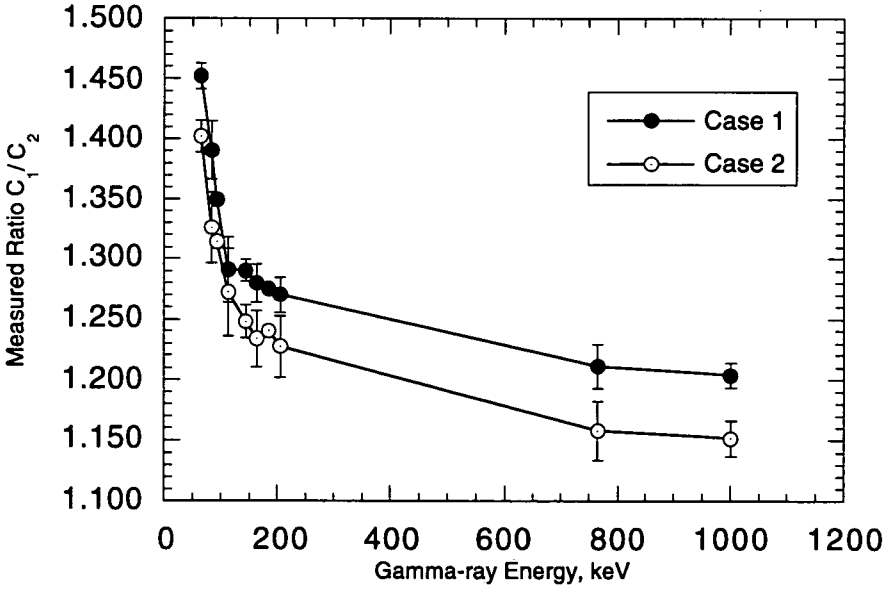


**Figure 5–8 Gamma-ray spectroscopy technique measured response ratios as a function of $\gamma$–ray energy for Case 1 ($a$=4.0 cm) and Case 2 ($a$=7.1 cm) for Sample C5a.**

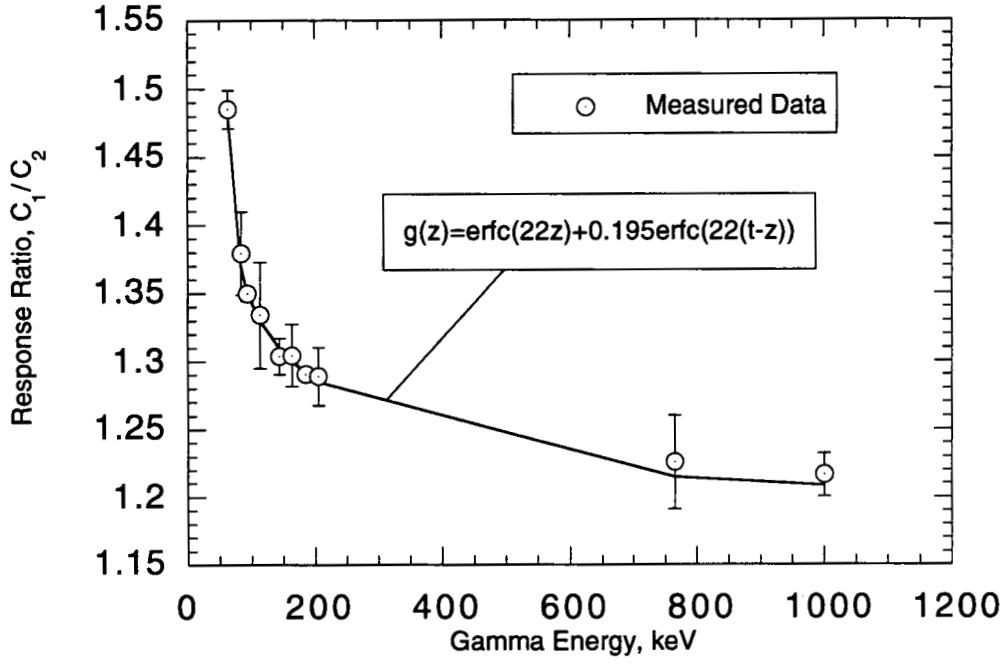


**Figure 5–9 Comparison of gamma-ray spectroscopy technique measured response ratios and the computed response ratios for Case 1 (*a*=4.0 cm) for Sample C5a.**

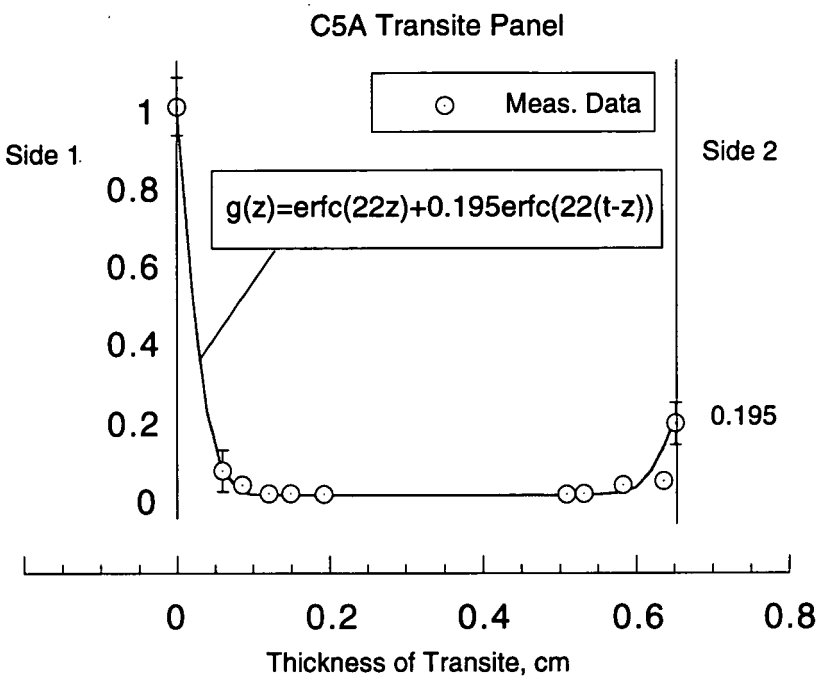


**Figure 5–10 Comparison of destructive G-M detector technique measured contamination distribution and the distribution predicted by the gamma-ray spectroscopy technique for transite sample C5a.**

## 5.3 METALS CHARACTERIZATION RESULTS

### 5.3.1 Metals Characterization Results - Leach Testing

Figures 5.11 through 5.14 depict results from the static leach tests on A6 transite samples. The principal contaminant of concern is lead; barium, chromium and uranium are also quantified. Results from the ICP metal analyses are listed in Tables 5.5 through 5.8.

Lead, chromium and uranium results indicate a peak release of contaminants following the 24 and 48 hour leach intervals. Subsequent leach intervals show decreased amounts of contaminants released. Barium results indicate a peak release after the first leach interval and decreased releases for each interval thereafter. Variations among samples A6b, A6c, A6e and A6f are considered minimal. Following 121 hours of leaching, the maximum cumulative amounts of lead, barium, chromium and uranium are 0.67 ppm, 0.35 ppm, 0.19 ppm and 1.92 ppm, respectively.

### 5.3.2 Metals Characterization Results - Surface Digestion

A total metals analysis was performed to determine the total amount of contamination in the surface layer of the transite. Lead was the principal contaminant of concern. Barium and uranium analyses were also performed.

Results of the digestion of surface transite are provided in Table 5.9. These results represent total surface extractable metals.

While these numbers for lead contamination seem large it is important to note that very little of this lead appears leachable (see Section 5.3.1). To produce these results, contaminated surface material was sanded off of the transite samples then digested in concentrated nitric acid at 200° C and 200 psi. Also, the final concentration (calculated) is based on the surface abraded material and not the complete sample.

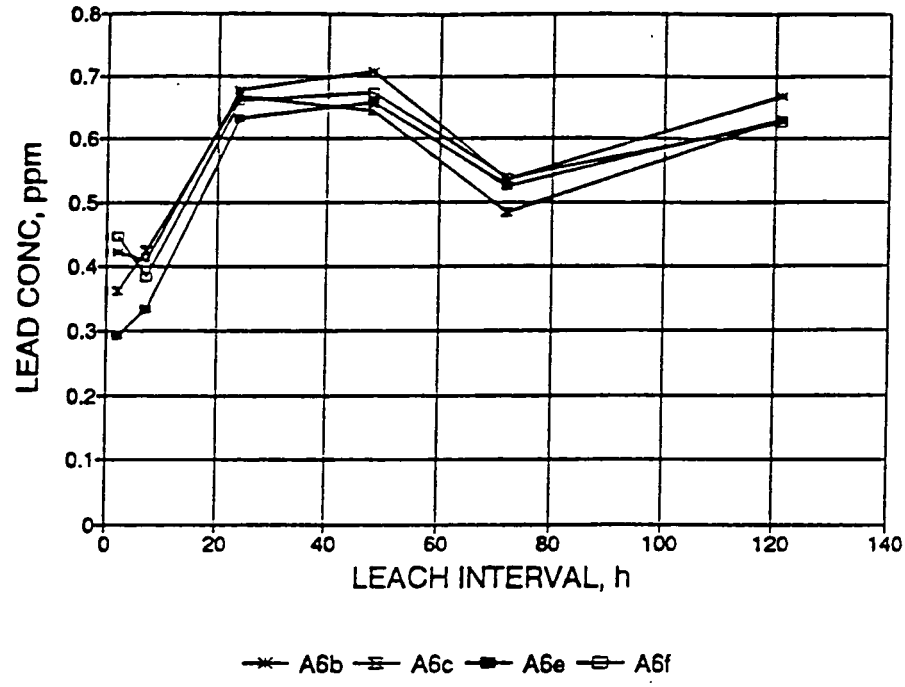


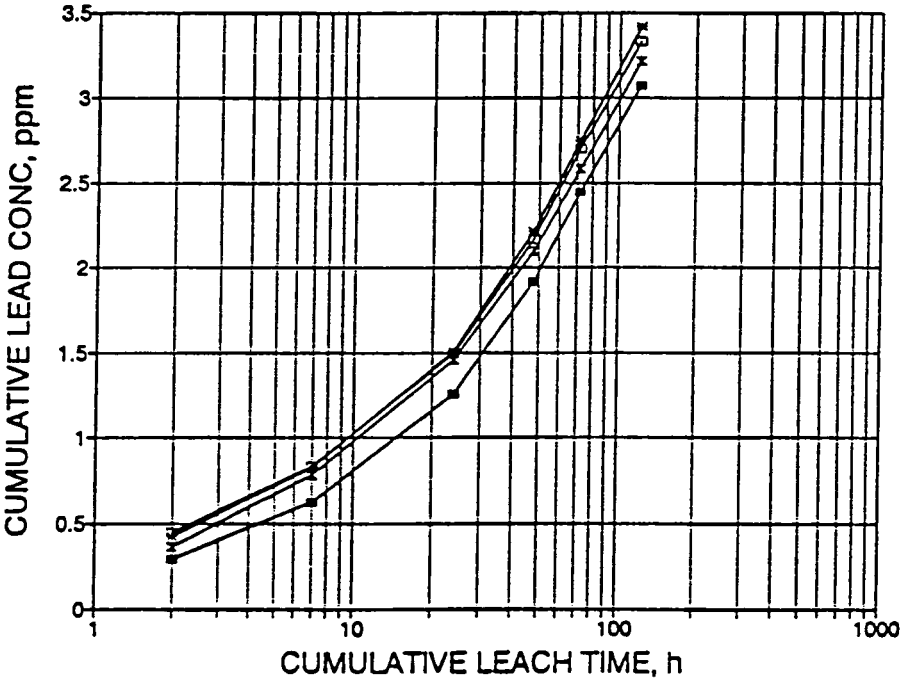


**Figure 5-11 Leached lead from A6 transite samples**

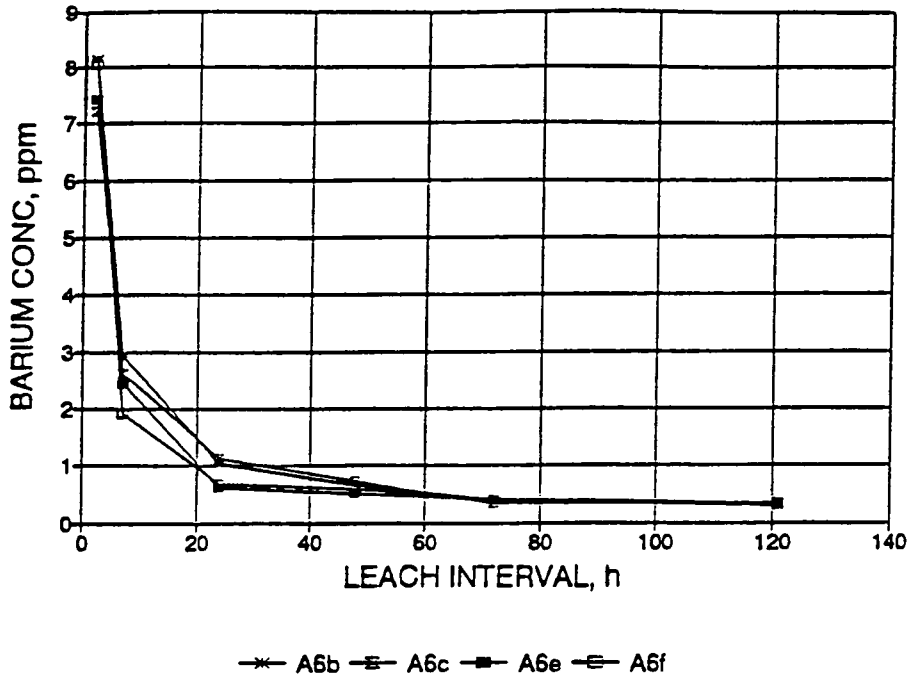


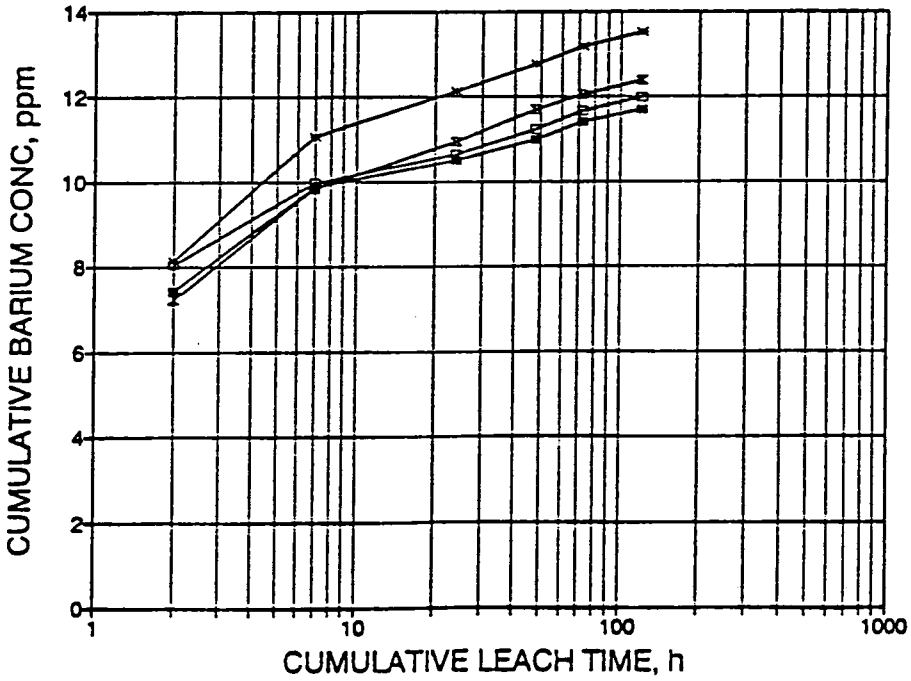


**Figure 5-12 Leached barium from A6 transite samples**

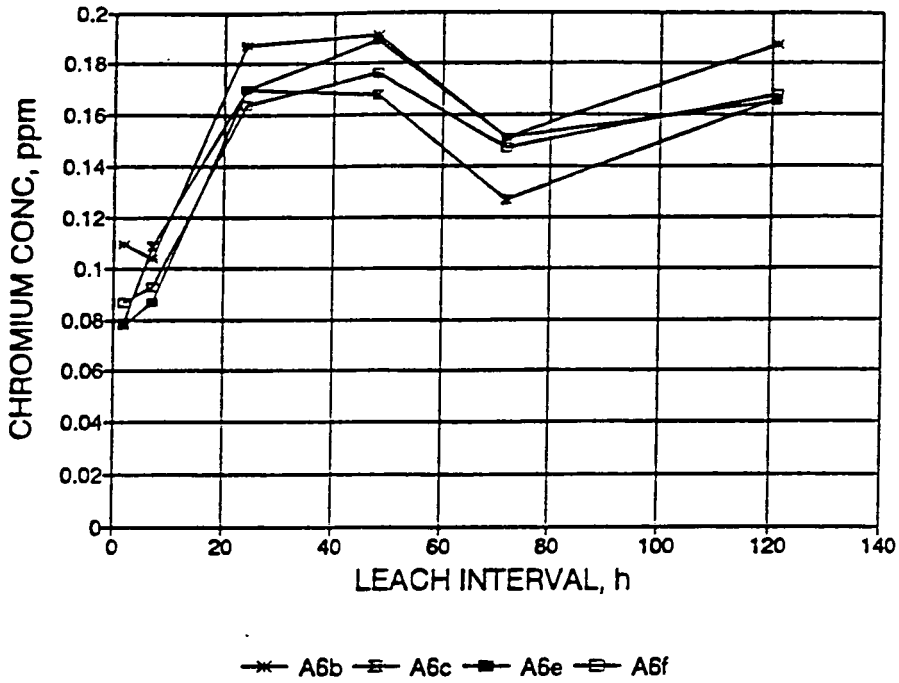


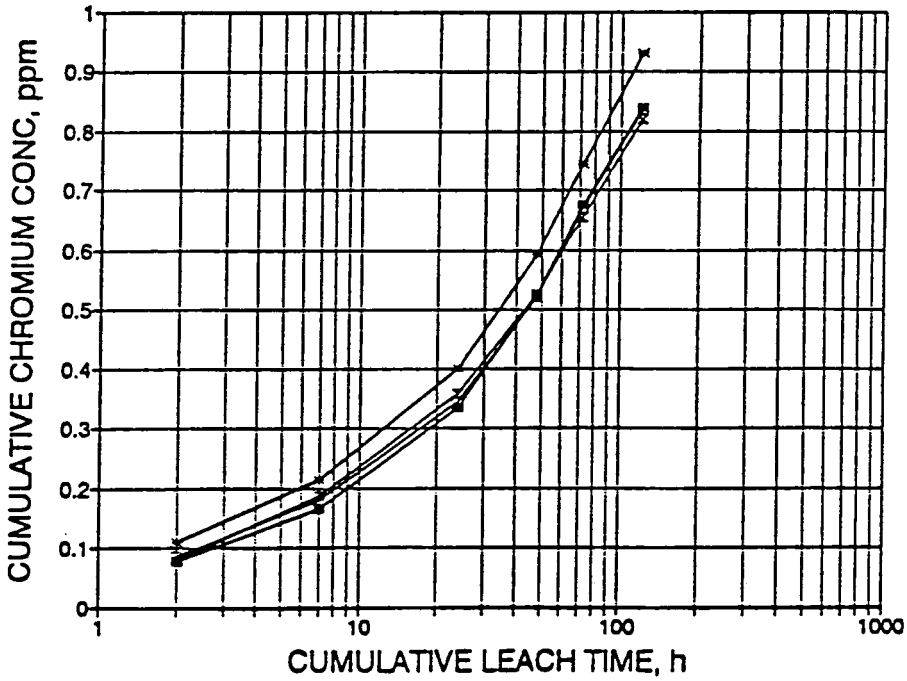


**Figure 5-13 Leached chromium from A6 transite samples**

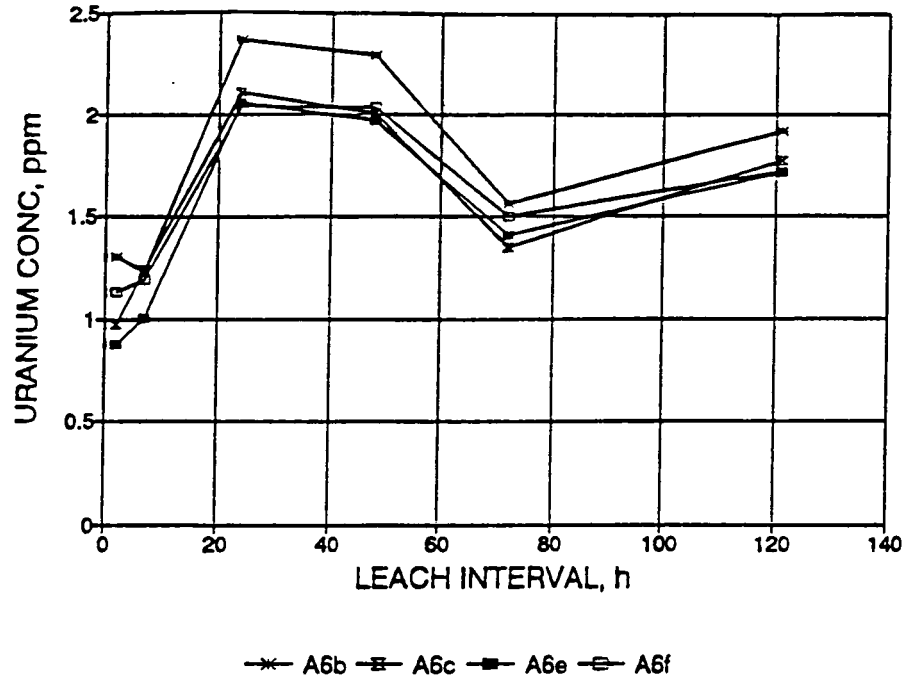


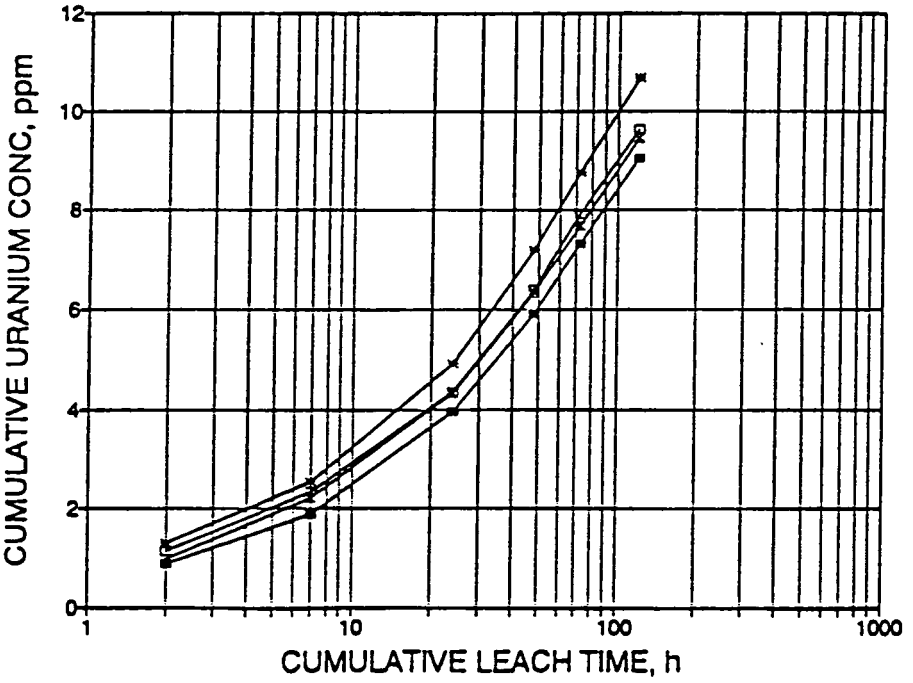


**Figure 5-14 Leached uranium from A6 transite samples**

Table 5-5A Lead conc, ppm

| TIME, h | SAMPLE | | | | | | | | | |
|---|---|---|---|---|---|---|---|---|---|---|
| | A6b | SD | A6c | SD | A6e | SD | A6f | SD | CONTROL | SD |
| 2 | 0.422 | 0.0065 | 0.362 | 0.012 | 0.293 | 0.0064 | 0.448 | 0.004 | 0.009 | 0.009 |
| 7 | 0.409 | 0.0082 | 0.425 | 0.0173 | 0.334 | 0.007 | 0.385 | 0.0038 | 0.023 | 0.0065 |
| 24 | 0.677 | 0.0086 | 0.669 | 0.0084 | 0.632 | 0.0105 | 0.660 | 0.0107 | 0.008 | 0.0108 |
| 48 | 0.708 | 0.0106 | 0.644 | 0.0067 | 0.659 | 0.0087 | 0.674 | 0.0028 | 0.016 | 0.0033 |
| 72 | 0.535 | 0.0077 | 0.484 | 0.0065 | 0.525 | 0.0097 | 0.537 | 0.0061 | 0.022 | 0.0048 |
| 121 | 0.668 | 0.0043 | 0.630 | 0.0067 | 0.631 | 0.0063 | 0.625 | 0.0064 | 0.013 | 0.0109 |

Table 5-5B Cumulative lead conc. ppm

| TIME, h | SAMPLE | | | |
|---|---|---|---|---|
| | A6b | A6c | A6e | A6f |
| 2 | 0.422 | 0.362 | 0.293 | 0.448 |
| 7 | 0.831 | 0.787 | 0.627 | 0.833 |
| 24 | 1.508 | 1.456 | 1.259 | 1.493 |
| 48 | 2.216 | 2.1 | 1.918 | 2.167 |
| 72 | 2.751 | 2.584 | 2.443 | 2.704 |
| 121 | 3.419 | 3.214 | 3.074 | 3.329 |

Table 5-6A Barium conc. ppm

| TIME, h | SAMPLE | | | | | | | | | |
|---|---|---|---|---|---|---|---|---|---|---|
| | A6b | SD | A6c | SD | A6e | SD | A6f | SD | CONTROL | SD |
| 2 | 8.153 | 0.0287 | 7.218 | 0.0164 | 7.433 | 0.021 | 8.047 | 0.0376 | 0.007 | 0.000 |
| 7 | 2.913 | 0.0069 | 2.611 | 0.0067 | 2.442 | 0.0144 | 1.916 | 0.0052 | 0.032 | 0.0001 |
| 24 | 1.044 | 0.0007 | 1.124 | 0.0097 | 0.621 | 0.001 | 0.682 | 0.0044 | 0.032 | 0.0022 |
| 48 | 0.666 | 0.0183 | 0.743 | 0.0112 | 0.499 | 0.0039 | 0.597 | 0.0051 | 0.028 | 0.0001 |
| 72 | 0.394 | 0.0019 | 0.347 | 0.004 | 0.399 | 0.0026 | 0.417 | 0.0035 | 0.032 | 0.0001 |
| 121 | 0.349 | 0.0028 | 0.342 | 0.0036 | 0.299 | 0.0016 | 0.320 | 0.0019 | 0.029 | 0.0003 |

Table 5-6B Cumulative barium conc, ppm

| TIME, h | SAMPLE | | | |
|---|---|---|---|---|
| | A6b | A6c | A6e | A6f |
| 2 | 8.153 | 7.218 | 7.433 | 8.047 |
| 7 | 11.066 | 9.829 | 9.875 | 9.963 |
| 24 | 12.11 | 10.953 | 10.496 | 10.645 |
| 48 | 12.776 | 11.696 | 10.995 | 11.242 |
| 72 | 13.17 | 12.043 | 11.394 | 11.659 |
| 121 | 13.519 | 12.385 | 11.693 | 11.979 |

Table 5-7A Chromium conc. ppm

| TIME, h | SAMPLE | | | | | | | | | |
|---|---|---|---|---|---|---|---|---|---|---|
| | A6b | SD | A6c | SD | A6e | SD | A6f | SD | CONTROL | SD |
| 2 | 0.11 | 0.0026 | 0.079 | 0.0025 | 0.078 | 0.0035 | 0.087 | 0.0017 | 0.011 | 0.0042 |
| 7 | 0.104 | 0.0013 | 0.109 | 0.0017 | 0.087 | 0.0009 | 0.093 | 0.0028 | 0.022 | 0.0018 |
| 24 | 0.187 | 0.0018 | 0.170 | 0.004 | 0.17 | 0.0042 | 0.164 | 0.0041 | 0.012 | 0.0028 |
| 48 | 0.191 | 0.0045 | 0.168 | 0.0031 | 0.189 | 0.0022 | 0.176 | 0.0006 | 0.016 | 0.0044 |
| 72 | 0.151 | 0.0032 | 0.127 | 0.002 | 0.151 | 0.0065 | 0.147 | 0.0007 | 0.014 | 0.0015 |
| 121 | 0.187 | 0.0032 | 0.166 | 0.0078 | 0.165 | 0.0047 | 0.168 | 0.0007 | 0.015 | 0.0008 |

Table 5-7 B Cumulative chromium conc. ppm

| TIME, h | SAMPLE | | | |
|---|---|---|---|---|
| | A6b | A6c | A6e | A6f |
| 2 | 0.11 | 0.079 | 0.078 | 0.087 |
| 7 | 0.214 | 0.188 | 0.165 | 0.18 |
| 24 | 0.401 | 0.358 | 0.335 | 0.344 |
| 48 | 0.592 | 0.526 | 0.524 | 0.52 |
| 72 | 0.743 | 0.653 | 0.675 | 0.667 |
| 121 | 0.93 | 0.819 | 0.84 | 0.835 |

Table 5-8A Uranium conc. ppm

| TIME, h | SAMPLE | | | | | | | | | |
|---|---|---|---|---|---|---|---|---|---|---|
| | A6b | SD | A6c | SD | A6e | SD | A6f | SD | CONTROL | SD |
| 2 | 1.306 | 0.002 | 0.976 | 0.0037 | 0.877 | 0.0139 | 1.133 | 0.0057 | -0.009 | 0.007 |
| 7 | 1.235 | 0.0093 | 1.238 | 0.0132 | 1.004 | 0.0064 | 1.190 | 0.0089 | -0.145 | 0.0063 |
| 24 | 2.365 | 0.0303 | 2.106 | 0.0091 | 2.058 | 0.0317 | 2.041 | 0.0162 | -0.138 | 0.003 |
| 48 | 2.289 | 0.0314 | 2.002 | 0.0323 | 1.971 | 0.0188 | 2.036 | 0.0209 | -0.131 | 0.0048 |
| 72 | 1.562 | 0.0128 | 1.349 | 0.0075 | 1.41 | 0.0064 | 1.503 | 0.0024 | -0.094 | 0.0008 |
| 121 | 1.918 | 0.0084 | 1.772 | 0.006 | 1.713 | 0.0114 | 1.720 | 0.0015 | -0.115 | 0.0045 |

Table 5-8B Cumulative uranium conc. ppm

| TIME, h | SAMPLE | | | |
|---|---|---|---|---|
| | A6b | A6c | A6e | A6f |
| 2 | 1.306 | 0.976 | 0.877 | 1.133 |
| 7 | 2.541 | 2.214 | 1.881 | 2.323 |
| 24 | 4.906 | 4.32 | 3.939 | 4.364 |
| 48 | 7.195 | 6.322 | 5.91 | 6.4 |
| 72 | 8.757 | 7.671 | 7.32 | 7.903 |
| 121 | 10.675 | 9.443 | 9.033 | 9.623 |

Table 5-9 Transite sample analysis
19 September 1995

Digestion: Method 3051 USEPA SW-846
Analysis: Method 6010A USEPA SW-846

| Sample ID | Vessel # | Transite dry weight (grams) | final sample volume (mL) | average measured Pb conc. [ug/L] | average measured U conc. [ug/L] | average measured Ba conc. [ug/L] | replicates | final Pb concentration (calculated) [mg/kg solids] | final U concentration (calculated) [mg/kg solids] | final Ba concentration (calculated) [mg/kg solids] |
|---|---|---|---|---|---|---|---|---|---|---|
| M1 | 1 | 0.55 | 100.0 | 2112.1 | 32989.3 | 827.4 | 3 | 384.0 | 5998.1 | 150.4 |
| M2 | 2 | 0.52 | 100.0 | 2402.3 | 38279.8 | 1002.8 | 3 | 462.0 | 7361.5 | 192.8 |
| M3 | 3 | 0.52 | 100.0 | 2332.4 | 38094.9 | 920.4 | 3 | 448.5 | 7325.9 | 177.0 |
| M4 | 4 | 0.54 | 100.0 | 2370.4 | 38313.9 | 879.8 | 3 | 439.0 | 7095.2 | 162.9 |
| M5 | 5 | 0.53 | 100.0 | 2373.5 | 38973.1 | 917.5 | 3 | 447.8 | 7353.4 | 173.1 |
| M6 | 6 | 0.55 | 100.0 | 2467.2 | 40032.9 | 950.6 | 3 | 448.6 | 7278.7 | 172.8 |
| M7 | 7 | 0.53 | 100.0 | 2078.3 | 32848.1 | 778.7 | 3 | 392.1 | 6197.8 | 146.9 |
| M8 | 8 | 0.51 | 100.0 | 2222.2 | 38088.1 | 851.4 | 3 | 435.7 | 7468.3 | 166.9 |
| M9 | 9 | 0.51 | 100.0 | 2349.2 | 38062.0 | 844.4 | 3 | 460.6 | 7463.1 | 165.6 |
| M10 | 10 | 0.53 | 100.0 | 2227.1 | 35534.7 | 822.8 | 3 | 420.2 | 6704.7 | 155.2 |
| M11 | 11 | 0.54 | 100.0 | 2317.5 | 37766.1 | 875.5 | 3 | 429.2 | 6993.7 | 162.1 |
| M12 | 12 | 0.51 | 100.0 | 2161.4 | 35595.3 | 882.9 | 3 | 423.8 | 6979.5 | 173.1 |
| M13 | 1 | 0.58 | 100.0 | 2673.7 | 43831.6 | 1023.9 | 3 | 461.0 | 7557.2 | 176.5 |
| M14 | 2 | 0.52 | 100.0 | 2143.2 | 34667.5 | 873.2 | 3 | 412.2 | 6666.8 | 167.9 |
| M15 | 3 | 0.52 | 100.0 | 2271.1 | 36122.8 | 918.7 | 3 | 436.8 | 6946.7 | 176.7 |
| M16 | 4 | 0.56 | 100.0 | 2233.1 | 35934.5 | 916.1 | 3 | 398.8 | 6416.9 | 163.6 |
| M17 | 5 | 0.54 | 100.0 | 1959.6 | 31148.6 | 806.0 | 3 | 362.9 | 5768.3 | 149.3 |
| M18 | 6 | 0.52 | 100.0 | 2392.3 | 39468.8 | 1038.0 | 3 | 460.1 | 7590.2 | 199.6 |
| M19 | 7 | 0.50 | 100.0 | 2123.8 | 34507.9 | 856.4 | 3 | 424.8 | 6901.6 | 171.3 |
| M20 | 8 | 0.51 | 100.0 | 2339.9 | 37143.0 | 934.1 | 3 | 458.8 | 7282.9 | 183.2 |
| M21 | 9 | 0.54 | 100.0 | 2056.7 | 33176.9 | 834.8 | 3 | 380.9 | 6143.9 | 154.6 |
| M22 | 10 | 0.59 | 100.0 | 2180.1 | 33985.6 | 847.3 | 3 | 369.5 | 5760.3 | 143.6 |
| M23 | 11 | 0.52 | 100.0 | 2298.5 | 36577.4 | 964.5 | 3 | 442.0 | 7034.1 | 185.5 |
| M24 | 12 | 0.53 | 100.0 | 2388.7 | 36969.8 | 921.6 | 3 | 450.7 | 6975.4 | 173.9 |

# 6.0 CONCLUSIONS

The results indicate the degree to which a given sample can be labeled as surface or volumetrically contaminated by showing a contamination penetration distribution. These distributions adhere closely to what is predicted by diffusion theory given the appropriate initial conditions. The subtle and gross variations of the distributions are derived from the differences in these initial conditions, the primary of which is the process exposure history of the sample. Given the primary concern of determining whether the transite can be decontaminated such that the bulk of the material is at or below background contamination levels, a key characteristic of interest is the depth to background or the depth of material that potentially requires removal. Should this characteristic be too great, decontamination may not be viable for a given method of removal. Figure 6.1 shows the number of sides of samples that were analyzed to have contamination down to a certain depth. The majority of the samples had a background depth of approximately 0.055 inches, all of which had a high level contamination process history. With an average total initial thickness of 0.259 inches and contamination on both sides of all samples, this represents about 40% of the total material. For samples with a much lower contamination process history, the background depth was only approximately 0.010 inches which would represent about 8% of the total material. The viability of decontamination is illustrated to be heavily dependent on the process history.

A new gamma-ray spectrometry based technique to evaluate the radiological contamination penetration depth for planar samples has been described and validated. This technique provides a qualitative and quantitative method to identify whether the radiological contamination is surface or volumetric. The technique predicts possible contamination distributions that may occur inside the samples non-destructively through the process of measuring response ratios and the boundary condition ratio, and a subsequent computer simulation using these data and corresponding geometric and material properties to obtain the predicted distributions. If the conditions under which the samples were contaminated are taken into consideration with reasonable assumptions, this technique produces satisfactory results. The value of this technique is its concept of using gamma-ray spectrometry without destroying the samples and that the computer simulations produce a reasonable representation of the actual contamination distribution. While this study has focused on the characterization of Fernald transite, other radiologically contaminated materials could also be characterized using this technique, as long as gamma-ray spectra can be acquired from two opposing sides, a range of photopeak energies are available, and the assumption of uniform contamination across the surface is not restrictive.

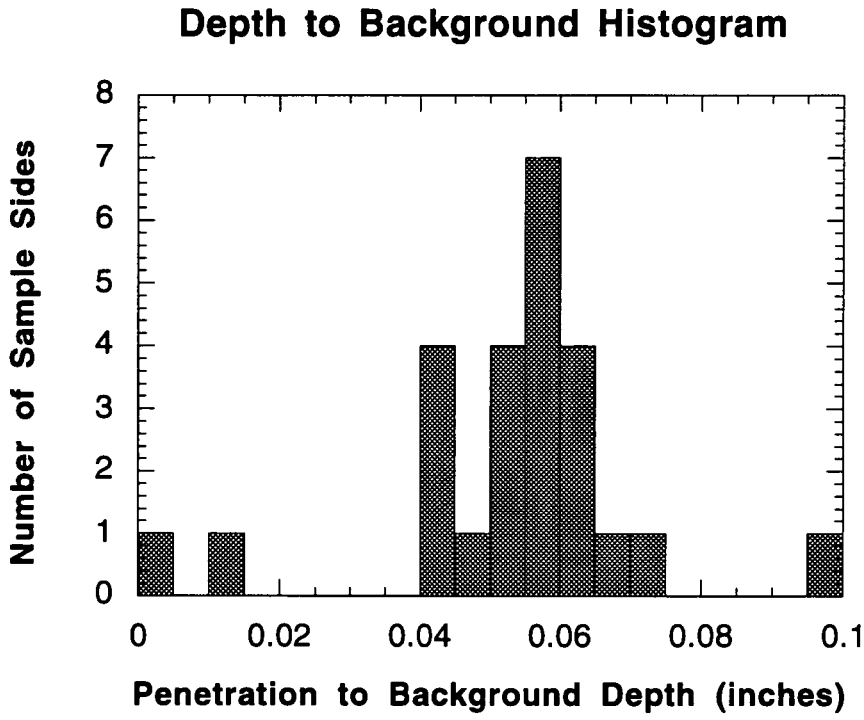


**Figure 6–1 Sample background depth distribution**

# Appendix A

# RADIOLOGICAL TECHNIQUES INVESTIGATED

## A.1 ACTIVATION ANALYSIS

Activation analysis is an important experimental technique arising as a by-product of the nuclear energy program developed during the last quarter century. It involves the production of radioactive nuclides from stable elements present in the sample under investigation. Each of these radioactive nuclides has characteristic properties including type, intensity and energy of the emitted radiations and half-life. These characteristics can be identified using relatively simple equipment with excellent sensitivity for quantitative estimation.

Activation analysis consists of two main steps:

- activation of the sample
- study of the induced radioactivity

### A.1.1 Method

In principle, activation analysis may be based on any artificially induced nuclear reaction. We may distinguish three main possibilities:

- First, the energy given to a nucleus by bombardment with energetic gamma-ray quanta or electrons may be used to promote emission of nuclear particles or translation of nuclei into excited states.
- Second, heavier particles, such as protons (such as PIXE or PIGE), deuterons and other nuclei may be accelerated by electrical means and used to bombard the sample. Such particles may be incorporated in the nucleus, altering its mass, charge and radioactive status or may bring about an internal rearrangement resulting in the emission of other nuclear particles. Electrically-charged projectiles may be furnished with any desired energy using particle accelerators, but have the disadvantage that they penetrate the sample short distances. Though this property can be turned to advantage in the analysis of surface layers. (Furthermore, the energy of the bombarding particles is largely transformed into heat without inducing any nuclear reactions.)
- Third, nuclear reactions of the kind desired for activation analysis are most generally induced by neutron bombardment. Neutrons may be used to produce radioactive nuclides

from almost every element. In general, neutrons have good penetration, allowing a homogeneous activation of the entire sample.

The optimum nuclear reaction is chosen with the following considerations in mind:

- Production of large activity should occur within a reasonable irradiation time.
- The radioisotope produced should have a reasonable half-life ($T_{1/2}$>1min).
- The type and energy of the radiation emitted by radioisotope should not present great counting difficulties.
- A minimum number of interfering reactions should be involved.

If the constituents of the sample are completely unknown, one starts with neutron irradiation because neutrons are absorbed by almost all isotopes. If the composition of the sample is known, then the best reaction for identification of the isotope of interest should be chosen. The "optimum nuclear reaction" depends not only on the isotope and the bombarding particles but also on the composition of the sample that is being analyzed.

### A.1.2 Advantages

The distinctive advantages of activation analysis are as follows:

- The ultimate sensitivity is excellent for nearly every element and is, for many elements, better than can be obtained by any other technique.
- Non-destructive analysis is often possible.
- Themethod has high sensitivity.
- It is generally possible to analyze for several elements in a single sample at a time.
- Requires a sample with very small mass.
- Provided that no pre-irradiation chemical manipulation is attempted, the technique is free from blank errors caused by the use of contaminated reagents.
- Activation analysis allows the opportunity to distinguish between different isotopes of an element.
- Provides results rapidly.

### A.1.3 Photon Activation

Photon activation complements neutron and charged-particle activation. (Photons are better than neutrons in certain cases.) For example, photons are preferred if the product of the neutron activation is an isotope that has a very short half-life or emits only low-energy betas or low-

energy X-rays. The cross-section for photonuclear reactions are generally smaller than those for neutrons and charged particles. The reactions most easily induced by photons are of the form ($\gamma$, $\gamma'$), ($\gamma$,p) and ($\gamma$,n) reactions.

### A.1.4 Activation with Charged Particles (and Proton Induced X-ray Emission, PIXE)

Such projectiles have very limited range in solid matter and it is, therefore, not possible to achieve uniform irradiation unless an extremely thin sample is used. A further difficulty arises because the energy spectrum of a beam of charged particles changes with depth of penetration into the analytical sample. It is not possible, therefore, to make calculations on the basis of a constant cross-section, as can normally be done for neutron and photon activation.

These reactions have a threshold.

Protons, deuterons and alpha particles are the most commonly used.

See Section A.2.

### A.1.5 Activation with Neutrons (Neutrons Activation Analysis, NAA)

Instrumental Neutron Activation Analysis (INAA) is a widely used technique for multi-element analysis of environmental, geological and biological samples. The identification and quantitative determination of activation products in INAA is conventionally achieved using high resolution gamma ray spectrometry (100-300 keV).

### A.1.6 The Reactions:

Although charged particles and gamma rays may be used as bombarding particles, neutrons are, by far, the most frequently utilized for irradiation of samples. A neutron, in motion as a certain distance from the nucleus, may deviate from its original path under the action of attractive forces and then continue moving in this altered direction. This type of neutron interaction is called potential scattering. If the neutron approaches sufficiently close to the nucleus, it can be caught due to the action of nuclear forces, penetrating the nucleus and forming a compound nucleus.

The compound nucleus can decay to a state of lower energy by the emission of one or more particles, for example a proton, alpha particle, triton, two neutrons, protons and neutrons, etc. Designation of these reactions are as follows: (n,p) (n,$\alpha$) (n,t) (n,2n) (n,pn) (n,3n)...

*A.1.6.1 Thermal neutron reactions*

The most commonly used reaction is the (n, $\gamma$) reaction, in which the excited nucleus passes to a lower energy state by emission of a gamma ray. This reaction takes place with almost all isotopes and has no threshold. In general, the (n, $\gamma$) cross section is higher for thermal neutrons than for fast neutrons. The reactions of this type (n, $\gamma$) are called radiative captures. This type of reaction is advantageous, especially in the determination of trace amounts of an element. This reaction type is only excluded in the case of several light elements ($Z<8$). Typical cross sections for (n, $\gamma$) reaction are about of 0.1-100 barns, whereas the majority of applicable reactions of the (n,p) or (n,$\alpha$) type have activation cross sections on the order of 1-100 millibarns.

*A.1.6.2 Fast neutron reactions*

Other neutron interactions are (n, $\alpha$), (n,p) and (n,2n) reactions. Except for a few exothermic (n, $\alpha$) reactions, the others have a threshold; therefore, they can be induced by fast neutrons only. The activation with fast neutrons usually involves the analysis of light elements which either do not form radioactive nuclides after reaction with thermal neutrons or, if they do, cannot be analyzed with sufficient sensitivity.

### A.1.7 Neutron Velocity

One can roughly separate neutrons into 2 classes: fast neutrons, which have energy higher than 0.5 MeV and slow neutrons, which have less energy. A more precise classification of neutrons is as follows: Thermal (energy of about 0.025 eV), epithermal (energy of about 0.2 eV), cadmium (0.4 eV), epicadmium (0.6 eV), slow (1-10 eV), resonance (1-300 eV), medium (500 eV-0.5 MeV), fast (energy above 0.5 MeV) and ultra-fast (above 20 MeV).

### A.1.8 Sources of Neutrons

Being uncharged particles, neutrons can not be accelerated. However they can be moderated. Neutron sources include reactors, accelerators and isotopic sources. Nuclear reactors are by far the most frequently used irradiation facilities. They provide high flux (an upper limit of about $10^{18}$ neutrons/cm$^2$•s, primarily thermal neutrons). Fast neutrons in the keV range are also available, but at lower flux levels.

Accelerators produce fast neutrons as a product of the charged-particle (d,t) reaction. The maximum flux provided by a neutron generator is on the order of $10^{12}$ neutrons/cm$^2$•s.

Neutrons with an average energy of about 2.5 MeV are produced by the (d,d) reaction. This reaction offers a neutron flux on the order of $10^9$ neutrons/cm$^2$•s. It is important to note that both the (d,d) and (d,t) reactions produce essentially monoenergetic neutrons.

Isotopic neutron sources are based on ($\alpha$,n) and ($\gamma$,n) reaction and on spontaneous fission ($^{252}$Cf). All produce fast neutrons.

### A.1.9 Disadvantages

- Change in neutron flux during passage through the sample: If the mass of the sample is too great or if it contains certain elements, changes in the flux can occur. These changes may occur in the total neutron flux or in the energy spectrum of the penetrating neutrons or in both.
- The most important factor causing changes is the absorption of neutrons inside the sample (self-absorption). This factor increases with increased sample mass and with an increase in the number of elements present which have a high absorption cross-section.
- Scattering is another factor to be considered, though it typically produces a small uncertainty. (Neutrons may deviate from their original direction because of a collision with atoms in the sample and thus the number of neutrons reaching the internal layers is decreased).
- Another source of uncertainty in activation analysis is the possibility of a reaction that produces the same isotope as the one being counted through the bombardment of a different isotope in the sample.

### A.1.10 Detector Used

To detect the gamma rays produced in NAA a high-purity germanium (HPGe) detector is used, due to its excellent energy resolution some 15 times better than that of a NaI(T1) scintillator detector.

### A.1.11 Use of X-Ray Emitters in Activation Analysis:

A number of authors have investigated the application of X-ray and low energy photon spectrometry (10-200 keV) in activation analysis. The use of X-ray spectrometry has been widely used as an analytical technique where gamma ray spectrometry fails to give satisfactory results. The possibility of using X-ray spectrometry in the activation analysis is based on the

property of a number of nuclides to decay after neutron capture by the emission of characteristic X-rays. The latter are due to the different nuclear process and as such may be divided into three groups:

- those due to internal conversion, X-rays of the parent element (Z)
- those due to electron capture, X-rays of the element (Z-1)
- those due to the beta decay followed by internal conversion, X-rays of the element (Z+1)

The X-rays from all three groups decay according to the half-life of the parent element (Z).

The technique of X-ray spectrometry is attractive since it presents several advantages which are a result of basic properties of X-rays. For example, the precise measurement of the energy of the emitted X-ray permits the unambiguous identification of the element due to the direct correlation between an element and its characteristic X-rays. Furthermore, the limited number of peaks in the X-ray spectrum of each element permits the analysis of many elements in a single spectrum. Finally, the reduced sensitivity of the Si(Li) and planar Ge photon detectors used for the measurement of X-rays, eliminates the interference of Compton scattered high energy gamma rays. As a result, the background is considerably lowered and the peak-to-background ration much increased.

Habib and Minski introduced the concept of `advantage factor' (AF) (i.e., the ratio of X-ray to gamma ray sensitivity for a particular isotope). The use of X-ray spectrometry is recommended in those cases where AF is significantly greater than unity.

### A.1.12 Interference with the Measurement of X-Rays

Possible interferences with the measurement of X-rays obtained following neutron activation may be due to the discrete x-rays and low energy gamma rays, secondary X rays, and beta particles.

#### A.1.12.1 Discrete X-rays

Due to the direct relationship between the atomic number of an element and the energy of its characteristic X-rays, the interference with the measurement of these X-rays will result chiefly from X-rays emitted by neighboring elements in the Periodic Table. Another possible source of interference is the L X-rays emitted by elements with high atomic numbers that have the same energy as the K X-rays of an element with a lower atomic number, or vice versa.

The possibility of distinguishing two elements with close X-ray energies in the same spectrum will depend on the resolution of the detector. In other words for two neighboring elements in the Periodic Table, the difference between the energy of the $K_1$ X-rays of one element and that of $K_2$ X-rays of its immediate predecessor should be greater than the resolution of the detector in order to distinguish the two.

A.1.12.2 Secondary fluorescent X-rays

Strong beta or gamma rays from the radioactive sample may interact with major elements present in the sample or materials in the vicinity of the detector and induce fluorescent X-rays. Generally the intensity of the X-rays and gamma rays obtained by NAA are too low to produce fluorescent X-rays in sufficient yield to interfere with the measurement. The possibility of secondary fluorescent X-rays must be taken into account only when very long irradiations are carried out or if one of the main components of the matrix is known to produce especially strong gamma or beta radiation following neutron activation.

A.1.12.3 Beta Particles

The beta particles emitted from an irradiated sample are another serious source of interference in X-ray spectrometry. These beta particles may produce a high background which completely obscures the X-ray peaks obtained from trace amounts of low and medium Z elements making their quantitative determination practically impossible. The interference of beta particles may be overcome by use of plastic absorbers or by the deflection of beta particles by magnetic fields (the intensity of the magnetic field depends on the beta energy and the source to detector distance).

The measurement of X-rays produces very satisfactory results for U (L X-rays) and Ba, Sm, Tb and Ta), with a flux of $1.5 \times 10^{13}$ n/cm$^2$•s and with a HPGe detector.

**A.1.13 Case of Uranium**

*Sensitivity:*

The sensitivity of neutron activation analysis in determination of Uranium by the (n,γ) reaction with a thermal neutron flux of $10^{13}$n/cm$^2$•s for a maximum irradiation time of one hour is about $10^{-10}$ gram. Activated $^{238}$U is a short-lived nuclide ($^{239}$U half life: 23.54 minutes) and emits low energy gamma-rays (74.6 keV) and beta particles.

Detection Limit: 0.1-1 ppm

AF of $^{238}$U = 1.4 (not enough to use X-rays, because of the interference applicable for X-rays)

## A.2 PROTON INDUCED X-RAY EMISSION (PIXE)

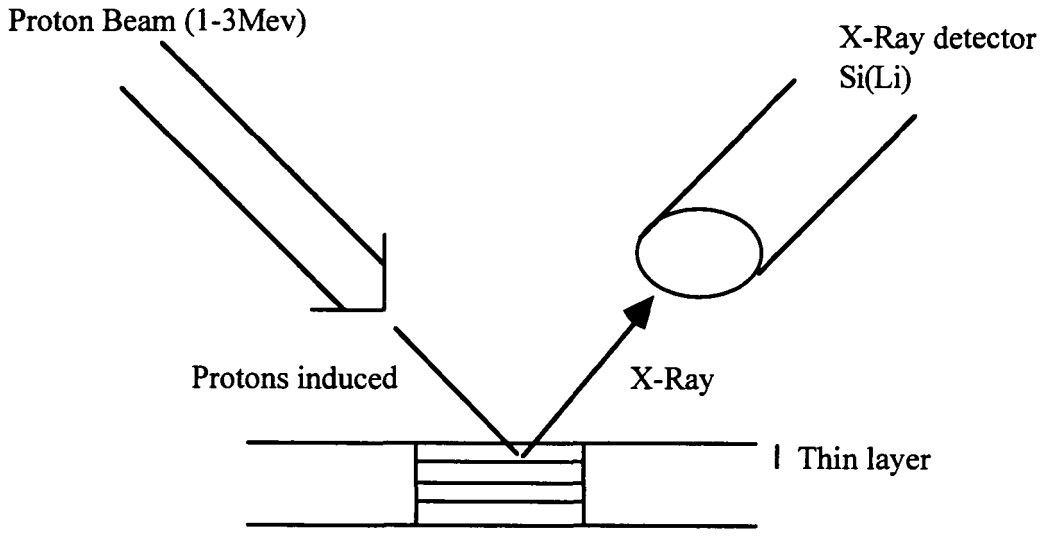


**Figure A–1 Schematic diagram of PIXE technique**

PIXE analysis can be used to:

- Identify the atomic species in the target from the energies of the characteristic peaks in the X-ray emission spectrum.
- Determine the amount of a particular element present in the target from the intensity of its characteristic emission spectrum. (This normally requires a knowledge of ionization cross-sections, fluorescence yields and absorption coefficient.)

### A.2.1 Method

When an energetic (MeV) proton impinges on a target atom there is a high probability, typically of the order of hundreds of barns (1 barn = $10^{-24}$ $cm^2$), that an inner-shell will be excited and removed from a target atom. The excited target atom seeks to regain a stable energy state by reverting to its original electron configuration. In so doing, the electronic transition which takes place may be accompanied by electromagnetic radiation in the form of X-rays, characteristic of

the excited atom. The emission consists of K, L, M, ... lines produced by electron transitions to the K, L, M shells of the target atom. The elements present can be identified by the corresponding characteristic X-ray energy (peaks recorded in spectrum).

Elemental quantitative analysis by PIXE based on the assumption that there is an unambiguous relationship between the number of characteristic X-rays of a particular element observed and the amount of this element present in the target sample. PIXE is done mainly in laboratories which have access to proton accelerator (usually Van de Graaf or Cyclotron). The typical geometry used in PIXE analysis is shown in Figure A–1.

The energy dispersive Si(Li) detectors have high count rate ability and a resolution high enough to distinguish between the X-rays of adjacent elements.

### A.2.2 Characteristics

PIXE is essentially a near-surface method. The best results are obtained by PIXE when thin samples are used, thickness less than about 1 mg/cm$^2$ (or approximately 10 mm). However, thick samples can be investigated by the analyses are invariably more complicated and the resulting sensitivity is poorer than with a thin target. Higher proton energies must be used in order to increase the penetration depth of particle.

It is difficult to obtain a good spatial resolution with PIXE. However, PIXE can be combined with other techniques to get a depth profiling. (Example: Rutherford Backscattering).

Protons provide better sensitivity over the whole Periodic Table than heavier projectiles of the same energy per nucleon.

### A.2.3 Advantages

In contrast with a number of other chemical and physical spectrometric techniques,

- high sensitivity for all elements, except the lightest ones (X<10),
- capable of multi-elemental analysis,
- practically all elements can be covered in a single experimental run
- need very short experimental time (typically between 5 and 20 minutes per sample
- good concentration sensitivity

- the basic advantage of characteristic X-ray analysis arises from the relative simplicity of the characteristic X-ray emission spectra
- the intrinsic capability for analysis without destructively interfering with the specimen
- requires only very small samples
- background effects are in almost all cases lower than those fort comparable X-ray techniques using electrons, photons
- cheaper in comparison with Neutron activation analysis per sample analyzed.

### A.2.4 Disadvantages

- inability to determine lightest elements (but coupled with PIGE, can cover the whole Periodic Table)
- difficult to provide depth information
- decreased sensitivity of the elements are too concentrated
- decreased sensitivity if the elements are too heavy (interferences between peaks)

### A.2.5 Detection Limits and Sensitivity

PIXE is a method of high sensitivity. The average detection limits for trace elements are typically as low as 0.1-1 ppm, as shown in Figure A–2.

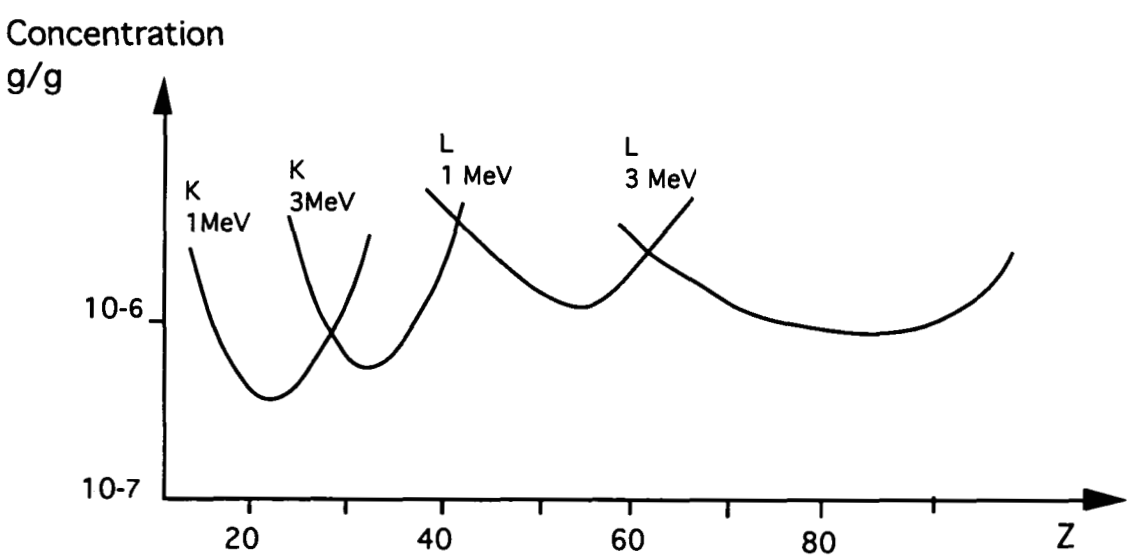


**Figure A–2 Theoretical minimum detectable concentration calculated for all elements.**

For high Z elements (beyond an atomic number of about 40), good elemental separation is provided by PIXE using the L X-ray lines rather than the K X-rays and K X-rays.

Optimum beam energy:

- The proton energy should be chosen according to the elemental region of interest. The lowest detection limit obtainable for a given range of elements depends on the energy of the proton.
- For heavy elements, we can increase the proton beam energy, however with a high concentration of several heavy elements in a sample, there is often interference between peaks, causing the sensitivity to deteriorate. One solution to this problem is to increase the beam energy so the cross-section for K X-ray production increases thus making it possible to also use the K X-ray peaks for analysis of the heavy elements

The sensitivity can be improved by increasing the count time.

### A.2.6 Proton Elastic Scattering Analysis (PESA)

Due to the degree of attenuation of softer X-rays by matter, X-ray analysis of the lightest elements is made difficult to impossible for practical sample loading. Proton elastic scattering analysis proves to be a useful compliment to PIXE since it has almost identical sample requirements and is also nondestructive. With modern commercially available solid state proton detectors and 16 MeV incident protons it is possible to resolve the light elements up through chlorine.

Two other advantages to the use of 16 MeV protons are their smaller specific energy loss (allowing the use of thicker samples) and relative freedom from resonant behavior of the excitation function.

One negative side, the nuclear scattering cross sections are approximately 1000 times smaller than the atomic cross sections for PIXE. The effect of this lower efficiency is greatly counterbalanced by the lower backgrounds for PESA spectra.

### A.2.7 Conclusion

These methods are fast, have a broad-range, are absolute, are subject to automation and are well-suited for samples having areas of a few square millimeters and thicknesses of 1 $mg/cm^2$.

Samples of uniform density are most convenient; however, non-uniform samples may be analyzed by using a uniform proton beam.

## A.3 ATOMIC ABSORPTION SPECTROMETRY

Techniques commonly referred to as atomic spectrometry usually include atomic emission, atomic absorption, and atomic fluorescence spectroscopy. These involve valence electron transitions yielding radiation with wavelengths in the ultraviolet-visible region of the spectrum.

### A.3.1 Atomic Spectra

An electron of an atom at its lowest energy state, the ground state, can absorb a quantum of energy (+ΔE) and undergo transition to a low-lying excited state. Emission occurs when this quantum of energy is released (–ΔE) and the electron returns to the ground state (Figure A–3). A transition to and from the ground state is called a resonance transition. Resonance lines are the most useful analytical lines for atomic absorption spectrometry.

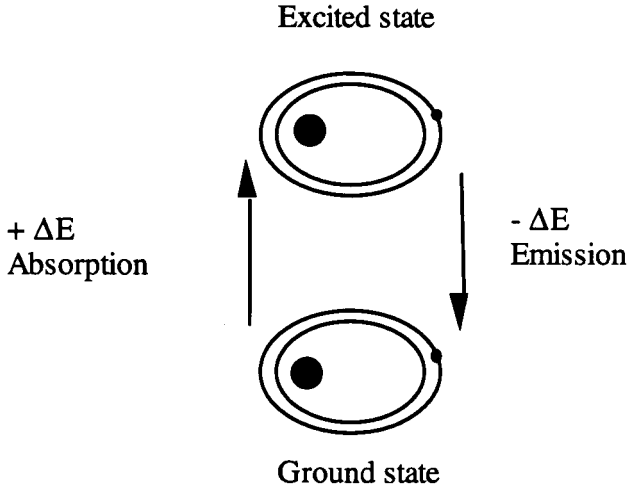


**Figure A–3 Relationship between emission and absorption of energy by a valence electron**

### A.3.2 Basic Concept

When a parallel beam of continuous radiation of intensity $I_0$ passes through a cell containing atomic species of an element., the transmitted radiation $I$ will show a frequency distribution as given in Figure A4. The atomic species is said to possess an absorption line at frequency $v_0$, where $v_0$ is the frequency at the center of the line.

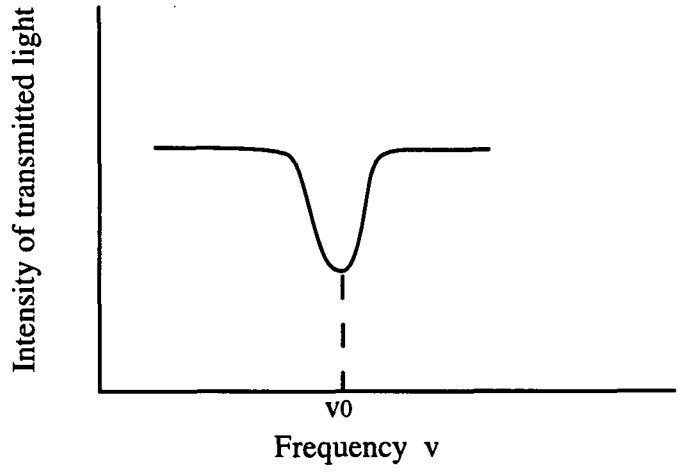


**Figure A–4 Intensity attenuation at characteristic frequency**

### A.3.3 Experimental Method

Since atoms are only able to absorb radiation within a very narrow frequency interval, certain demands must be placed upon the radiation source. Although continuum radiation sources afford a high total illumination intensity, the illumination intensity in the interval of interest of about 0.5 ppm to 5 ppm is nevertheless too weak. For this reason, one recommends that the radiation source used for absorption measurements should emit the spectrum of the element to be quantified. With such an arrangement the required resonance line merely has to be separated from the spectral lines of the same element by means of a monochromator.

The spectrum of the element (usually a single element) under study is emitted from a hollow cathode lamp. This beam, consisting largely of resonance radiation, is electronically or mechanically pulsed. Analyte atoms are produced thermally in the atom reservoir. Ground state

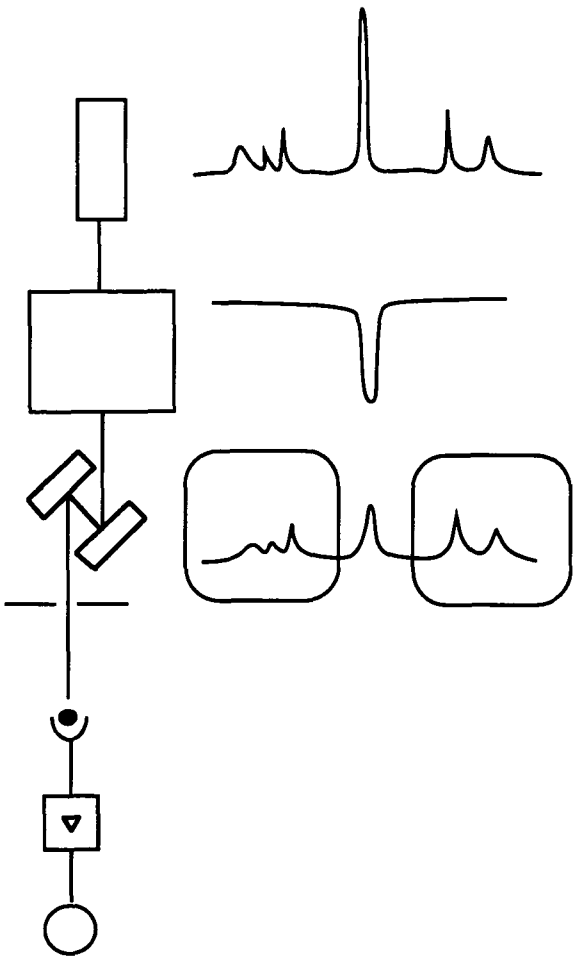

**Figure A–5 Atomic absorption spectrometry equipment diagram**

atoms, which predominate under the experimental conditions, absorb a portion of resonance radiation from the lamp corresponding to the concentration of this element, reducing the intensity of the incident beam. Lines that do not occur in absorption are not attenuated. After dispersion of the radiation in a monochromator, the resonance line is separated by the exits lit and all other lines are masked. The detector 'sees' only the resonance line, whose attenuation is then displayed.

### A.3.4 Instrumentation

The general construction of an atomic absorption spectrometer is simple. The most important components are:

- A radiation source, which emits the spectrum of the analyte element. Hollow-cathode atomic spectral lamps are the most common radiation sources for atomic absorption spectroscopy. These lamps can produce resonance radiation of narrow linewidth, typically <10 Å, for most elements that can be quantified by atomic absorption.
- An atomizer, in which the atoms of the sample to be analyzed are formed. It produces free ground-state atoms of the element of interest. A variety of commercial atomizers are available for use with AA equipment, the most common being flames and furnaces.
- A monochromator for the spectral dispersion of the radiation with an exit slit for selection of the resonance line. Because of the simplicity of the spectrum emitted by most radiation line sources, the monochromator in atomic absorption spectroscopy need not be of high resolution required for emission work.
- A detector permitting measurement of radiation intensity, followed by an amplifier and a readout device to record the intensity.

### A.3.5 Advantages

- Simple spectra

### A.3.6 Disadvantages

- Destructive method
- No depth information (only total amount)
- Better with just one element

### A.3.7 Case of Uranium

Uranium can be determined in a nitrous oxide/acetylene flame at the 351.5 nm resonance line with a characteristic concentration of 50 mg/L and a detection limit of about 30 mg/L. The resonance lines at 358.5 nm and 356.7 nm exhibit better sensitivity, but a less favorable signal to noise ratio.

### A.3.8 Interferences

*A.3.8.1 Atomic Spectral Interferences*

This type of problem occurs when the radiation being measured is attenuated by substances other than the atoms of interest. Atomic spectral interference occurs when the absorption profile of

another element overlaps that of the analyte within the spectral linewidth of the atomic emission line of the source. Because of the narrow width of atomic emission lines, atomic spectral interference causes very few problems.

*A.3.8.2 Nonspecific Interferences*

Nonspecific interference occurs due to molecular absorption or light scattering in the atomizer. These effects, seldom encountered in flames except in work near the detection limit, are very serious problems in most work with electrothermal atomizers.

*A.3.8.3 Chemical Interferences*

Chemical interference occurs when the analyte is contained in a chemical compound that is not broken down by the flame or furnace. This results in a lower concentration of 'free' analyte atoms than would occur in the absence of the interference. Atomic absorption can only occur by free atoms.

In work with flames, chemical interferences can be minimized either by using a higher temperature flame and/or through addition of a releasing agent.

*A.3.8.4 Ionization Interferences*

In atomic absorption, the flame should ideally be an absorption cell in which the sample is atomized and only atoms at the ground state are produced. Although the number of excited atoms at normal flame temperatures is always considerable lower than the number of atoms in the ground state, many practical examples are known in which the emission of the flame interferes with absorption measurements in this type of instrument. To eliminate this interference due to flame emission, virtually all atomic absorption spectrometers currently operate with a chopped or pulsed radiation system instead of a direct current. the radiation beam is modulated either electrically or mechanically at a fixed frequency and the amplifier electronics are tuned to the same frequency. In this system, only the radiation from the primary source having the modulation frequency is amplified, while the emission from the flame, which is not modulated is neglected. Accordingly, spectral interferences caused by emission of sample atoms in the flame are practically negligible in such a system. Elements that commonly present a problem are cesium, rubidium, potassium and sodium.

## A.4 X-RAY FLUORESCENCE (XRF)

X-ray fluorescence is an application of X-ray emission spectrometry using X-ray and gamma-ray sources for excitation. X-ray fluorescence is described as an incident beam of photons which impinging on specimens and resulting in the fluorescence emission of X-rays characteristic of the elements present.

### A.4.1 History of this Method

The excitation of characteristic X-rays using a radioisotope source was first reported in 1966. By that time, several measurement techniques had been developed and analysis was proven feasible. Also a range of sealed, radioisotope, low-energy X-ray and gamma ray sources and a few instruments, were commercially available. These techniques are based on detection and low resolution energy selection of characteristic X-rays using ordinary scintillation or proportional counters, and the use of filters for discriminating between X-rays from adjacent elements. An event of more general significance is the recent availability of lithium-drifted silicon and high-purity detectors (Si(Li) and HPGe detectors), whose energy resolution is good enough to resolve K X-rays from the adjacent elements down to sodium.

### A.4.2 X-rays Fluorescence System Basic Concepts

Primary radiation is incident on the sample where it interacts to produce vacancies in the inner atomic shells, which then de-excite to produce the characteristic X-rays of interest which are then defined by a collimator or silt arrangement and are absorbed by an appropriate detector. These X-rays from the sample are then detected, and their energies are measured by detector spectrometer. The detector spectrometer converts the energy of the incident X-ray into a voltage pulse whose amplitude is proportional to that energy. A multichannel analyzer is used to accumulate a histogram of the pulse amplitude spectrum. The energy resolution of the detector is more than adequate to separate X-ray lines from elements of adjacent atomic number. The area under the individual characteristic X-ray peaks in the spectrum is proportional to the concentration of the various elements in the sample.

A radioisotope X-ray fluorescence analyzer consists of the following basic components:

- a sealed radioisotope excitation source
- a detection system which selects the energy of characteristic X-ray excited and measures their intensity

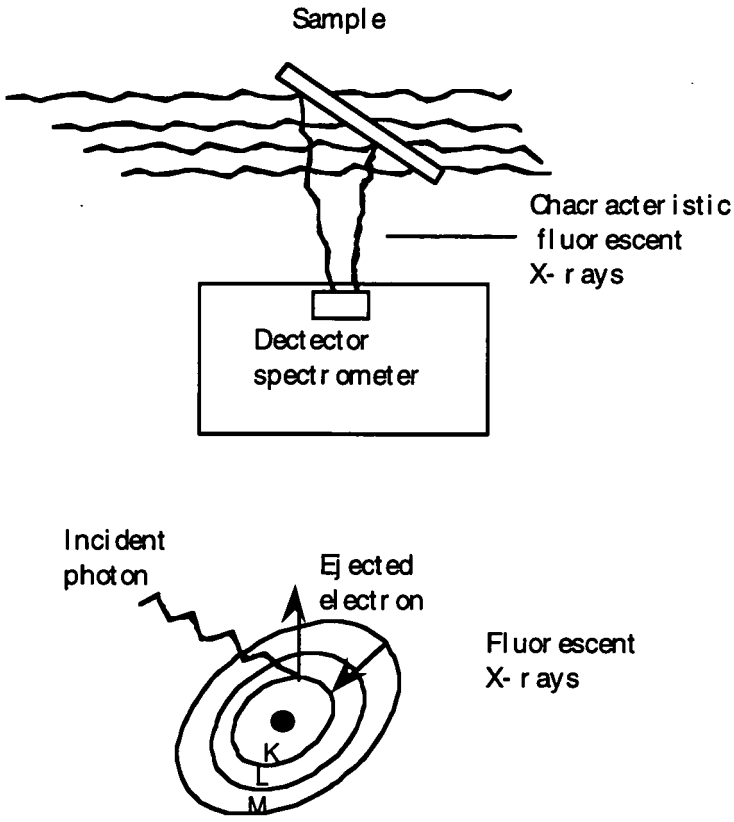


**Figure A–6 Schematic of the X-ray fluorescence technique**

- an electronic amplification and a read out system whose output can be correlated with the elements present in the specimen and their concentration.

X-ray photons incident on the sample interact either by the photoelectric effect to produce the desired inner shell atomic vacancies in the elements of interest or by scattering mainly from the atoms in the low atomic number substrate. These scattered X-rays constitute an unwanted background that determines the detection limit for the fluorescence measurement.

### A.4.3 Sources

Alpha, beta, gamma and X-ray emitting isotopes have all been used as sources to excite characteristic X-rays.

The most widely used excitation method is by primary or secondary gamma or X-ray sources, preferably those that emit one or a few spectral lines rather than a high proportion of continuous radiation. But characteristic X-rays can be excited by radiation; from an X -ray tube or a radioactive source. Each method has its own problems and advantages.

The major advantage of the preferred sources is that they excite characteristic X-rays efficiently with minimum background in the energy region of interest. It is preferred to use monoenergetic X-ray excitation sources (especially source-target assemblies) rather than broadband excitation, which distribute the scattered radiation over the entire range of energies. The main advantages of radioisotope sources are that they are small and are independent of any external power. The most important limitation of radioisotopes as excitation sources for XRF is their low intensity of primary radiation ($10^{-6}$ to $10^{-7}$ less than conventional X-ray tubes). The probability of producing fluorescent excitation of an element is greatest when the incident X-ray energy just exceeds the binding energy of the electrons in the appropriate shells. This probability falls off rapidly with increasing excitation energy. This implies that very low energy characteristic X-rays are not efficiently produced by monochromatic radiation of high energy, thus limiting the range of elements that can be sensitively measured with a single exciting energy. In some case, such as the analysis for very light elements ($Z<20$), the use of continuum excitation may give better sensitivity than monochromatic excitation. An X-ray tube is typically chosen as the primary excitation source because of its higher output compared to generally available radioisotope sources. X-ray tubes offer the advantages of being large, high speed, and having stable power supply, but are also costly and less compact.

Bremsstrahlung emitters are secondary sources excited by beta particles. Bremsstrahlung spectra are continuous and have similar shapes to spectra emitted by X-ray tubes. Their main disadvantage is the continuous scattered background which accompanies excitation of characteristic X-rays.

Direct excitation by beta particles has two major disadvantages; excitation of Bremsstrahlung background in the specimen and backscatter of a large proportion of the incident beta particles.

Excitation by alpha emitters becomes efficient below about 2 keV and complements X-ray and gamma-ray excitation.

The criteria of a good source are:

- a simple line spectrum at an appropriate energy below 150 keV

- no high energy beta or gamma radiation
- half year of at least one year
- specific activity high enough to yield a source emission of $10^7$ to $10^8$ photons/s from 1 $cm^2$ surface.

The resolving energy required of the energy selection apparatus varies from virtually none for certain very simple measurements to several hundred when complex groups of K and L X-rays have to be resolved.

### A.4.4 Conditions

It is assumed that the specimen is homogeneous, flat and infinitely thick with respect to the X-ray fluorescence emission. But XRF has found wide application in the analysis of thin films. Depending on the nature of the specimen being irradiated by a beam of X-rays. (i.e., pure element, binary or multi-element system), the emitted characteristic radiation may be the resultant of more than one process:

*A.4.4.1 Primary Fluorescence*

Some K level electrons are ejected directly after interaction, with the incident beam photons.

*A.4.4.2 Secondary Fluorescence*

Some K level electrons are ejected indirectly; some incident beam photons eject K level electrons, leading to the emission of photons, which in turn have enough energy to eject target level electron. This process is called the process of enhancement.

*A.4.4.3 Tertiary Fluorescence*

The realization that an element enhancing another may already be enhanced by a third element results in an additional component of fluorescent emission.

In multi-element specimens, some emitted X-ray lines are likely to be the resultant of enhancement by more than one element. In the absence of enhancement effects, the emitted intensity of a function of:

- the intensity emitted by the pure element
- the concentration of the element in the specimen
- the total mass absorption coefficient

### A.4.5 Advantages

- Requires very small samples
- Non destructive analysis
- Simple method
- Better relative sensitivity for heavier elements than NAA
- Low costs (lower than PIXE and NAA, but more expensive than ICP-AES)
- Greater depth of analysis

### A.4.6 Disadvantages

- Poor results with highest elements (covers elemental analysis from Aluminum to Uranium)
- Mostly used on solid samples
- Requires homogeneous solid sample (it is better to analyze heterogeneous solid samples, after dissolution, by ICP-AES)
- Can be slow, particularly for trace determination, because it needs longer counting time.

## A.5 ULTRAVIOLET LIGHT AND RADIOGRAPHY METHODS

An inspection of the remaining transite surface by observing the ultra-violet light emitted by activated uranyl ion phosphorescence may be used as an indicator of local contamination. Samples of transite containing uranium and thorium isotopes were viewed under short-wave length (254 nm) ultraviolet light to determine:

- whether the specimens contain fluorescent species on the surface,
- whether the appearance under UV changes with depth by removing sample layers.

One control specimen with no uranium or thorium content showed no fluorescence. Samples containing radioactive contamination emit bright yellow-green fluorescence from a number of discrete, specific sources. This method is mainly qualitative, but when coupled with imaging software can be quantitative.

### A.5.1 Basic Concepts

The term 'fluorescence' as commonly used refers to the emission of light (usually in the visible range) from a material in response to the absorption of incident energy, which is commonly

ultraviolet light. The emission of light is caused by energy released when the electrons in the excited material return to their ground state (true fluorescence), or when the spins of excited electrons return to ground state (fluorescence). The term 'luminescence' properly includes both phenomena, and whether a particular atom or molecule will absorb and re-emit radiant energy depends on its unique atomic structure. As cataloged by several authors, many uranium and thorium compounds emit radiant energy in the visible range upon absorbing ultraviolet light. While there is evidence to suggest that it is actually phosphorescence rather than fluorescence, the latter term is in common use when describing uranium and thorium behavior.

Not all species fluoresce under UV excitation nor do all uranium and thorium compounds fluoresce. Uranium and thorium are key constituents of radioactive waste and many compounds of these elements fluoresce under ultraviolet light. (Frondel lists 82 fluorescent uranium and thorium compounds.) One of the most common of such fluorescent species, the most colorful and well-documented fluorescent species, which is known to fluoresce an intense yellow-green under short-wave length (254 nm), is the uranyl ion ($UO_2+^2$) under UV light. The uranyl ion is present in all fluorescing uranium compounds. While the uranyl ion will fluoresce weakly under ordinary or long wave length ultraviolet light (365 nm wavelength), the yellow-green fluorescent emission is far more intense under short-wave length UV incident radiation (254 nm).

This fluorescence may be useful in identifying fluorescent species in radioactive wastes. This can be useful since uranium and thorium compounds are not necessarily distinguishable by visual inspection of a mixed waste.

### A.5.2 Experiment Procedure

The procedures very simple. The sample of transite is viewed under the short wave length (254 nm) ultraviolet light. The specimen containing uranium or thorium emits bright yellow-green fluorescence from a number of discrete, specific points. These point sources are on the order of 1 to 5 mm in diameter and are non-uniformly distributed. Fluorescence is readily observed against the dark non-fluorescent background or other non-fluorescent background or other non-fluorescent materials present, and specimens with higher measured radioactivity show a larger number of fluorescent point sources. One can also use a camera and filter and take photos useful for later study.

This method is a near surface method, but one can use it to determine the depth profiling of uranium in the samples by removing successive layers of sample between two ultraviolet light exposures.

### A.5.3 Advantages

- simple method both in execution and in interpretation,
- fast method.

### A.5.4 Disadvantages

- gives relative intensities,
- low sensitivity,
- surface method,
- no quantitative determination.

### A.5.5 Coupling

*A.5.5.1 Imaging Software*

This method is just a qualitative method, but it may be possible, by coupling with imaging software to scan the photo into a computer, digitize the picture, and analyze the image. This can produce a correspondence between the colors and the intensities obtained with the UV method, and quantify, the concentration of uranium contained in the samples.

### A.5.6 Radiograph

Radiographs can be used to confirm the presence of radioactivity in the sample. The radiograph is sensitive to the short range radiation ($\alpha$ and $\beta$ particles).

*A.5.6.1 Experimental procedure*

The samples have to be manipulated under a safety light. One puts the sample's side that one is studying against the film in a dark place. After a time, one develops the film. The film appears marked where it received beta and alpha particles emitted by the uranium atoms and their daughters present in the sample. In this way, one can directly deduce the position of the uranium atoms present on the sample's surface.

*A.5.6.2 Advantages/disadvantages:*

The radiograph's sensitivity is not higher than that of the UV method. In fact, the sensitivity of this method depends on the time of irradiation of the film. Then for a sample containing a few atoms that emit radioactive particles, one will need a long exposure time, on the order of hours or days, for the film to be sufficiently irradiated. This method can be lengthy, especially for samples with low activity. For example, the lowest sensitivity for an exposure of 48 h is around 500 counts per minute (cpm) over a 3"x3" area.

The sensitivity for an exposure of 24 h is twice that (around 1000 cpm).

## A.6 BACKSCATTERING SPECTROMETRY

In 1967, the purpose of the alpha-scattering experiment was to analyze the composition of the nuclear soil.

### A.6.1 Basis

Both in its concept and in its elementary execution, Rutherford scattering is a simple experiment. A beam of monoenergetic and collimated alpha particles impinges perpendicularly on a target. When the sample that constitutes the target is thin, almost all of the incident particles reappear at the far side of the target with some slightly reduced energy and only slightly altered direction. The few alpha particles that are lost undergo large changes in energy and direction, changes due to close encounters of the incident particles scattered backward by angles of more than 90° from the incident direction can be detected. This is the situation that is used in the analytical technique called Backscattering spectrometry.

*A.6.1.1 Generality*

Charged particles are generated in an ion source. Their energy is than raised to several MeV by an accelerator. The high-energy beam than passes through a series of devices which collimate or focus the beam and filter it for a selected type of particle and energy. The beam then enters the scattering chamber and impinges on the sample to be analyzed. Some of the backscattered particles impinge on the defector, where they generate an electrical signal. This signal is amplified and processed with fast analog and digital electronics. The final stage of the data

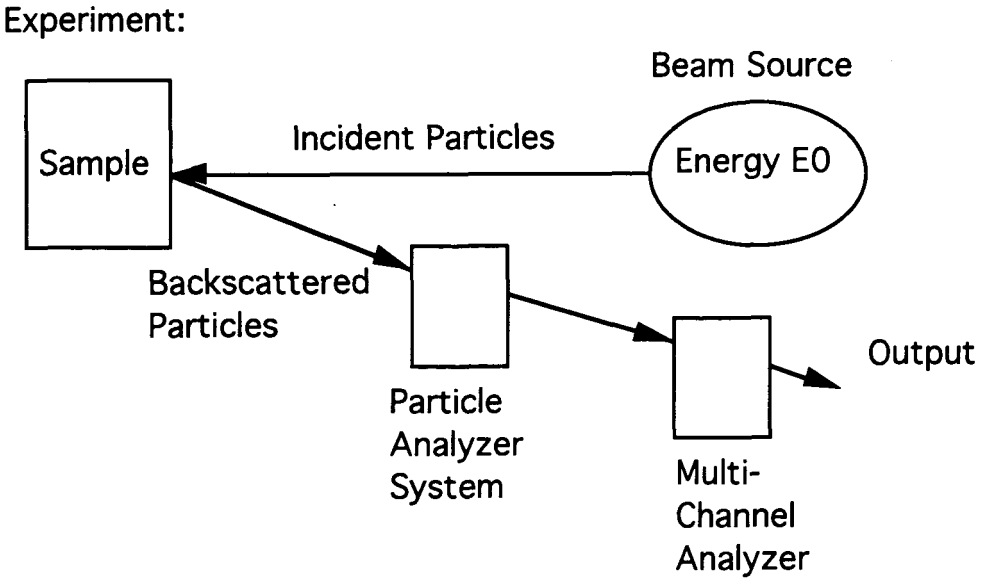


**Figure A–7 Backscattering spectrometry geometry**

acquisition usually is to store the signals in the form of a spectrum, hence the name backscattering spectrometry.

*A.6.1.2 Specifications and properties*

- The BS system has only 3 elements: the beam, the detector and the vacuum pump. The requirements of the vacuum are quite modest by today's standard: $10^{-5}$ Torr expedient and $10^{-6}$ Torr is quite adequate.

- The source generates a beam of collimated and monoenergetic particles of energy $E_0$. The projectile energy $E_0$ must be much larger than the binding energy of the atoms in the target. Chemical bonds are of the order of 10 eV, so that $E_0$ should be very much larger than that. Chemical bonds and binding energy are not the same. The angular effect of the elastic backscattering factor decreases as the scattering angle increases, up to 180°, so that large scattering angles are usually preferable, i.e. $\theta>160°$. To maximize count rate, the detector can be located close to the sample. A distance of 10–15 cm between the detector and the target has been found quite sufficient for a 25 $mm^2$ detector.

  A typical case is a monoenergetic 10. MeV H+ ion beam with a current of 10 to 100 nA of in a 1 $mm^2$ area, with scattering through $\theta=170°$. These particles impinge on the sample

which is the object to be analyzed. Almost all of the incident particles are absorbed within the sample. A few (much less than one in $10^4$) are scattered back out of the sample. Of these, a small fraction are incident on the area defined by the aperture of an analyzing system.

The scattered particles are analyzed with a solid-state detector located about 10 cm from the target and with a solid angle between 3 and 4 mSr. The detector resolution is between 15 and 20 keV, and the multichannel analyzer is set up with a channel width E between 3 and 5 keV.

- The collision then must be an elastic one. The phenomenon is similar to the collisions of two hard spheres and can be solved exactly. Nuclear reactions and resonances must be absent. With a H+ beam, nuclear effects can appear even below 1 MeV; with He+, they begin to appear at 2 to 3 MeV. Several elements have just one stable isotope (for example Au), whereas several others have more than one stable isotope. Sometimes the different signals from the different isotopes cannot be distinguished because the energy resolution of the detection system is too coarse.

- Scratches, cavities, dust particles and any other surface non-uniformities can drastically modify the spectrum, if present in sufficient amounts (even if they are of a sub-micron size). The lateral uniformity of a sample must therefore be assured on the surface as well as in depth.

### A.6.2 Accelerator

Many commercially available accelerators can be used for backscattering spectrometry. The most widely used available electrostatic accelerator is the Van de Graaf generator.

### A.6.3 Advantages

Compared to other methods-for example, neutron activation analysis or secondary ion mass spectroscopy - backscattering spectrometry is not very sensitive. However backscattering spectrometry is capable of quantitative measurements without recourse to standards.

One of the advantages of this method is that the spectrum can be interpreted rather easily.

The increase in sensitivity for heavy elements is an asset for the detection of these elements, but a severe limitation for the detection of light elements.

Two elements of similar mass cannot be distinguished when they appear together in a sample.

One of the main applications of backscattering spectrometry is the analysis of thin films and layered structures. With spectra analysis of thick samples, only the surface is clearly recognizable as the high-energy edges of the signals in the spectrum.

### A.6.4 Four Basic Physical Concepts Enter into Backscattering Spectrometry

- Energy transfer from a projectile to a target nucleus in an elastic two-body collision. This process leads to the concept of the kinematic factor and the capability of mass perception.
- Likelihood of occurrence of such a two-body collision. This leads to the concept of scattering cross section and to the capability of quantitative analysis of atomic composition.
- Average energy loss of an atom moving through a dense medium. This process leads to the concept of stopping cross section and to the capability of depth perception..
- Statistical fluctuation in the energy loss of an atom moving through a dense medium. This process leads to the concept of energy straggling and to a limitation in the ultimate mass and depth resolution of backscattering spectrometry.

## A.7 INDUCTIVELY COUPLED PLASMA ATOMIC EMISSION SPECTROMETRY (ICP - AES)

The development of inductively coupled Plasma (ICP) technology began in 1942. The plasma possesses three important characteristics which can be exploited and used as vaporization cells and free atom reservoirs for analytical atomic emission spectrometry (AES):

- high gas temperature
- capability of being sustained in a noble environment
- freedom from contamination

These characteristics have been used and now the Inductively Coupled Plasma - Atomic Emission Spectrometry (ICP-AES) has become one of the most advanced techniques for elemental analysis. ICP-AES is an elemental analysis technique suing spectra emitted by free atoms or ions generated within a source such as an ICP.

### A.7.1 Basic Concept

The ICP-AES is a conventional spectroscopy technique; its unique properties derive from the particular excitation source, the ICP.

The method is based on AES coupled with an ICP source. The ICP source produces a stream of high energy ionized gas known as a plasma by inductively coupling an inert gas (most commonly argon) with a high-frequency field. The resulting plasma has an internal temperature up to 10,000 K which dissolves, dissociates, atomizes, and excites the elements present when a sample is injected through its center. This results in the emission of light of unique frequencies from the constituent element(s). The light emitted from the plasma is proportional to the concentration of the elements in the sample. The light is transferred to an emission spectrometer which has the capability of separating the unique frequencies into discrete wavelengths (each wavelength or frequency being associated with an element in the sample). The intensity of light is measured at a wavelength which is unique to that element. The fundamental assumption in quantitative analysis is that the intensity of a line emitted within an excitation source is directly proportional to the concentration of the atoms of the emitter which are present in the discharge. The electronics of the spectrometer calculate the correlation and quantify the results. The presence of a background or residual impurity in standards causes deviation from linearity.

### A.7.2 Basic Elements of the ICP-AES

The basic elements of an ICP-AES instrument are source, optics, detector and processor.

*A.7.2.1 Source*

The source produces the emission spectra characteristic of the elements present in a sample. Under ideal conditions the excitation source should:

- excite lines of all elements of interest
- provide constant excitation conditions over a period of time corresponding to the sample excitation
- provide reproducible excitation conditions from sample to sample
- provide sufficient line intensity to achieve the required detection limit
- provide a low spectral background

One source with these characteristics is the ICP. By definition, a plasma is simply a very hot gas in which a significant fraction of the atoms or molecules are ionized. This ionized nature means that a plasma reacts in a number of ways when subjected to electromagnetic influences. The hot plasma ionized a portion of the incoming flow of non ionized gas so that the process is repeated continuously. Most commonly, a sample is introduced into the ICP in the form of an aqueous aerosol produced by pneumatic or ultrasonic nebulization. As aerosol droplets enter the aqueous aerosol produced by pneumatic or ultrasonic nebulization. As aerosol droplets enter the base of the plasma discharge and progress up through the aerosol channel, a variety of processes take place. The aerosol droplets that are passed into the plasma by the spray chamber are dissolved to yield a solid salt particle. The salt particles produced are subsequently vaporized to yield gas-phase molecular species. Then molecular dissociation yields free atoms (atomization) that may, given sufficient excitation energy, lose an electron to form free ions (ionization).

*A.7.2.2 Optics*

The spectrometer which optically collects light from the source (plasma) and separates the spectral details of the elements present in a sample for measurement. The primary function of the spectrometer is to isolate light from the various wavelength corresponding to emission lines of the different analyte elements and to differentiate this light from the plasma background emission. The better the resolution the less likely that adjacent lines will overlap.

*A.7.2.3 Detector*

A detector is generally a photomultiplier tube with associated electronics. The photomultiplier tube has a current that is proportional to the intensity of the elements line. The intensity must be averaged over the measuring time.

*A.7.2.4 Processor*

A computer system is used to calculate, calibrate, analyze and store the analytical data generated during analysis.

### A.7.3 Sample Preparation by Dissolution and Digestion Methods

All samples have to be in solution form for ICP-AES analysis. Traditionally, samples can be divided into a solution or liquid state, inorganic solid, and solids containing a high proportion of organic matter. The most common dissolution procedures for solid sample are:

- to heat the sample in a gas (thermal decomposition or pyrolysis)
- to treat the sample with liquids such as water, acids, organic solvents, etc.

- to form a melt or a flux by fusion with a salt or salts (fusion with ammonium salts, peroxides, borates, perchlorates, etc.).

The normally very long drawn-out process of dissolution can be accelerated by making the sample into a fine particle size, adding a catalyst, or sing ultrasonic agitation. The sample is then introduced, reduced to atomic vapor and quantified by the intensity of the light emitted by excited atoms and ions.

### A.7.4 Detection Limit

The detection limits (the lowest concentration of analyte which gives rise to a detectable signal) are generally very low for most element failing within the range 1-100 μg/l. It is recommended that an analyte should be present in the sample at a concentration approximately ten times that of its detection limit before a reasonably precise determination can be made. To attain reasonable accuracy, long integration period of 3 to 5 seconds and frequent recalibration are recommended. A judicious choice of analyte wavelength allows the analyst to assure detection of the selected analyte and minimize or avoid spectral interferences from the plasma background and the sample matrix. For example, for uranium the best wavelength is 385.96 nm with a detection limit around 100 μg/l and a standard concentration around 500 μg/l. The wavelength can also be used with a detection limit around 200 μg/l and the same standard concentration.

### A.7.5 Interferences

Not a single analytical technique can be claimed as free of interferences for quantitative analysis. ICP-AES is no exception to this claim. Some of the common interferences which can affect an analysis follows.

#### *A.7.5.1 Chemical and Physical Interference*

The ICP is relatively free from chemical interferences due to the high operating temperature of the argon plasma, which is enough to cause dissociation of most chemical bonds and compounds to the atomic state.

#### *A.7.5.2 Ionization Interference*

This interference arises from donation of electrons from concomitant species in the sample, which alter the atom or ion concentration of the species being determined.

*A.7.5.3 Spectral or Background Interference*

This interference is due to light emission at the analyte wavelength by the excitation source or some component of the sample (e.g., a spectral interference occurs when the spectrometer is set to measure the emission of an element at a particular wavelength, and another element is also present in the sample and has an emission line very close to the analyte wavelength).

Interference effects are generally small and easily manageable..

### A.7.6 Advantages

- covers most of the periodic table elements (rare earth elements, refractory elements),
- all concentration levels,
- sensitivity (increase detection limits). Excellent detection for many light elements, but less effective for heavy elements, such as lead or uranium,
- speed,
- accuracy and precision (around 1%),
- convenience unequaled by any other elemental analytical technique,
- no chemical interferences,
- minimum inter-element effects,
- simultaneous analysis of 20-40 elements,
- need a small volume of solution and consequently a small quantity of rock, mineral, etc.

### A.7.7 Disadvantages

- no depth analysis,
- destructive method,
- it's conventional form requires the analyte to be in solution.

## A.8 INDUCTIVELY COUPLED PLASMA MASS SPECTROMETRY (ICP-MS)

ICP-MS is an alternative use of ICP, as a source of ions, for mass spectrometry. The original concept of ICP-MS was developed from a requirement, expressed in 1970, for the next generation of multi-element analytical instrument systems needed to follow the then rapidly developing technique of ICP-AES. ICP-MS was introduced in commercial form in 1983.

After a survey of available and emerging techniques, it was concluded that atomic mass spectrometry was the only basic spectrometric technique that potentially had the wide element coverage, element specificity and relatively uniform sensitivity across the periodic table essential to provide a viable successor to powerful too that ICP-MS was promising to become.

### A.8.1 Basic Concept

The bases are the same for ICP-AES, just the optics used are different. The classic spectrometer is replaced by a mass spectrometer. The plasmas used at present for ICP-MS are essentially those developed for AES, and do not necessarily represent the optimum choice for ion source applications.

### A.8.2 Detection Limits

The detection limit around 50 ng/l is obtained for many elements in solution in real samples and around a mg/g in a solid. In extreme cases, the detection of an element at or even below these levels may be achieved on examination of a spectrum, because of the ability of the eye to recognize the shape of a very small peak in the presence of background. The detection limit for uranium in a solid is around 0.02 mg/g (6 mg/g for XRF).

Although detection limits for AAS, ICP-AES and XRF have now reached a plateau, the detection limits reported here for the ICP-MS may be improved in the future.

### A.8.3 Advantages

- qualitative and quantitative method
- the instrumental background is extremely small, typically a few ions per second
- can count individual ions (very low concentration range, typically two orders of magnitude lower than ICP-AES)
- extreme simplicity of the spectra obtained: spectra contain peaks mainly from singly charged ions
- excellent detection over the complete Periodic Table, especially good for heavy elements

### A.8.4 Disadvantages

- instrument tends to saturate at high ion currents ( restrict the range)

- more expensive than ICP-AES
- slower operation than ICP-AES

### A.8.5 Interferences

This technique suffers from the same interferences as the ICP-AES, because sample introduction constraints are similar.

- interface effects: this term may be used to describe any perturbation in the detected ion signal caused during the transmission of the sample from ICP tailflame into the first vacuum stage of the mass spectrometer.
- matrix effects: these effects are more serious in ICP-MS than ICP-AES.
- doubly ionized species: elements with low second ionization energy can partly be doubly ionized. This effect is less important in new systems.
- polyatomic ion interference: interferences may be produced in the sample itself.

These interferences are produced from different acids, some of which are used in dissolution procedure for geological samples.

# Appendix B

## INITIAL SURVEY DATA FOR ALL PANELS

**Samples from interior of Plant 7**

**Sample A-1** Measurement Date: 10/21/94

| | | | |
|---|---|---|---|
| A-1<br>β–γ 100cpm<br>α 10 cpm | β–γ 100 cpm<br>α 5 cpm | β–γ 110cpm<br>α 10 cpm | β–γ 110 cpm<br>α 10 cpm |

Side 1* – Painted

| | | | |
|---|---|---|---|
| A-1<br>β–γ 90cpm<br>α 0 cpm | β–γ 90 cpm<br>α 0 cpm | β–γ 80cpm<br>α 0 cpm | β–γ 90 cpm<br>α 0 cpm |

Side 2 – Painted

Comments:

| Background Activity | |
|---|---|
| β–γ | 50 cpm |
| α | 0 cpm |

**Sample A-2** Measurement Date: 10/21/94

| | | | |
|---|---|---|---|
| A-2<br>β–γ 70 cpm<br>α 0 cpm | β–γ 60 cpm<br>α 0 cpm | β–γ 70 cpm<br>α 0 cpm | β–γ 60 cpm<br>α 0 cpm |

Side 1 – Painted

| | | | |
|---|---|---|---|
| A-2<br>β–γ 70cpm<br>α 10cpm | β–γ 50 cpm<br>α 5 cpm | β–γ 100 cpm<br>α 15cpm | β–γ 70 cpm<br>α 10 cpm |

Side 2 – Unpainted

Comments: Left part of Side 2 appears to have been wet at some point

| Background Activity | |
|---|---|
| β–γ | 50 cpm |
| α | 0 cpm |

**Figure B–1 Initial survey data for panels A–1 and A–2**

**Samples from interior of Plant 7**

**Sample A-3** Measurement Date: 10/21/94

| A-3 | |
|---|---|
| β–γ 100 cpm<br>α 0 cpm | β–γ 100 cpm<br>α 5 cpm |
| β–γ 160 cpm<br>α 0 cpm | β–γ 120 cpm<br>α 5 cpm |

Side 1 – Painted

| A-3 | |
|---|---|
| β–γ 60cpm<br>α 15cpm | β–γ 100 cpm<br>α 30cpm |
| β–γ 240 cpm<br>α 40cpm | β–γ 120 cpm<br>α 50cpm |

Side 2 – Unpainted

Comments: Side 2 has large chip in upper left corner,

| Background Activity | |
|---|---|
| β–γ | 50 cpm |
| α | 0 cpm |

**Sample A-4** Measurement Date: 10/21/94

| A-4 | |
|---|---|
| β–γ 60cpm<br>α 5 cpm | β–γ 80cpm<br>α 0 cpm |
| β–γ 70cpm<br>α 0 cpm | β–γ 70cpm<br>α 0 cpm |

Side 1 – Painted

| A-4 | |
|---|---|
| β–γ 130 cpm<br>α 0 cpm | β–γ 130 cpm<br>α 0 cpm |
| β–γ 140 cpm<br>α 0 cpm | β–γ 130 cpm<br>α 0 cpm |

Side 2 – Painted

Comments:

| Background Activity | |
|---|---|
| β–γ | 50 cpm |
| α | 0 cpm |

**Figure B–2 Initial survey data for panels A–3 and A–4**

**Samples from interior of Plant 7**

**Sample A-5** Measurement Date: 10/21/94

| | |
|---|---|
| A-5<br>β–γ 90cpm<br>α 0 cpm | β–γ 150 cpm<br>α 5 cpm |
| β–γ 110 cpm<br>α 0 cpm | β–γ 150 cpm<br>α 0 cpm |

Side 1 – Painted

| | |
|---|---|
| A-5<br>β–γ 80cpm<br>α 0 cpm | β–γ 100 cpm<br>α 0 cpm |
| β–γ 60cpm<br>α 5 cpm | β–γ 70cpm<br>α 0 cpm |

Side 2 – Painted

Comments:

| Background Activity | |
|---|---|
| β–γ | 50 cpm |
| α | 0 cpm |

**Sample A-6** Measurement Date: 10/21/94

| | |
|---|---|
| A-6<br>β–γ 270 cpm<br>α 0 cpm | β–γ 180 cpm<br>α 0 cpm |
| β–γ 140 cpm<br>α 0 cpm | β–γ 110 cpm<br>α 0 cpm |

Side 1 – Painted

| | |
|---|---|
| A-6<br>β–γ 130 cpm<br>α 5 cpm | β–γ 180 cpm<br>α 5 cpm |
| β–γ 80cpm<br>α 10cpm | β–γ 110 cpm<br>α 10cpm |

Side 2 – Unpainted

Comments: Looks to be a separate panel that was bolted on all 4 corners and thus was not cut specifically for this project nor should it be expected to be similar to the others

| Background Activity | |
|---|---|
| β–γ | 50 cpm |
| α | 0 cpm |

**Figure B–3 Initial survey data for panels A–5 and A–6**

**Samples from exterior of building 7**

**Sample B-1** Measurement Date: 10/25/94

| | |
|---|---|
| B-1<br>β–γ 150 cpm<br>α 0 cpm | β–γ 150 cpm<br>α 0 cpm |
| β–γ 400 cpm<br>α 0 cpm | β–γ 700 cpm<br>α 30cpm |

Side 1 – unpainted

| | |
|---|---|
| B-1<br>β–γ 500 cpm<br>α 20cpm | β–γ 550 cpm<br>α 20cpm |
| β–γ 400 cpm<br>α 30cpm | β–γ 650 cpm<br>α 30cpm |

Side 2 – paint stripes

Comments: corrugated

| Background Activity | |
|---|---|
| β–γ | 70 cpm |
| α | 0 cpm |

**Sample B-2** Measurement Date: 10/25/94

| | |
|---|---|
| B-2<br>β–γ 100 cpm<br>α 0 cpm | β–γ 50cpm<br>α 0 cpm |
| β–γ 600 cpm<br>α 0 cpm | β–γ 250 cpm<br>α 0 cpm |

Side 1 – unpainted

| | |
|---|---|
| B-2<br>β–γ 400 cpm<br>α 50cpm | β–γ 500 cpm<br>α 20cpm |
| β–γ 500 cpm<br>α 30cpm | β–γ 500 cpm<br>α 30cpm |

Side 2 – paint stripes

Comments: corrugated

| Background Activity | |
|---|---|
| β–γ | 70 cpm |
| α | 0 cpm |

**Figure B–4 Initial survey data for panels B–1 and B–2**

**Samples from exterior of building 7**

**Sample B-3** Measurement Date: 10/25/94

| | |
|---|---|
| B-3<br>β–γ 70cpm<br>α 10cpm | β–γ 250 cpm<br>α 40cpm |
| β–γ 70cpm<br>α 10cpm | β–γ 200 cpm<br>α 40cpm |

Side 1 – unpainted

| | |
|---|---|
| B-3<br>β–γ 650 cpm<br>α 10cpm | β–γ 550 cpm<br>α 20cpm |
| β–γ 350 cpm<br>α 50cpm | β–γ 500 cpm<br>α 50cpm |

Side 2 – paint stripes

Comments: corrugated

| Background Activity | |
|---|---|
| β–γ | 70 cpm |
| α | 0 cpm |

**Sample B-4** Measurement Date: 10/25/94

| | |
|---|---|
| B-4<br>β–γ 1.4k cpm<br>α 40cpm | β–γ 70cpm<br>α 10cpm |
| β–γ 1.5k cpm<br>α 40cpm | β–γ 120 cpm<br>α 20cpm |

Side 1 – unpainted

| | |
|---|---|
| B-4<br>β–γ 450 cpm<br>α 20cpm | β–γ 500 cpm<br>α 20cpm |
| β–γ 800 cpm<br>α 40cpm | β–γ 1.1k cpm<br>α 50cpm |

Side 2 – paint stripes

Comments: corrugated

| Background Activity | |
|---|---|
| β–γ | 70 cpm |
| α | 0 cpm |

**Figure B–5 Initial survey data for panels B–3 and B–4**

**Samples from exterior of building 7**

**Sample B-5** Measurement Date: 10/25/94

| | |
|---|---|
| B-5<br>β–γ 70cpm<br>α 0 cpm | β–γ 1.8k cpm<br>α 20cpm |
| β–γ 70cpm<br>α 0 cpm | β–γ 1.1k cpm<br>α 0 cpm |

Side 1 – adhesive

| | |
|---|---|
| B-5<br>β–γ 600 cpm<br>α 0 cpm | β–γ 700 cpm<br>α 0 cpm |
| β–γ 600 cpm<br>α 20cpm | β–γ 550 cpm<br>α 30cpm |

Side 2 – paint stripes

Comments: corrugated

| Background Activity | |
|---|---|
| β–γ | 70 cpm |
| α | 0 cpm |

**Sample B-6** Measurement Date: 10/25/94

| | |
|---|---|
| B-6<br>β–γ 1.5k cpm<br>α 50cpm | β–γ 1.4k cpm<br>α 20cpm |
| β–γ 150 cpm<br>α 40cpm | β–γ 100 cpm<br>α 20cpm |

Side 1 – unpainted

| | |
|---|---|
| B-6<br>β–γ 400 cpm<br>α 20cpm | β–γ 600 cpm<br>α 30cpm |
| β–γ 350 cpm<br>α 30cpm | β–γ 800 cpm<br>α 40cpm |

Side 2 – paint stripes

Comments: corrugated

| Background Activity | |
|---|---|
| β–γ | 70 cpm |
| α | 0 cpm |

**Figure B–6 Initial survey data for panels B–5 and B–6**

**Samples from interior of building 2A**

**Sample C-1**

Measurement Date: 10/26/94

| | |
|---|---|
| C-1<br>β–γ 15k cpm<br>α 600 cpm | β–γ 13k cpm<br>α 700 cpm |
| β–γ 11k cpm<br>α 500 cpm | β–γ 13k cpm<br>α 400 cpm |

Side 1 – unpainted

| | |
|---|---|
| C-1<br>β–γ 2.5k cpm<br>α 300 cpm | β–γ 2kcpm<br>α 800 cpm |
| β–γ 2.5k cpm<br>α 400 cpm | β–γ 2.5k cpm<br>α 400 cpm |

Side 2 – liquid stains

Comments:

| Background Activity | |
|---|---|
| β–γ | 50 cpm |
| α | 0 cpm |

**Sample C-2**

Measurement Date: 10/26/94

| | |
|---|---|
| C-2<br>β–γ 9kcpm<br>α 800 cpm | β–γ 1kcpm<br>α 300 cpm |
| β–γ 8kcpm<br>α 500 cpm | β–γ 1kcpm<br>α 400 cpm |

Side 1 – unpainted

| | |
|---|---|
| C-2<br>β–γ 1.5k cpm<br>α 400 cpm | β–γ 1.5k cpm<br>α 500 cpm |
| β–γ 2.5k cpm<br>α 600 cpm | β–γ 3.5k cpm<br>α 700 cpm |

Side 2 – liquid stains

Comments:

| Background Activity | |
|---|---|
| β–γ | 50 cpm |
| α | 0 cpm |

**Figure B–7 Initial survey data for panels C–1 and C–2**

**Samples from interior of building 2A**

**Sample C-3** Measurement Date: 10/26/94

| C-3 | |
|---|---|
| β–γ 11k cpm<br>α 800 cpm | β–γ 10k cpm<br>α 700 cpm |
| β–γ 10k cpm<br>α 700 cpm | β–γ 10k cpm<br>α 1.1k cpm |

Side 1 – unpainted

| C-3 | |
|---|---|
| β–γ 2kcpm<br>α 300 cpm | β–γ 2kcpm<br>α 300 cpm |
| β–γ 3kcpm<br>α 500 cpm | β–γ 4.5k cpm<br>α 700 cpm |

Side 2 – unpainted

Comments:

| Background Activity | |
|---|---|
| β–γ | 50 cpm |
| α | 0 cpm |

**Sample C-4** Measurement Date: 10/26/94

| C-4 | |
|---|---|
| β–γ 25k cpm<br>α 1.3k cpm | β–γ 25k cpm<br>α 1.1k cpm |
| β–γ 25k cpm<br>α 900 cpm | β–γ 25k cpm<br>α 900 cpm |

Side 1 – unpainted

| C-4 | |
|---|---|
| β–γ 15k cpm<br>α 4kcpm | β–γ 4kcpm<br>α 1.4k cpm |
| β–γ 15k cpm<br>α 2kcpm | β–γ 8kcpm<br>α 1.5k cpm |

Side 2 – unpainted

Comments:

| Background Activity | |
|---|---|
| β–γ | 50 cpm |
| α | 0 cpm |

**Figure B–8 Initial survey data for panels C–3 and C–4**

**Samples from interior of building 2A**

**Sample C-5** Measurement Date: 10/26/94

| | |
|---|---|
| C-5<br>β–γ 20k cpm<br>α 900 cpm | β–γ 15k cpm<br>α 1.1k cpm |
| β–γ 18k cpm<br>α 1.2k cpm | β–γ 15k cpm<br>α 1kcpm |

Side 1 – unpainted

| | |
|---|---|
| C-5<br>β–γ 6kcpm<br>α 1.2k cpm | β–γ 15k cpm<br>α 5kcpm |
| β–γ 10k cpm<br>α 1kcpm | β–γ 18k cpm<br>α 6kcpm |

Side 2 – unpainted

Comments:

| Background Activity | |
|---|---|
| β–γ | 50 cpm |
| α | 0 cpm |

**Sample C-6** Measurement Date: 10/26/94

| | |
|---|---|
| C-6<br>β–γ 18k cpm<br>α 800 cpm | β–γ 13k cpm<br>α 900 cpm |
| β–γ 15k cpm<br>α 900 cpm | β–γ 12k cpm<br>α 1.1k cpm |

Side 1 – unpainted

| | |
|---|---|
| C-6<br>β–γ 20k cpm<br>α 4kcpm | β–γ 6kcpm<br>α 2kcpm |
| β–γ 20k cpm<br>α 2kcpm | β–γ 8kcpm<br>α 1kcpm |

Side 2 – unpainted

Comments:

| Background Activity | |
|---|---|
| β–γ | 50 cpm |
| α | 0 cpm |

**Figure B–9 Initial survey data for panels C–5 and C–6**

# Appendix C

## RADIOLOGICAL CHARACTERIZATION SAMPLE SPECIFIC RESULTS BASED ON DESTRUCTIVE ANALYSIS TECHNIQUES

**Table C–1 Layer removal results based on geiger-mueller detector $\beta - \gamma$ measurements for sample A3c**

original thickness: 0.252 inches

side 1

| Total Thickness Removed (inches) | Activity (cpm) |
|---|---|
| 0 | 110 |
| 0.005 | 70 (background) |

side 2

| Total Thickness Removed (inches) | Activity (cpm) |
|---|---|
| 0 | 220 |
| 0.006 | 120 |
| 0.010 | 90 |
| 0.013 | 70 (background) |

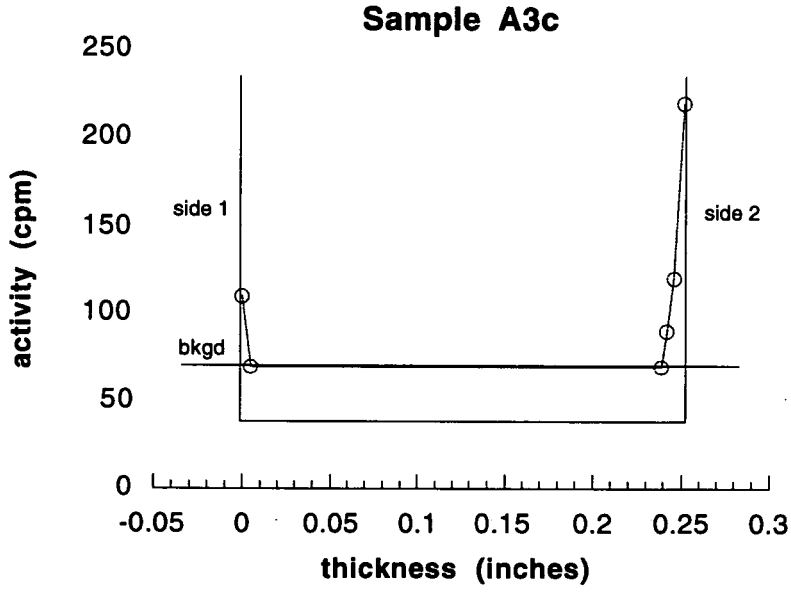


**Figure C–1 Graph of the contamination penetration distribution for sample A3c**

**Table C–2 Layer removal results based on geiger-mueller detector $\beta - \gamma$ measurements for sample A3e**

side 2

original thickness: 0.251 inches

| Total Thickness Removed(inches) | Activity (cpm) |
|---|---|
| 0 | 130 |
| 0.067 | 50 (background) |

**Table C–3 Layer removal results based on geiger-mueller detector $\beta - \gamma$ measurements for sample C4b**

original thickness: 0.261 inches

side 2

| Total Thickness Removed (inches) | Activity (cpm) |
|---|---|
| 0 | 8000 |
| 0.006 | 4000 |
| 0.009 | 3000 |
| 0.013 | 1000 |
| 0.019 | 600 |
| 0.031 | 240 |
| 0.047 | 130 |
| 0.055 | 70 (background) |

side 1

| Total Thickness Removed (inches) | Activity (cpm) |
|---|---|
| 0 | 23000 |
| 0.012 | 12000 |
| 0.023 | 2400 |
| 0.026 | 900 |
| 0.034 | 240 |
| 0.041 | 120 |
| 0.053 | 70 (background) |

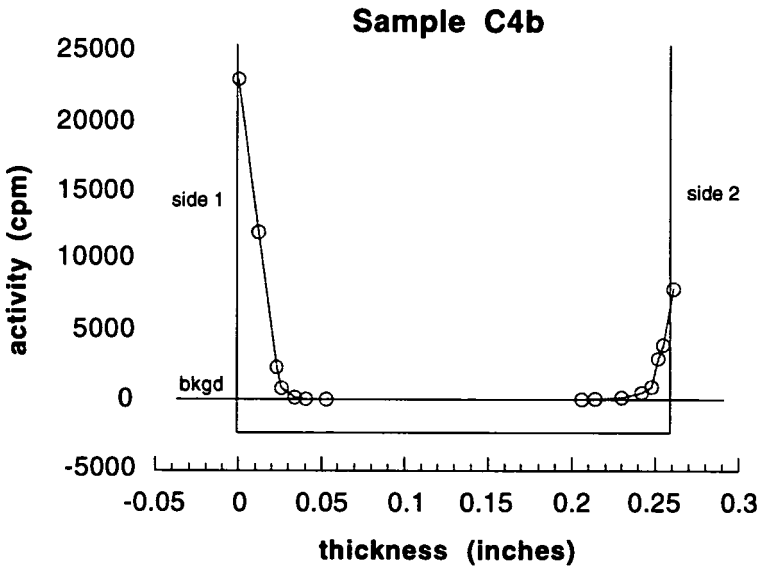


**Figure C–2 Graph of the contamination penetration distribution for sample C4b**

**Table C–4 Layer removal results based on geiger-mueller detector $\beta - \gamma$ measurements for sample C4e**

original thickness: 0.260 inches

side 2

| Total Thickness Removed (inches) | Activity (cpm) |
|---|---|
| 0 | 6000 |
| 0.005 | 4000 |
| 0.010 | 1400 |
| 0.016 | 900 |
| 0.023 | 700 |
| 0.033 | 300 |
| 0.043 | 130 |
| 0.054 | 70 (background) |

side 1

| Total Thickness Removed (inches) | Activity (cpm) |
|---|---|
| 0 | 20000 |
| 0.015 | 17000 |
| 0.026 | 1700 |
| 0.031 | 400 |
| 0.033 | 200 |
| 0.045 | 120 |
| 0.060 | 70 (background) |

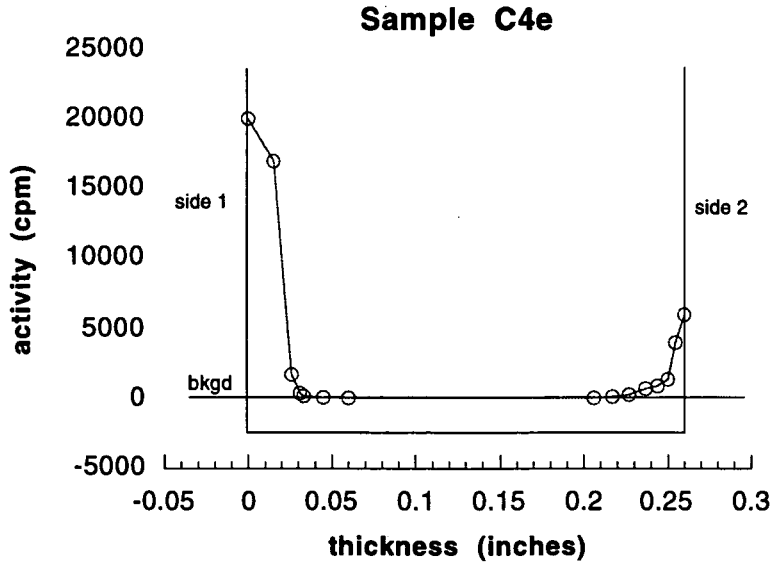


**Figure C–3 Graph of the contamination penetration distribution for sample C4e**

**Table C–5 Layer removal results based on geiger-mueller detector $\beta - \gamma$ measurements for sample C5b**

original thickness: 0.257 inches

side 2

| Total Thickness Removed (inches) | Activity (cpm) |
|---|---|
| 0 | 4000 |
| 0.004 | 1600 |
| 0.008 | 1000 |
| 0.015 | 700 |
| 0.024 | 350 |
| 0.037 | 180 |
| 0.046 | 120 |
| 0.055 | 70 (background) |

side 1

| Total Thickness Removed (inches) | Activity (cpm) |
|---|---|
| 0 | 13000 |
| 0.013 | 5000 |
| 0.022 | 300 |
| 0.026 | 200 |
| 0.030 | 170 |
| 0.035 | 120 |
| 0.043 | 70 (background) |

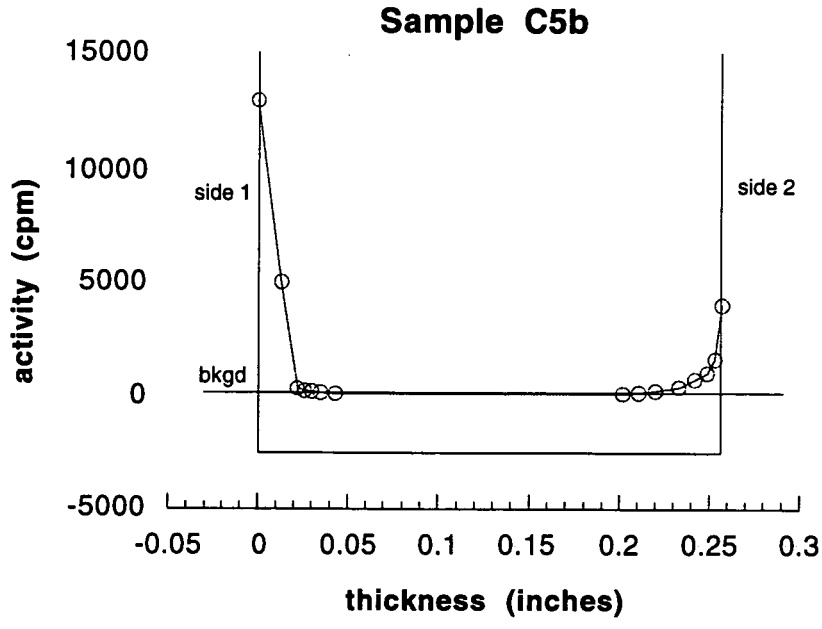


**Figure C–4 Graph of the contamination penetration distribution for sample C5b**

**Table C–6 Layer removal results based on geiger-mueller detector $\beta - \gamma$ measurements for sample C5c**

original thickness: 0.259 inches

side 2

| Total Thickness Removed (inches) | Activity (cpm) |
|---|---|
| 0 | 5000 |
| 0.007 | 1700 |
| 0.012 | 800 |
| 0.019 | 600 |
| 0.031 | 300 |
| 0.039 | 220 |
| 0.050 | 110 |
| 0.061 | 70 (background) |

side 1

| Total Thickness Removed (inches) | Activity (cpm) |
|---|---|
| 0 | 11000 |
| 0.014 | 1700 |
| 0.019 | 300 |
| 0.025 | 180 |
| 0.034 | 130 |
| 0.044 | 70 (background) |

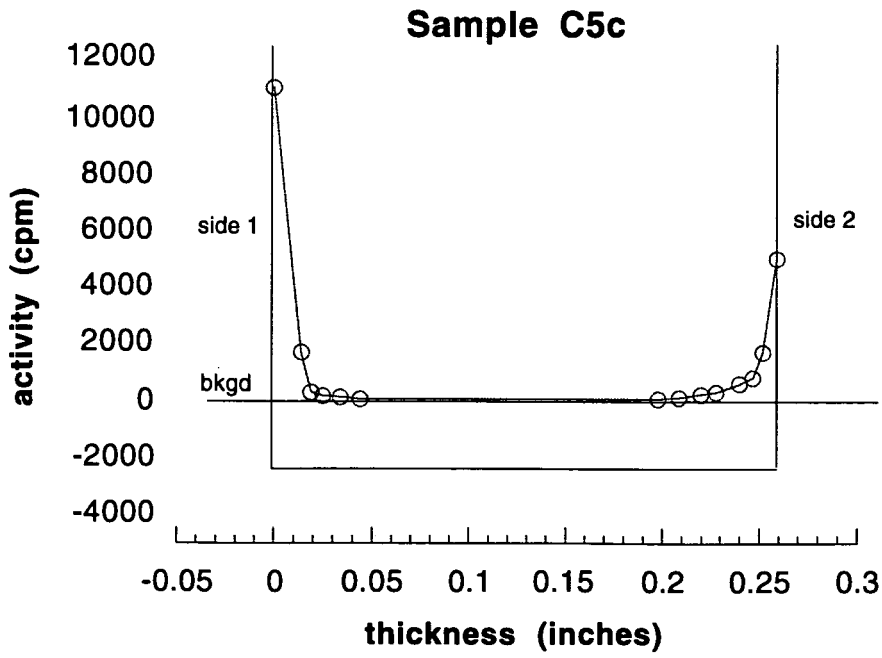


**Figure C–5 Graph of the contamination penetration distribution for sample C5c**

**Table C–7 Layer removal results based on geiger-mueller detector $\beta - \gamma$ measurements for sample C5d**

original thickness: 0.259 inches

side 1

| Total Thickness Removed (inches) | Activity (cpm) |
|---|---|
| 0 | 18000 |
| 0.011 | 15000 |
| 0.017 | 6000 |
| 0.024 | 700 |
| 0.029 | 240 |
| 0.037 | 130 |
| 0.058 | 70 (background) |

side 2

| Total Thickness Removed (inches) | Activity (cpm) |
|---|---|
| 0 | 6000 |
| 0.004 | 4500 |
| 0.006 | 3100 |
| 0.009 | 1900 |
| 0.016 | 900 |
| 0.028 | 400 |
| 0.045 | 140 |
| 0.060 | 70 (background) |

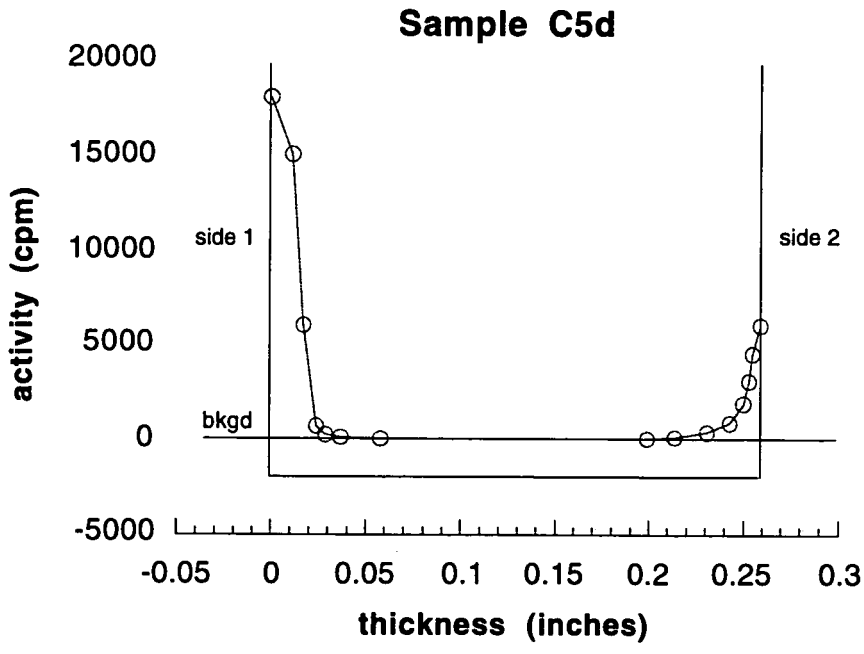


**Figure C–6 Graph of the contamination penetration distribution for sample C5d**

**Table C–8 Layer removal results based on geiger-mueller detector $\beta - \gamma$ measurements for sample C5e**

original thickness: 0.258 inches

side 2

| Total Thickness Removed (inches) | Activity (cpm) |
|---|---|
| 0 | 7000 |
| 0.007 | 2100 |
| 0.011 | 1100 |
| 0.020 | 500 |
| 0.028 | 400 |
| 0.038 | 350 |
| 0.051 | 210 |
| 0.061 | 70 (background) |

side 1

| Total Thickness Removed (inches) | Activity (cpm) |
|---|---|
| 0 | 13000 |
| 0.018 | 500 |
| 0.024 | 240 |
| 0.028 | 180 |
| 0.039 | 120 |
| 0.058 | 70 (background) |

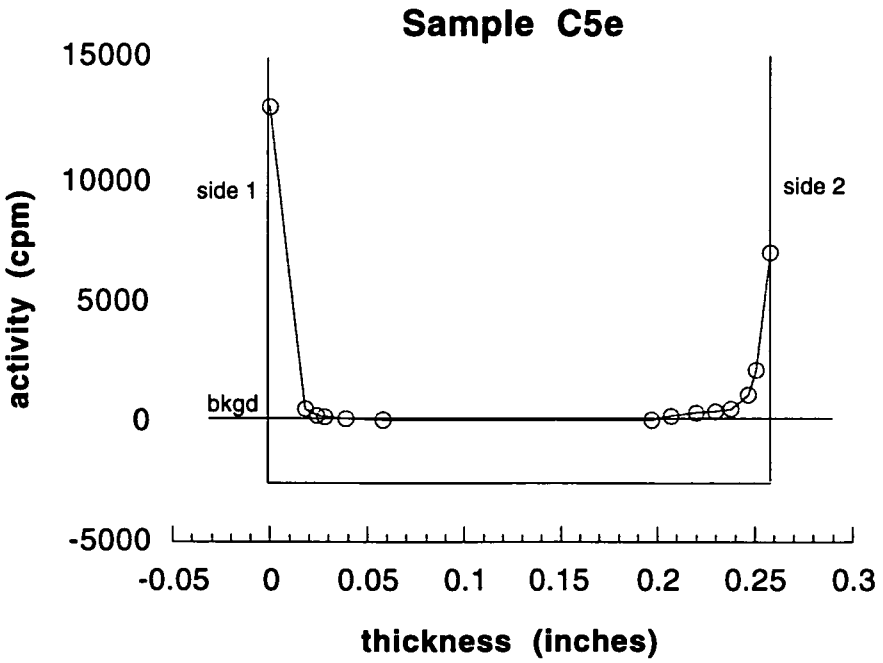


**Figure C–7 Graph of the contamination penetration distribution for sample C5e**

**Table C–9 Layer removal results based on geiger-mueller detector $\beta - \gamma$ measurements for sample C5f**

original thickness: 0.258 inches

side 2

| Total Thickness Removed (inches) | Activity (cpm) |
|---|---|
| 0 | 6000 |
| 0.007 | 1600 |
| 0.012 | 1000 |
| 0.024 | 500 |
| 0.033 | 280 |
| 0.044 | 180 |
| 0.059 | 120 |
| 0.064 | 70 (background) |

side 1

| Total Thickness Removed (inches) | Activity (cpm) |
|---|---|
| 0 | 11000 |
| 0.021 | 1100 |
| 0.032 | 280 |
| 0.039 | 190 |
| 0.049 | 140 |
| 0.059 | 70 (background) |

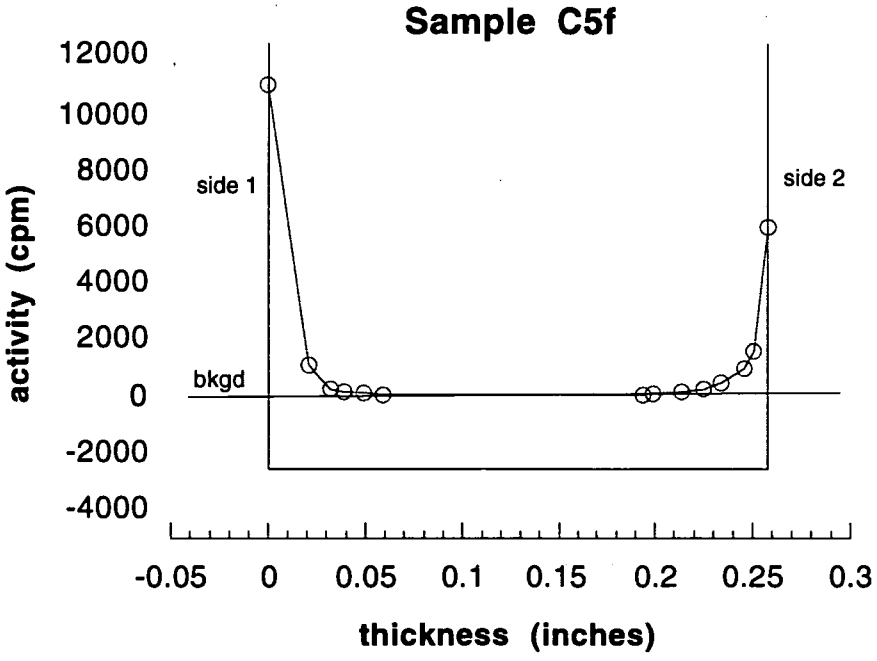


**Figure C–8 Graph of the contamination penetration distribution for sample C5f**

**Table C–10 Layer removal results based on geiger-mueller detector $\beta - \gamma$ measurements for sample C5g**

original thickness: 0.258 inches

side 2

| Total Thickness Removed (inches) | Activity (cpm) |
|---|---|
| 0 | 13000 |
| 0.006 | 5000 |
| 0.009 | 1400 |
| 0.013 | 700 |
| 0.022 | 360 |
| 0.031 | 280 |
| 0.039 | 170 |
| 0.049 | 130 |
| 0.059 | 70 (background) |

side 1

| Total Thickness Removed (inches) | Activity (cpm) |
|---|---|
| 0 | 17000 |
| 0.009 | 12000 |
| 0.019 | 1300 |
| 0.029 | 180 |
| 0.035 | 110 |
| 0.042 | 70 (background) |

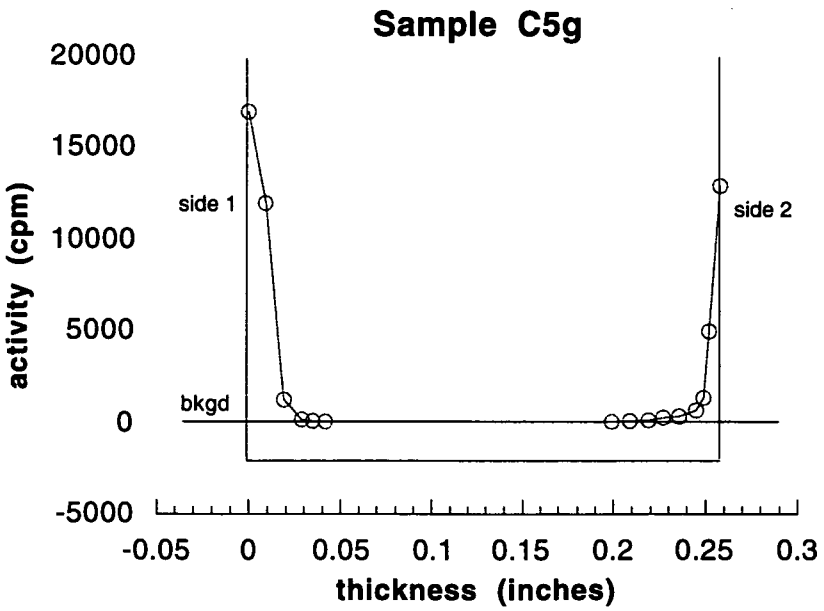


**Figure C–9 Graph of the contamination penetration distribution for sample C5g**

**Table C–11 Layer removal results based on geiger-mueller detector $\beta - \gamma$ measurements for sample C5h**

original thickness: 0.260 inches

side 2

| Total Thickness Removed (inches) | Activity (cpm) |
|---|---|
| 0 | 15000 |
| 0.005 | 7000 |
| 0.008 | 4000 |
| 0.011 | 2000 |
| 0.016 | 1000 |
| 0.051 | 240 |
| 0.074 | 140 |
| 0.096 | 70 (background) |

side 1

| Total Thickness Removed (inches) | Activity (cpm) |
|---|---|
| 0 | 13000 |
| 0.012 | 8000 |
| 0.017 | 2100 |
| 0.021 | 500 |
| 0.026 | 200 |
| 0.033 | 120 |
| 0.048 | 70 (background) |

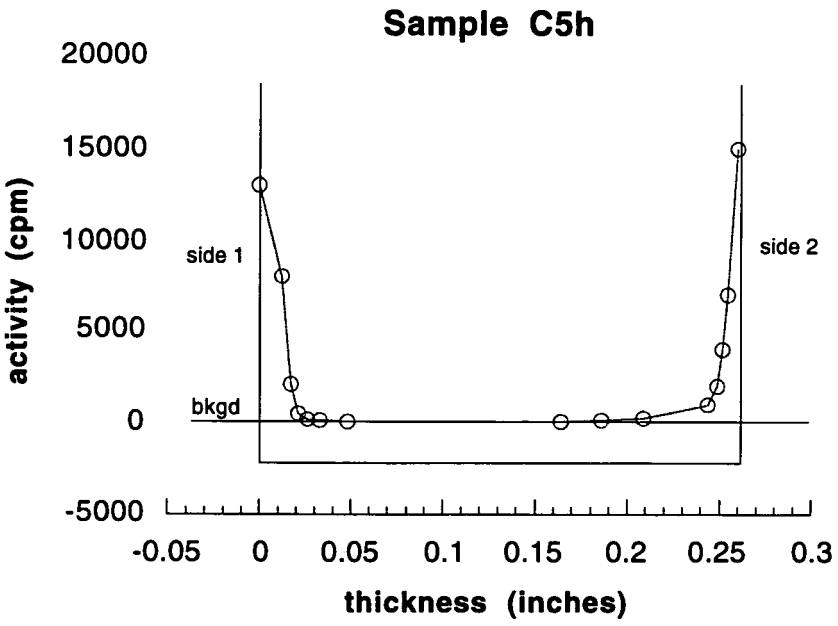


**Figure C–10 Graph of the contamination penetration distribution for sample C5h**

**Table C–12 Layer removal results based on geiger-mueller detector**
$\beta - \gamma$ measurements for sample C5i

original thickness: 0.258 inches

side 2

| Total Thickness Removed (inches) | Activity (cpm) |
|---|---|
| 0 | 17000 |
| 0.005 | 3000 |
| 0.009 | 1100 |
| 0.015 | 700 |
| 0.022 | 400 |
| 0.034 | 270 |
| 0.041 | 190 |
| 0.050 | 140 |
| 0.063 | 70 (background) |

side 1

| Total Thickness Removed (inches) | Activity (cpm) |
|---|---|
| 0 | 12000 |
| 0.010 | 3400 |
| 0.020 | 360 |
| 0.026 | 200 |
| 0.035 | 130 |
| 0.041 | 70 (background) |

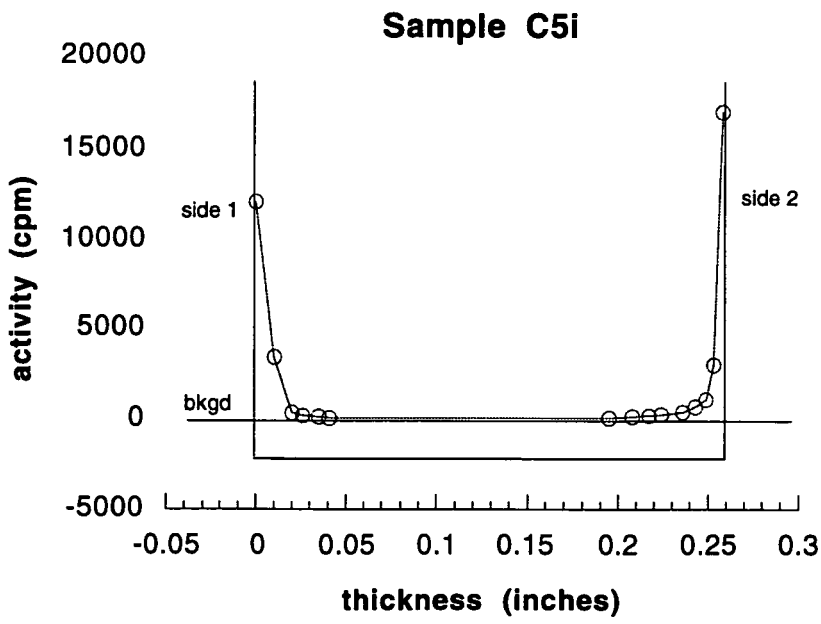


**Figure C–11 Graph of the contamination penetration distribution for sample C5i**

# Appendix D

## RADIOLOGICAL CHARACTERIZATION SAMPLE SPECIFIC RESULTS BASED ON GAMMA-RAY SPECTROSCOPY TECHNIQUE

### D.1 PREDICTED CONTAMINATION DISTRIBUTIONS

#### D.1.1 Sample C5d

Sample C5d is of dimension: 8.5 cm by 8.5 cm by 0.657 cm. The measured response ratios are listed in Table D–1 and shown in Figure D–1 for spacing $a$=4.0 cm.

In order to compare the measured data with simulated data, it was assumed that the distribution in the transite sample was the error complementary function, and that the boundary condition ratio $S_2/S_1$=0.33 ± 0.058 (as measured using a G-M detector). With these conditions, the predicted distribution $g(z) = erfc(12z) + 0.34erfc(12(t-z))$ produces response ratios similar to the measured data, FigureD–1.

#### D.1.2 Sample C5e

Sample C5e is of dimension: 8.5 cm by 8.5 cm by 0.654 cm. The measured response ratios are listed in Table D–2 and shown in Figure D–2 for spacing $a$=7.1 cm.

In order to compare the measured data with computed data by computer simulation program, it was assumed that the distribution in the transite sample was error complementary function, erfc(z). The measured boundary condition ratio is $S_2/S_1$=0.54 ± 0.1 (as measured using a G-M detector). With these conditions, the predicted distribution $g(z) = erfc(27z) + 0.53erfc(27(t-z))$ produces response ratios similar to the measured data, Figure D–2.

#### D.1.3 Sample C5f

Sample C5f is of dimension: 8.5 cm by 8.5 cm by 0.655 cm. The measured response ratios are listed in Table D–3 and shown in Figure D–3 for spacing $a$=4.0 cm.

In order to compare the measured data with computed data by computer simulation program, it was assumed that the distribution in the transite sample was the error complementary function, erfc(z). The measured boundary condition ratio is $S_2/S_1$=0.538 ± 0.0873 (as measured using a G-M detector). With these conditions, the predicted distribution $g(z) = erfc(18z) + 0.555erfc(18(t-z))$ produces response ratios similar to the measured data, Figure D–3.

**Table D–1 Measured response ratio ($C_1/C_2$) for C5d ($a$=4.0 cm)**

| Energy, keV | $C_1$ | $C_2$ | Ratio ($C_1/C_2$) | σ |
|---|---|---|---|---|
| 63.91 | 83796 | 64619 | 1.3063 | 0.009840 |
| 84.60 | 36620 | 29454 | 1.2433 | 0.01985 |
| 93.11 | 476180 | 385261 | 1.2353 | 0.003178 |
| 113.24 | 21874 | 18346 | 1.1979 | 0.02264 |
| 144.09 | 88242 | 73044 | 1.2080 | 0.008082 |
| 163.56 | 39667 | 33039 | 1.2006 | 0.01370 |
| 185.54 | 447395 | 381041 | 1.1741 | 0.002771 |
| 205.35 | 35796 | 30461 | 1.1751 | 0.01274 |
| 765.35 | 11908 | 13494 | 1.1332 | 0.02154 |
| 1001.00 | 33766 | 38100 | 1.1284 | 0.009145 |

Where, $C_1$ is the photopeak area for detector 1;
$C_2$ is the photopeak area for detector 2.

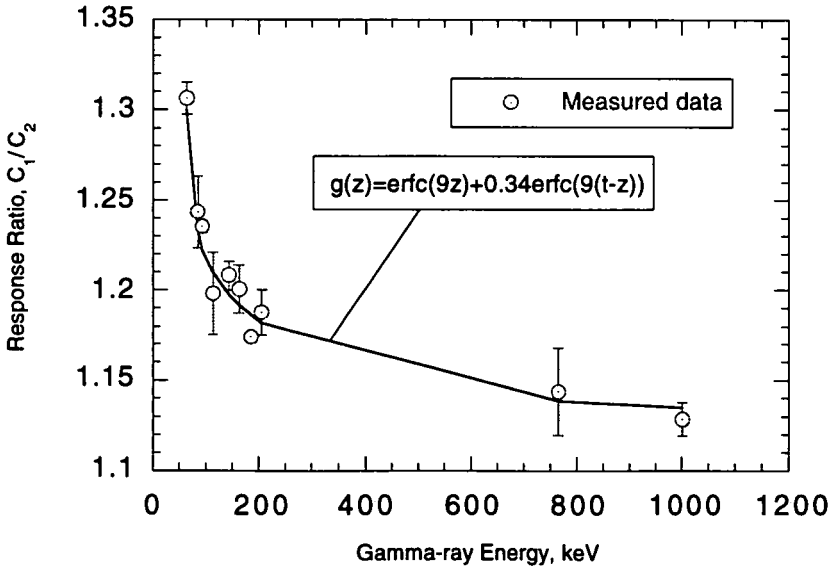


**Figure D–1 Comparison of measured data and the computed data for transite sample C5d.**

**Table D–2 Measured response ratios ($C_1/C_2$) for C5e ($a$=7.1 cm)**

| Energy, keV | $C_1$ | $C_2$ | Ratio ($C_1/C_2$) | σ |
|---|---|---|---|---|
| 63.91 | 35610 | 30683 | 1.1605 | 0.01150 |
| 84.60 | 14597 | 12864 | 1.1347 | 0.02591 |
| 93.11 | 176798 | 157472 | 1.1227 | 0.004523 |
| 113.24 | 8539 | 7675 | 1.1126 | 0.03145 |
| 144.09 | 29478 | 26487 | 1.1129 | 0.01212 |
| 163.56 | 12981 | 11699 | 1.1096 | 0.02036 |
| 185.54 | 162788 | 148305 | 1.0977 | 0.004205 |
| 205.35 | 12444 | 11393 | 1.0922 | 0.01938 |
| 765.35 | 4666 | 4360 | 1.0701 | 0.03536 |
| 1001.00 | 13883 | 13022 | 1.0661 | 0.01413 |

Where, $C_1$ is thephotopeak area for detector 1;
$C_2$ is thephotopeak area for detector 2.

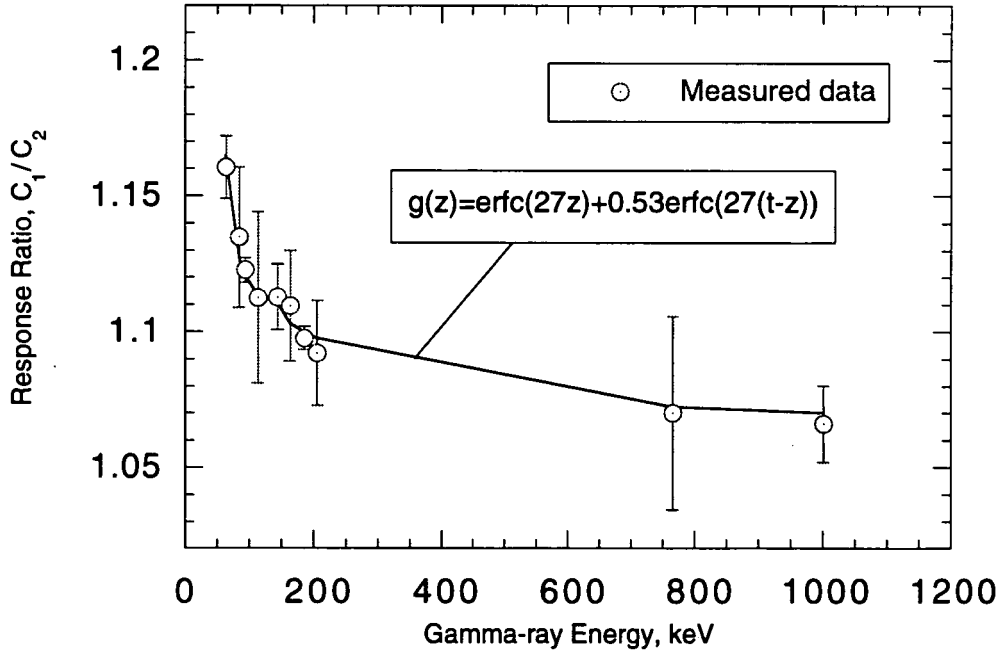


**Fig D–2 Comparison of measured data and the computed data for transite sample C5e.**

**Table D–3 Measured response ratio ($C_1/C_2$) for C5f ($a$=4.0 cm)**

| Energy, keV | $C_1$ | $C_2$ | Ratio ($C_1/C_2$) | σ |
|---|---|---|---|---|
| 63.91 | 52152 | 43646 | 1.1948 | 0.00984 |
| 84.60 | 22246 | 19228 | 1.1569 | 0.02134 |
| 93.11 | 302864 | 265726 | 1.1397 | 0.003518 |
| 113.24 | 14348 | 13157 | 1.1160 | 0.02529 |
| 144.09 | 53142 | 47858 | 1.1305 | 0.00921 |
| 163.56 | 23837 | 21237 | 1.1224 | 0.01611 |
| 185.54 | 285393 | 256941 | 1.1107 | 0.003253 |
| 205.35 | 22519 | 20282 | 1.1099 | 0.01512 |
| 765.35 | 7534 | 6853 | 1.0993 | 0.02957 |
| 1001.00 | 24462 | 22639 | 1.0805 | 0.01102 |

Where, $C_1$ is the photopeak area for detector 1;
$C_2$ is the photopeak area for detector 2.

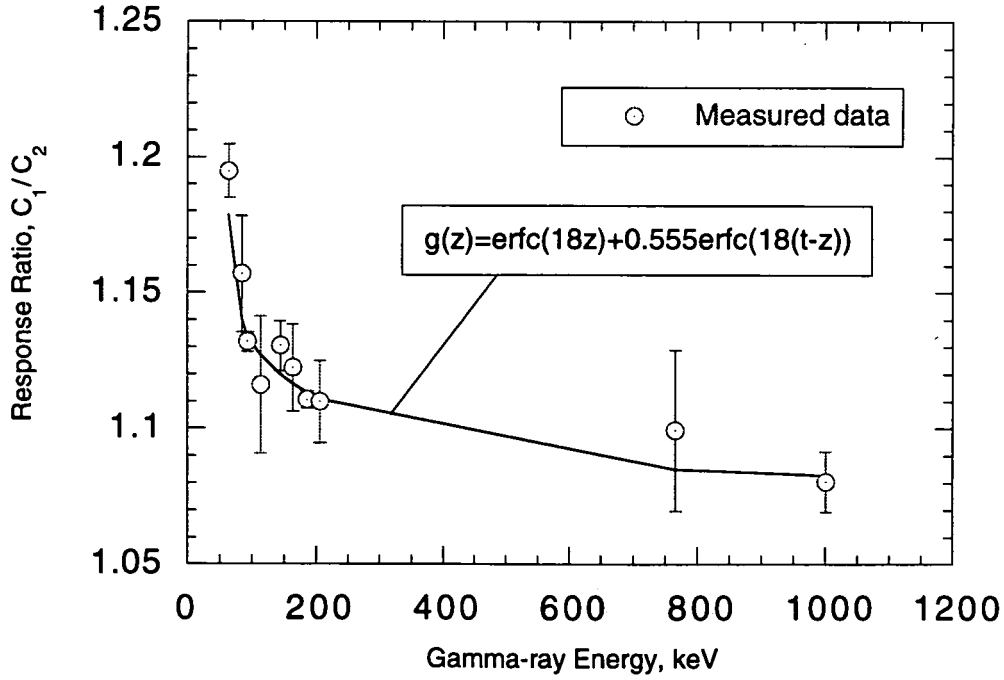


**Figure D–3 Comparison of measured data and the computed data for transite sample C5f.**

## D.2 VERIFICATION BY LAYER REMOVAL MEASUREMENT

### D.2.1 Sample C5a

In order to verify these results, a destructive layer removal technique was used to measure the actual decontamination distribution for sample C5a. The measured layer removal results are shown and compared to the best fitted distribution of $g(z)= erfc(22z) + 0.195erfc(22(t-z))$ in Figure D–4.

### D.2.2 Sample C5f

Sample C5f was destructively analyzed to verify the gamma-ray spectroscopy technique. The measured layer removal results are shown and compared to the predicted distribution in Figure D–5. The predicted distribution is determined with distribution function $g(z)=erfc(9z) + 0.34erfc(9(t-z))$. Comparing the layer removal and the predicted results, it appears that the predicted distribution on side-2 is significantly different from the layer removal results. This was observed for other samples as well, and is likely due to the choice of equal constants $\lambda_1= \lambda_2$, which assumes the two sides were similarly exposed to the contamination. Actually the two sides were exposed differently. Therefore, it is suggested that the constants $\lambda_1$ and $\lambda_2$ should be considered separately when this occurs.

### D.2.3 Sample C5d

Sample C5d was destructively analyzed to verify the gamma-ray spectroscopy technique. The measured layer removal results are shown and compared to the predicted distribution in FigureD–6. Note that the layer removal results have boundary ratio $S_2/S_1$=0.33 which is in the range of the measured ratio $S_2/S_1$=0.33 ± 0.058. The predicted distribution is of the form $g(z)=erfc(9z) + 0.34erfc(9(t-z))$. The difference between the predicted and measured distributions appears significant. These differences could be due to the uncertainties of the gamma-ray spectrum analyses, especially the choice of ROIs for the full-energy peaks. Other potential sources for the differences include the uncertainty of the destructive measurements.

### D.2.4 Sample C5e

Sample C5e was destructively analyzed to verify the gamma-ray spectroscopy technique. The measured layer removal results are shown and compared to the predicted distribution in Figure D–7. The predicted distribution is of distribution form with $g(z)=erfc(27z) + 0.53erfc(27(t-z))$.

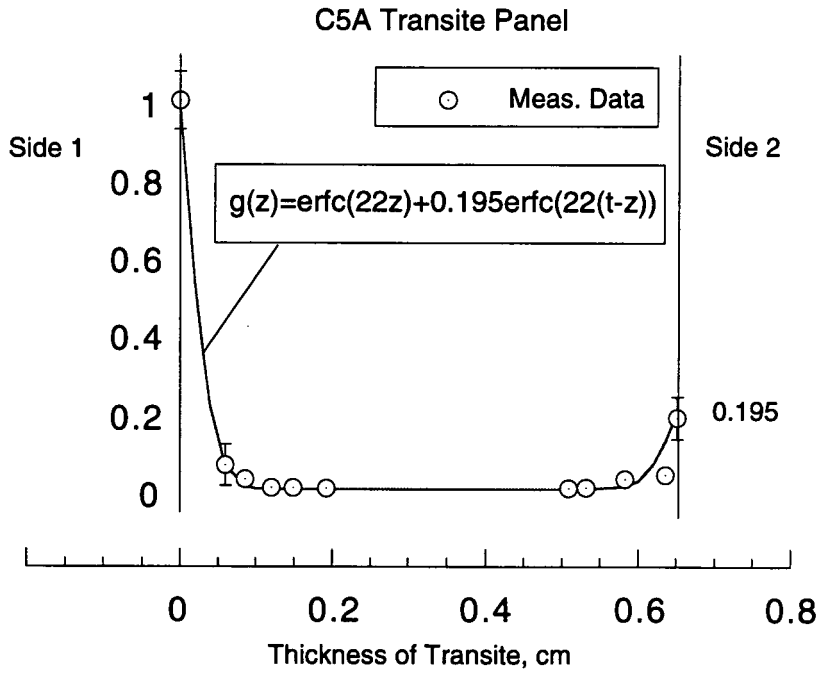


**Figure D–4 The comparison of measured distribution by layer removal and the predicted distribution for transite sample C5a**

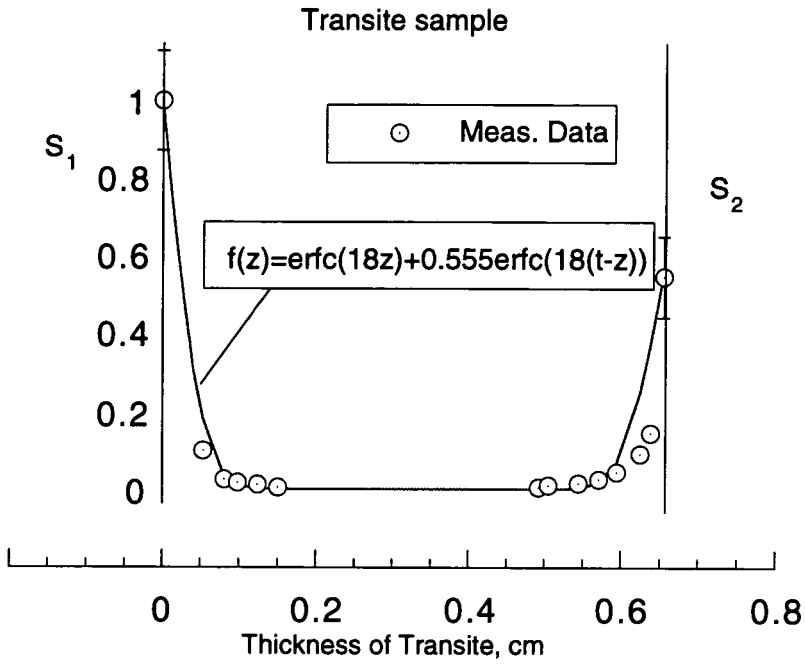


**FigureD–5 The comparison of measured distribution by layer removal and the predicted distribution for transite sample C5f.**

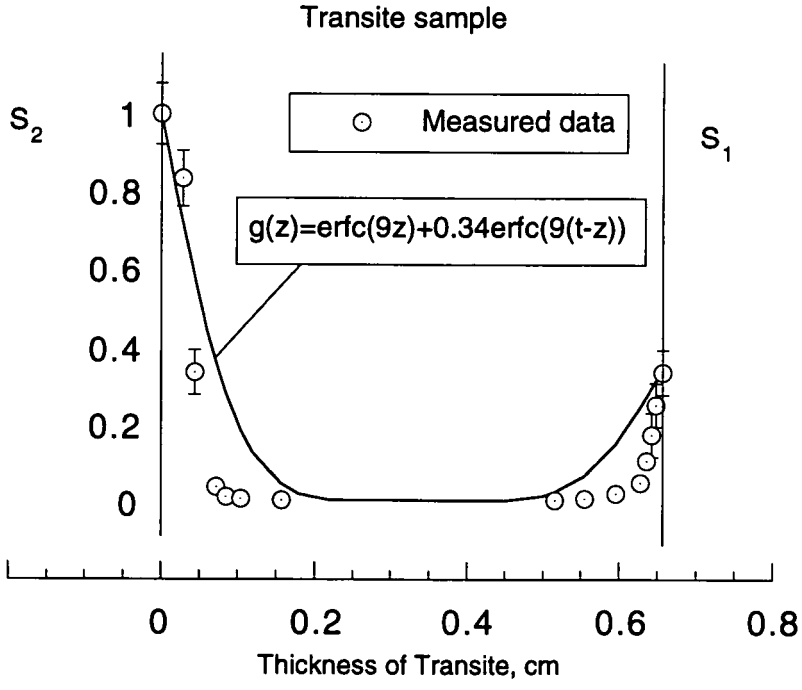


**Figure D–6 The comparison of measured distribution by layer removal and the predicted distribution for transite sample C5d**

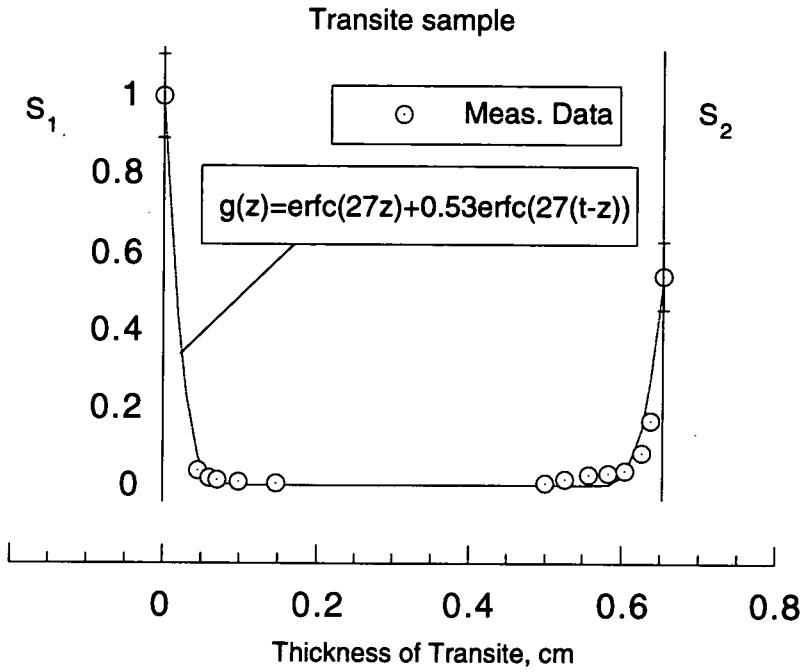


**Figure D–7 Comparison of measured data by layer removal and predicted distribution for transite sample C5e.**

# REFERENCES


Z. B. Alfassi, *Activation Analysis,* (volume 1, CRC Press, Boca Raton, Florida, 1990)

E.F. Arniella and L.J. Blythe, "Solidifying Traps Hazardous Wastes", *Chemical Engineering,* (February, 1990), pp. 92-102.

Asha Varma, *Handbook of Inductively Coupled Plasma Atomic Emission Spectroscopy,* (CRC Press, Boca Raton, Florida, 1991)

P.R. Bevington, *Data Reduction and Error Analysis for the Physical Sciences,* (McGraw-Hill, New York, 1969), chap. 5, pp. 66-91, chap. 10, pp. 187-203.

P.L. Bishop, "Contaminant Leaching from Solidified/Stabilized Wastes", *Emerging Technologies in Hazardous Waste Management II,* D.W. Tedder and F. G. Pohland Eds., (American Chemical Society, 1991), pp. 302-315.

E. Browne, R.B. Firestone, and V.S. Shirley, *Table of Radioactive Isotopes,* (John Wiley and Sons, New York, 1986), pp. 1431-1443.

Y.K. Cheng, P. Bishop and J. Isenburg, "Leaching Boundary in Cement-Based Waste Forms", *Journal of Hazardous Materials,* (Vol 9, No. 2, 1992), pp. 285-295.

Y.K. Cheng and P. Bishop, "Metal Distribution in Solidified/Stabilized Waste Forms After Leaching", *Journal of Hazardous Materials,* (Vol. 30, 1992), pp. 163-171.

P.L. Cote and T.R. Bridle, "Long-Term Leaching Scenarios for Cement-Based Waste Forms", *Waste Management and Research,* (Vol 5, 1987), pp. 55-66.

P.S. Daley, "Cleaning up Sites with On-Site Process Plants", *Environmental Science and Technology,* (Vol 23, No. 8, 1989), pp. 912-916.

A. R. Date and A. L. Gray, *Inductively Coupled Plasma Mass Spectrometry,* (Chapman and Hall, New York, 1989)

K. Debertin and R.G. Helmer, *Gamma- and X-ray Spectrometry with Semiconductor Detectors,* (North-Holland, New York, 1988), chap. 6, pp. 339-367.

T. G. Dzubay, *X-Ray Fluorescence Analysis of Environmental Samples,* (Ann Arbor Science Publishers, Ann Arbor, Michigan, 1977)

C.W. Groetsch, *The Theory of Tikhonov Regulation for Fredholm Equation of the First Kind,* (Pitman Advanced Publishing Program, Boston, 1984), chap. 1, pp. 1-14, chap. 3, pp. 31-63.

M. Hinsenveld, *A Shrinking Core Model As A Fundamental Representation of Leaching Mechanisms in Cement Stabilized Waste,* Doctoral Dissertation, University of Cincinnati, Cincinnati, chap. 4, pp. IV1-IV27, chap. 5, pp. V1-V20, (1992).

K. C. Hover and L. A. Rieser, *Practical Application of Ultraviolet Inspection Techniques in Processing Radioactive Waste,* (Draft #4 , unpublished paper, July 2, 1993)

R.G. Jaeger, et al., *Engineering Compendium on Radiation Shielding,* Vol. I, *Shielding Fundamentals and Methods*, (Herdelberg, New York, 1968), chap. 4, pp. 167-258.

S. A. E. Johansson and J. L. Campbell, *PIXE: a Novel Technique for Elemental Analysis*, (Wiley, Chichester, New York, 1988)

G. R. Lachance, F. Claisse and H. Chessin, *Quantitative X-Ray Fluorescence Analysis: Theory and Application,* (Wiley, Chichester, New York, 1995)

J. M. A. Lenihan and S. J. Thomson, *Advances in Activation Analysis,* (Academic Press, New York, 1969-1972)

C.V. McIsaac and S.T. Croney, "Effect of Waste Form Size on the Leachability of Radionuclides Contained in Cement-Based Evaporator Concentrates Generated at Nuclear Power Stations", *Waste Management*, (Vol. 11, 1991), pp. 271-282.

F. Medici, C. Merli and R. Volpe, "Experimental Evaluation of Limiting Factors for Leaching Mechanism in Solidified Hazardous Wastes", *Environmental Aspects of Stabilization and Solidification of Hazardous and Radioactive Wastes, ASTM STP 1033*, P.L. Cote and T.M. Gilliam, Eds.,(American Society for Testing and Materials, Philadelphia, 1989), pp. 229-237.

J. Millette, "Investigation of the Protective Effect of Iron Containing Coatings on Asbestos-Cement Pipe Exposed to Aggressive Water", Thesis submitted to the University of Cincinnati in partial fulfillment of the requirements for the degree of Doctor of Philosophy, (1983).

I. V. Mitchell, *Nuclear Science Applications- Section B: Particle Induced X-Ray Emission Analysis Application to Analytical Problems*, (Harwood Academic, Chur, Switzerland, 1981)

J. Philibert, *Atom Movements: Diffusion and Mass transport in Solids,* (Les Editions de Physique, 1991), chap. 1, pp. 1-31.

C.S. Poon, A.I. Clark and R. Perry, "Permeability Study on the Cement-Based Solidification Process for the Disposal of Hazardous Wastes", *Cement and Concrete Research,* (Vol. 16, 1986), pp. 161-172.

C.S. Poon, A. I., Clark and R. Perry, 'Investigation of the Physical Properties of Cement-Based Fixation Processes for a the Disposal of Toxic Wastes", *The Public Health Engineer*, (Vol. 13, 1985), pp. 108-110.

C.S. Poon, A.I. Clark and R. Perry, "Mechanisms of Metal Fixation and Leaching by Cement Based Fixation Processes", *Waste Management and Research*, (Vol. 3, 1985), pp. 127-142.

C.S. Poon, A.I. Clark and R. Perry, "Use of Stabilization Processes in the Control of Toxic Wastes", *Effluent and Water Treatment Journal,* (November, 1983), pp. 451-459.

W.H. Press, et al., *Numerical Recipes,* (Cambridge University Press, Cambridge, 1987), chap. 4, 5, and 6, pp. 102-190.

M. Rakovic, *Activation Analysis*, (CRC Press, Cleveland, 1970)

A. Roy, H.C. Eaton, F.K. Cartledge and M.E. Tittlebaum, "Solidification/Stabilization of Hazardous Waste: Evidence of Physical Encapsulation", *Environmental Science and Technology*, (Vol. 26 No. 7, 1992), pp. 1349-1353.

A. Roy, H.C. Eaton, F.K. Cartledge and M.E. Tittlebaum, "Solidification/Stabilization of a Heavy Metal Sludge by a Portland Cement/fly ash Binding Mixture", *Hazardous Waste and Hazardous Materials*, (Vol. 8 , No. 1, 1991), pp. 33-41.

W.R. Russ, J.D. Valentine, and W. Chung, *Radiological Contamination Penetration Depth in Fernald Transite Panels,* submitted for presentation at the *WM'96* conference in Tucson, AZ, February 25-29, 1996.

M.R. Schock and R.W. Buelow, "The Behavior of Asbestos-Cement Pipe Under Various Water Quality Conditions: Part 2, Theoretical Considerations", *Journal AWWA*, (Vol. 73, No. 12, 1981), pp. 636-651.

M. Sittig, "Pollution Control in the Asbestos, Cement, Glass and Allied Mineral Industries", *Pollution Technology Review*, (Park Ridge, N.J., Noyes Data Corporation, No. 19, 1975).

S.C. Taunton, "Manufacture and Use of Asbestos Cement Pipe", *Chemistry and Industry*, (Vol. 17, September 5, 1983), pp. 667-670.

M. Thompson, J. N. Walsh, *Handbook of Inductively Coupled Plasma Spectroscopy,* (2nd edition, Chapman and Hall, New York, 1989)

N. Tsoulfanidis, *Measurement and Detection of Radiation- McGraw Hill Series in Nuclear Engineering*, (Hemisphere Pub. Corp., New York, 1983)

G.C.C. Yang, "Durability Study of a Solidified Mercury-Containing Sludge", *Journal of Hazardous materials*, (Vol. 34, 1993), pp. 217-223.

H.A. Van der Sloot, J. de Groot and J. Wijkstra, "Leaching characteristics of Construction Materials and Stabilization; Products Containing Waste Materials", *Environmental Aspects of Stabilization and Solidification of Hazardous and Radioactive Wastes*, ASTM STP 1033, P.L. Cote and T.M. Gilliam, Eds. (American Society for Testing and Materials, Philadelphia, 1989), pp. 125-149.

J. C. Van Loon, *Analytical Atomic Absorption Spectrometry: Selected Methods*, (Academic Press, New York, 1980)

Wei-Kan Chu, J. W. Mayer, M. A. Nicolet, *Backscattering Spectroscopy,* (Academic Press, New York, 1978)

B. Welz, *Atomic Absorption Spectrometry,* 2nd edition, (Weinheim, Deerfield Beach, Florida,1985)

J. Wood, *Computational Methods in Reactor Shielding,* (Pergamon Press, New York, 1982), chap. 5, pp. 119-191.